Mag.pharm. Ramona Baumgartner

A ONE-STEP PROCESS TO MANUFACTURE SOLID NANO-PARTICLE FORMULATIONS DIRECTLY FROM THE LIQUID PHASE

DOCTORAL THESIS

to achieve the university degree of

Doktorin der Naturwissenschaften

submitted to

Graz University of Technology

Supervisor

Univ.-Prof. Dipl.-Ing. Dr.techn. Johannes Khinast

Institute of Process and Particle Engineering

Second Supervisor

Assoz. Prof. Mag.pharm. Dr.rer.nat. Eva Roblegg

Institute of Pharmaceutical Sciences, University of Graz

Graz, Mai 2016

AFFIDAVIT

I declare that I have authored this thesis independently, that I have not used other than the declared sources/resources, and that I have explicitly indicated all material which has been quoted either literally or by content from the sources used. The text document uploaded to TUGRAZonline is identical to the present thesis.

Date Signature

EIDESSTATTLICHE ERKLÄRUNG

Ich erkläre an Eides statt, dass ich die vorliegende Arbeit selbstständig verfasst, andere als die angegebenen Quellen/Hilfsmittel nicht benutzt, und die den benutzten Quellen wörtlich und inhaltlich entnommenen Stellen als solche kenntlich gemacht habe. Das in TUGRAZonline hochgeladene Textdokument ist mit der vorliegenden Dissertation identisch.

Datum Unterschrift

DANKSAGUNG

Ich möchte mich in erster Linie bei Prof. Johannes Khinast dafür bedanken, dass er die Erstbetreuung meiner Arbeit übernommen hat.

Allen voran gilt mein besonderer Dank Assoz. Prof. Eva Roblegg, die nicht nur durch ihren wissenschaftlichen Input, sondern auch durch ihre wertvollen Ratschläge beim Verfassen von Publikationen die Arbeit so erfolgreich gemacht hat.

Weiters danke ich Prof. Andreas Zimmer, dass er die Zweitbeurteilung der Arbeit übernommen hat.

Als nächstes gilt mein Dank meinen Arbeitskollegen am RCPE, wobei hier vor allem das Extrusionsteam hervorzuheben ist, welches mir stets bei den jeweiligen Versuchen tatkräftig unter die Arme griff. Außerdem möchte ich Dr. Andreas Eitzlmayr für die sehr angenehme und vor allem wertvolle Zusammenarbeit im NANEX-Projekt danken. Mit fortwährendem Optimismus hat er immer wieder versucht, mir ein grundlegendes Prozessverständnis beizubringen.

Ebenso danke ich dem gesamten Team der Pharmazeutischen Technologie an der Karl-Franzens Universität. Hierbei sind mir vor allem die Hobbits ans Herz gewachsen. Die tiefgründigen Gespräche und intensiven Freizeitaktivitäten formten sowohl Geist als auch Charakter und erweiterten meinen Horizont. Ihr habt meine Zeit als Dissertantin zu einer unvergesslichen werden lassen und dafür danke ich euch von ganzen Herzen.

Meiner Familie und damit meinen Eltern, Beate und Herbert, meiner Schwester Beatrice und meinem Freund Peter gilt jedoch mein größter Dank. Ihr habt mich die ganze Zeit begleitet, mich durch eure immerwährende Motivation unterstützt und all meine Höhen und Tiefen ertragen. Ohne euch hätte ich das nicht geschafft.

Während meiner Dissertation habe ich außerdem das wertvollste Geschenk bekommen, das man sich nur wünschen kann: meine Tochter Linda. Sie hat mit mir gemeinsam den Großteil dieser Arbeit verfasst, und daher widme ich ihr diese Arbeit.

ABSTRACT

New “designer-made” drug molecules are becoming increasingly complex and as a consequence, they are more lipophilic and less soluble in aqueous media. Currently, 90% of drugs in the pipeline have poor water solubility, which poses a great challenge since drug solubility is frequently the rate-limiting step in drug absorption. To overcome this obstacle, novel methods to convert complex molecules into effective medicines are an important objective. One highly promising approach in this field is particle size reduction to the nano-scale, where solubility enhancement is achieved by making use of the high surface-to-volume ratio. Such nano-systems show a decreased stability and immediately need to be converted into safe and effective high-quality medicines. Since most of the processes available are batch based and thus, time-consuming and cost-intensive, we developed a continuous nano-extrusion (NANEX) process, where an aqueous nano-suspension is directly transformed into a stable solid product using a hot melt extrusion process (HME). On that account, the objective of this thesis was:

i) to design and characterize a stable aqueous nano-suspension of a poorly soluble model API (i.e., phenytoin),
ii) to transform the nano-suspension into a stable solid product via the NANEX-process,
iii) to carefully characterize the obtained nano-extrudates and
iv) to optimize the NANEX process (with respect to the process parameters and distinct polymer matrices).

We showed that smallest particle sizes of bulk phenytoin were obtained by wet media milling using Tween® 80 as stabilizing agent. Nano-crystalline phenytoin displayed a faster and higher drug release and a markedly higher permeability compared to the bulk material. Next, Soluplus® was used as matrix material for the HME process. The screw configuration was designed according to the material´s characteristics (i.e., melting/glass temperature), the nano-suspension was added via side feeding, devolatilization was performed to remove the residual water and the obtained extrudates were characterized. Investigations showed that the nano-crystals were homogenously distributed in the matrix material, which in turn increased drug release compared to the bulk material. To extend the NANEX process, a variety of matrix materials were tested (i.e., Kollidon® VA64, Eudragit® EPO, HPMCAS and PEG 20000). We specifically focused on the maximum water integration and removal capacity to reach sufficiently high drug loadings in the final product. For this, process parameters (i.e., throughput and screw speed) were varied and the influence of the residence time and the filling degree on the process stability was investigated. It was found that water soluble/miscible matrix systems are appropriate candidates for the NANEX process. Long residence times and low filling degrees of the melt-

water mixture in the degassing zone favor the addition of high water amounts and as a consequence, improve the final product stability.

KURZFASSUNG

Neu designte Arzneistoffmoleküle sind zunehmend komplexer und besitzen dadurch häufig einen lipophilen Charakter und sind schlecht wasserlöslich. Derzeit weisen rund 90% aller Arzneistoffe in den pharmazeutischen Pipelines eine schlechte Wasserlöslichkeit auf. Die Auflösungsgeschwindigkeit eines Arzneistoffes stellt jedoch meist den geschwindigkeitsbestimmenden Schritt in der Arzneistoffabsorption dar. Dementsprechend werden verschiedenste Technologien angewendet, um die komplexen Moleküle in effektive Darreichungsformen mit ausreichender Arzneistofflöslichkeit zu überführen. Eine besonders vielversprechende Methode in diesem Bereich ist die Partikelgrößenreduktion in den Nanometerbereich. Durch ein großes Oberfläche-zu-Volumen Verhältnis von nanopartikulären Stoffen wird die Löslichkeit gesteigert. Da diese Nanosysteme jedoch eine schlechte Stabilität besitzen, müssen sie in eine sichere, effektive und qualitativ hochwertige Darreichungsform überführt werden. Die dafür vorhandenen Prozesse sind allerdings chargenbasiert und daher kostenintensiv und zeitaufwendig. Aus diesem Grund wurde der kontinuierliche Nanoextrusions-Prozess (NANEX) entwickelt. Dieser innovative Schmelzextrusionsprozess ermöglicht die Überführung von wässrigen Nanosuspensionen in stabile, feste Darreichungsformen direkt aus der flüssigen Phase. Demnach war das Ziel dieser Arbeit:

i) die Herstellung und Charakterisierung einer stabilen, wässrigen Nanosuspension eines schlecht wasserlöslichen Modelarzneistoffes (i.e., Phenytoin),
ii) die Überführung dieser Nanosuspension in ein festes Produkt mittels NANEX-Prozess,
iii) eine detaillierte Charakterisierung der erhaltenen Nanoextrudate und
iv) eine NANEX-Prozessoptimierung (hinsichtlich der Prozessparameter und verschiedener Matrixsysteme).

Es konnte gezeigt werden, dass die kleinsten Phenytoinpartikel mittels Nassvermahlung und der Zugabe von Tween® 80 als Stabilisator erhalten wurden. Das Nanomaterial zeigte eine erheblich gesteigerte Wirkstofffreisetzung und eine verbesserte Permeabilität im Vergleich zum Ausgangsmaterial. Im nächsten Schritt wurden die NANEX Versuche unter Verwendung von Soluplus® als Matrixmaterial durchgeführt. Die Schnecke wurde den Polymereigenschaften entsprechend designt (i.e., Schmelz-/Glasübergangstemperatur) und die Nanosuspension mittels Flüssigdosiereinheit dem Schmelzextruder zugeführt. Über einen internen Entgasungsschritt wurde das (überschüssige) Wasser entfernt. Die erhaltenen Extrudate wurden anschließend charakterisiert. Die Untersuchungen zeigten, dass die Nanokristalle de-agglomeriert eingebettet im Matrixmaterial vorlagen, wodurch eine Zunahme der Wirkstofffreisetzung im Vergleich zum Ausgangsmaterial erzielt wurde. Um künftig weitere Matrixmaterialien für den NANEX-Prozess verwenden zu können,

wurden Kollidon® VA64, Eudragit® EPO, HPMCAS und PEG 20000 hinsichtlich ihrer NANEX-Tauglichkeit untersucht. Dabei wurde vor allem die maximal zuführbare Nanosuspensionsmenge (bzw. die maximal abdampfbare Wassermenge) evaluiert, um ausreichend hohe Wirkstoffbeladungen im finalen Produkt zu erzielen. Zu diesem Zweck wurden die Prozessparameter Durchsatz und Schneckenumdrehungszahl variiert und die daraus resultierenden Verweilzeiten und Füllgrade hinsichtlich ihres Einflusses auf die Prozess- und Produktstabilität untersucht. Es konnte gezeigt werden, dass wasserlösliche/mischbare Matrixmaterialien für den NANEX-Prozess geeignet sind. Lange Verweilzeiten und niedrige Füllgrade des Polymer-Wasser Gemisches begünstigten dabei die Zugabe von hohen Nanosuspensions-/Wassermengen und steigerten die finale Produktstabilität.

TABLE OF CONTENTS

1. Introduction

1.1. Oral drug delivery

Drugs can be administered to patients via several routes, including parenteral, oral, transdermal, inhalative, vaginal and intraoral application. Among these routes, oral administration with intestinal absorption is with a market share of 90% the most common way [1].

R.J. Mrsny stated in his article "Oral drug delivery research in Europe" [2], that "…it *is unclear why people prefer taking a drug by the oral route over just about every other method.…Thinking about it, swallowing an object without mastication is contrary to all our default mechanisms for items that enter our mouth.…While the reason(s) behind man`s willingness to so readily swallow unknown materials remain obscure and quite debatable, it leaves the pharmaceutical industry with a huge challenge in finding new therapeutic entities that can be delivered by this preferred route of administration.*"

When active pharmaceutical ingredients (APIs) are orally administered, they are confronted with various obstacles of the oro-gastro-intestinal uptake route. The pH varies from 1.5 to 3.5 in the stomach, 5.5-6.8 in the small intestine to 6.4 in the colon. For APIs showing a pH dependent dissolution behavior and spectrum of activity, these variations may hamper drug absorption and thus, lead to an inadequate drug performance. Moreover, the API is exposed to various enzymes and metabolic processes of the digestive system, which may lead to degradation and as a consequence, inactivation of the API. Finally, the API must overcome the biological barriers of the gastro-intestinal tract to reach the systemic circulation [2]–[5]. Since the main function of the GI tract is to prevent an uncontrolled uptake of xenobiotics, intestinal absorption is challenging [2]–[5].
However, the uptake efficacy can be controlled by optimal formulation parameters and physicochemical properties of the drug [4].
One of the most important properties is a sufficient solubility of the API in gastric and intestinal fluids, since only dissolved molecules diffuse across biological membranes. Moreover, a moderate degree of lipophilicity facilitates the permeation across the lipophilic cell membrane. Thus, solubility and/or permeability of the API strongly define API absorption and bioavailability [6], [7]. For this, the Biopharmaceutics Classification System (BCS) was established [6]. It comprises four categories, which categorize APIs based on their solubility (in water) and permeability characteristics (see Fig. 1). Class II and IV contain APIs yielding poor solubility, while APIs of class III have a poor permeability. APIs of class IV exhibit both, poor solubility and permeability [6].

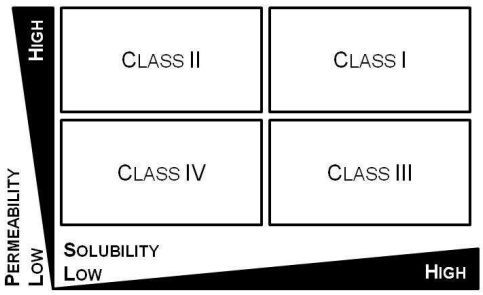

Fig. 1. *Biopharmaceutics Classification System (BCS)* [6]

Nearly a third of APIs listed in the United States Pharmacopeia are lipophilic and thus poorly soluble or insoluble in water [8]. On that account, new chemical entities (NCEs) featuring improved physicochemical characteristics are urgently needed. However the average costs for developing NCEs is often substantially higher compared to innovative drug delivery strategies to enhance the efficacy of an existing API [9].

1.2. Strategies for solubility enhancement

An ample body of technologies exists to improve API performance, mostly focusing on strategies for solubility enhancement of the API. These approaches encompass

- chemical and
- physical/technological modifications on the drug molecule.

1.2.1. Chemical modifications

Chemical modifications involve the formation of more soluble salts (of acidic and basic drugs) or co-crystals (i.e., molecular complexes). Thereby, the events of in-vivo salting-out, GI irritations, diarrhea or constipation have to be taken into account [4], [10]. Modifications can also be performed by introducing hydrophilic functional groups to the molecule to develop water-soluble derivates [11]. Nevertheless, alterations of the chemical structure may harmfully change the pharmacological activity, and thus, additional costs emerge for safety and efficacy studies [11].

1.2.2. Physical/technological modifications

Physical/technological modifications include the alteration of the crystal habit (i.e., lattice structure or crystallinity). In general, the free energy of polymorphs (e.g. the amorphous form) or pseudopolymorphs is higher compared to the crystalline form, which is related to

a higher solubility. However, polymorphs are metastable and tend to convert to the more stable but least soluble form over time [11].
A further opportunity is complexation of the API using complexing agents (e.g. cyclodextrins). Here, the limitations are the lack of universal applicability due to specifically required properties of the API (e.g., size, solubility, affinity, etc.) and a high amount of complexing agents for a sufficient drug loading[11].
The use of solubilizing excipients or co-solvents is also restricted by potential toxic or adverse pharmacological effects [11].
There exists also the possibility of a co-medication to modify motility or the pH to promote solubility [4], [11]. In the case of extreme pH conditions, chemical instabilities and/or local tissue irritations or necrosis might occur [11].
Solubility enhancement and thus, oral delivery can also be improved by tuning formulation parameters, including pH-dependent, controlled and site specific drug delivery via polymeric coatings, oral osmotic pumps and the density of dosage forms [4].

Another promising strategy is displayed by the use of solid dispersions, where the API is embedded or even dissolved in a matrix carrier. Solubility enhancement is achieved by using soluble/solubilizing carrier systems and/or by converting the API into the more soluble amorphous form. In the past decades, hot melt extrusion (HME) has emerged as a new platform technology for the production of solid dispersions for various routes of administration [12]–[16].

1.2.2.1. Hot melt extrusion (HME)

Before HME processing was applied in the pharmaceutical sector in the 1970s, it was established in the early 1930s in the plastic and rubber industry for the production of plastic bags, pipes and sheets [12]–[18]. In the pharmaceutical industry, HME is used to prepare solid dosage forms that comprise a drug embedded or dissolved in a thermoplastic polymer, low-melting wax or lipid (i.e., carrier). To improve process stability and/or to improve the drug performance, components like plasticizers, fillers, thermal lubricants, release modifying agents, antioxidants, miscellaneous additives and stabilizers are added optionally to the carrier/API mixture [14], [16]–[18].

There are different types of extruders used in the pharmaceutical industry, i.e., single-, twin- or multi-screw extruders. However, due to some considerable advantages, including shorter residence times, self-cleaning features, minimum supply, flexibility (in terms of operating parameters, screw configuration, etc.), and enhanced mixing (compared to a

single screw extruder) co-rotating, intermeshing twin-screw extruders are typically applied in the pharmaceutical sector [14], [19].

The HME-equipment of a twin-screw extruder basically comprises two screws, which can be individually designed (i.e., conveying, mixing and kneading elements) based on the requirements of the used formulation (e.g., required shear forces) and the desired results (e.g., degree of mixing). The screws are inside a cylindrical barrel. Since HME is most likely performed at accelerated temperatures (i.e., above the glass transition temperature (T_g) of thermoplastic polymers or the melting temperature (T_m) of lipids and waxes), barrels can be individually heated with electric heaters and/or cooled with water. At the end of the extruder, a die plate or an orifice is mounted, which serves as shaping tool for the extrudates [14], [16]–[18] (see Fig. 2).

In general, the HME process includes, feeding of the formulation via gravimetric or volumetric feeders to the hot melt extruder. Subsequently, the feedstock is transported in axial direction via the rotating screws to the compression and melting zone, where the mass is compressed, plasticized and/or molten. In the mixing zone, the carrier is mixed (on a molecular level) and homogenized with all other components. Finally, the homogenous mass is forced through a die plate or an orifice and the obtained rods, tubes or films of uniform shape and density solidify at the outlet [14], [16]–[18]. By installing a downstream-equipment like calandering, injection molding and strand cutting devices, granules or pellets can be obtained, which can be further pressed into tablets or filled into capsules [20]. Moreover, implants [21]–[25], patches and films [26]–[31] can be manufactured. Thus, this approach allows the manufacturing of dosage forms intended for the oral, transdermal or transmucosal route [14] (see Fig. 2).

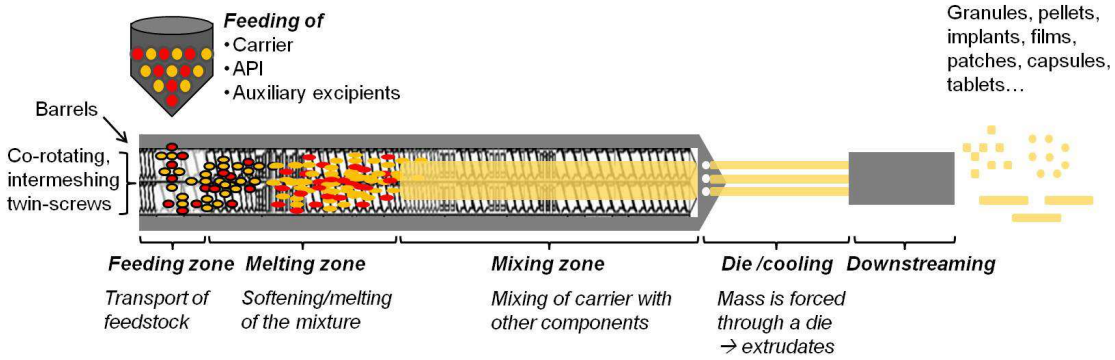

Fig. 2. *Schematic illustration of the HME process.*

The combination of feeding, conveying, melting, mixing, homogenizing, degassing and extruding in a single processing-unit made the HME to a continuous, cost-efficient, robust

and quick process over the past decades while offering the opportunity to produce targeted [32]–[34], controlled, modified [16]–[18], [35]–[40] or taste masked [41]–[48] drug delivery systems. Since the drug is embedded into the carrier or even dissolves in it, no solvent is required, making this approach environmental friendly and solvent related instabilities are eliminated [49]–[56]. Moreover, during HME, the API is (often) converted via accelerated temperatures, shear forces or solubilizing properties of the carrier into the amorphous form, yielding a higher solubility, faster dissolution velocities and thus, an enhanced bioavailability [14], [16]–[18], [49]–[56].

However, amorphous solid dispersions often struggle against long-term stability due to recrystallization, which in turn could affect dissolution characteristics over time.

Another possible solubility enhancing physical/technological strategy, which is not associated with changes in the crystal habit, is displayed by the particle size reduction of poorly soluble APIs to the nano-mater range (i.e., nano-technology).

1.2.2.2. Nano-technology: Nano-sizing of poorly soluble APIs

In the past decades, drug nano-crystals, which mainly consist of pure API, reached high popularity. Nano-sized materials exhibit larger specific surface areas and a decreased hydrodynamic boundary layer thickness during dissolution. These two factors are conducive for a faster transfer of solvated molecules from the surface area into the bulk solution and thus, enhance dissolution velocity of nano-crystals compared to larger crystals [57]–[60]. This relationship is illustrated in the Noyes-Whitney equation (Equation 1), which was extended by Nernst and Brunner [61]–[63],

Equation 1

$$\frac{dC_t}{dt} = \frac{DA}{h}(C_s - C_t)$$

where C_s stands for equilibrium solubility of the substance, C_t for the concentration at time t, D for the diffusion coefficient, A for the surface area of the particles and h for the hydrodynamic boundary layer thickness (see Fig. 3).

In addition to the improved dissolution velocity, nano-crystals (< 1 µm) yield increased saturation solubility due to a higher curvature of the particle surface, which is elucidated in the Ostwald-Freundlich equation (Equation 2) [58] (see Fig. 3).

Equation 2

$$log\frac{C_r}{C_\infty} = \frac{2\,\sigma\,V}{2.303\,RT\,\rho\,r}$$

C_r stands for the solubility of particles with radius r, C_∞ for the solubility of infinitely large particles, σ for the interfacial tension of the substance, V for the molar volume of the particle material, R for the absolute gas constant, T for the absolute temperature and ρ for the density of the solid.

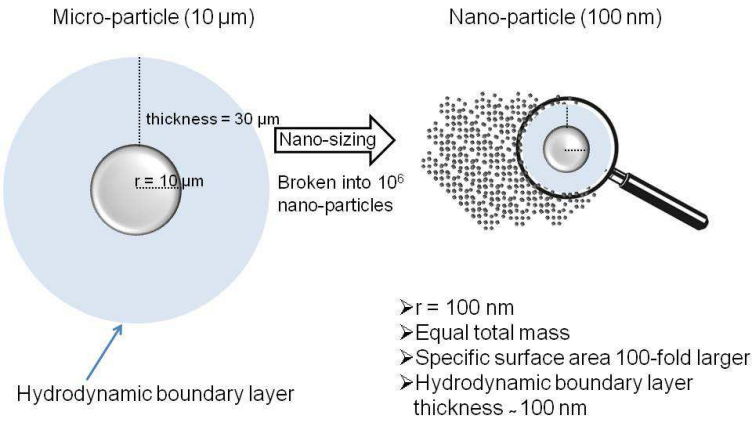

Fig. 3. *Effects of nano-sizing.*

Drug nano-crystals can be obtained by two different techniques: large particles can be broken into nano-scaled crystals via *top-down approaches* or built up from molecular solutions via *bottom-up approaches* (e.g. precipitation). Precipitation could not be established to a standard approach in pharmaceutical industry due to limitations concerning particle growth- and/or process control, low drug loading efficiencies and the need of organic solvents [57], [64]–[68]. In contrast, two *top-down techniques* have already served as production technique for marketed products [60] (see Table 1). In the 1990s, Liversidge et al. established the NanoCrystal® technology, which is a wet media-based milling technique [69]–[71]. With the marketed products Rapamune®, Emend®, Tricor®, Lyphantyl®, Megace® ES, Invega®, Sustenna® and Xeplion, this approach is seen as the most successful [57], [72]. Contemporaneously, Müller et al. developed the DissoCubes™ technology (acquired by SkyePharma PLC), which is based on piston gap high pressure homogenization [65], [66], [73]–[79]. Later on, modified techniques have emerged out of it, i.e., IDD-P™ (i.e., microfluidizer technology) [64], [66] and Nanopure® technology (i.e., piston gap homogenization in water mixtures or in nonaqueous media) [80]. However, Triglide® (i.e., IDD-P™ technology) is currently the only product available on the market [57].

All techniques are liquid phase processes, resulting in nano-suspensions. Owing to their small size and increased specific surface area, drug particles in the nano-meter range

yield an increased surface energy (i.e., Gibbs free energy). Thus, nano-suspensions are thermodynamically unstable systems since they possess the natural tendency to reduce this excess surface energy by agglomeration [81]. In addition to this, Ostwald-ripening might occur, which is described as crystal growth over time initiated by smaller particles yielding a higher saturation solubility compared to larger ones. Thus, larger particles grow while smaller dissolve [11]. Secondary and polymorphic nucleations are also well known instability problems, leading to re-crystallization of supersaturated solutions or converting a polymorph into a more stable form. Thus, a major issue is long-term stabilization against the thermodynamics of metastable, dispersed systems [11].

In general, parameters affecting the stability are first of all the solid properties (i.e., density, hardness, quality and quantity of lattice defects) of the drug, since they affect the particle size reduction by impact forces. Surface properties like the interfacial and the surface tension as well as the structure of the solid-liquid interface (e.g., the zeta potential at the interface) also determine the promoting or hindering forces for nano-particle agglomeration. Moreover, important characteristics of the dispersant are viscosity, solubility capacity for nano-crystals, and micellization activity of surfactants, since they are decisive for the rate of particle diffusion in the dispersant [11], [82].

Thus, in order to prepare stable nano-suspensions, inter-particle forces and the potential energy caused by the large interface between the particle and the dispersant have to be reduced. This can be achieved by the addition of surface-active agents. Charged surfactants (i.e., electrostatic stabilization) hinder nano-particle agglomeration by repulsive forces. Hydrophobic domains of non-ionic surfactants/polymers (i.e., steric stabilization) attach to the particle surface and the more hydrophilic part of the polymer extend into the aqueous dispersant providing a physical barrier. A combination of both types of stabilizers result in an electrosteric stabilization [57], [64], [71], [82]–[92] (see Fig. 4).

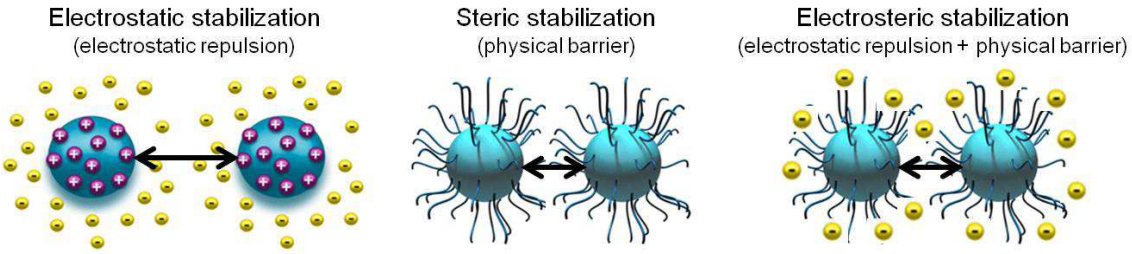

Fig. 4. *Nano-suspension stabilization: Hindering inter-particle interactions via electrostatic (i.e., introducing additional electrostatic repulsive forces via charged surfactants) and steric stabilization (i.e., providing a physical barrier via polymer adsorption onto the particle surface). Electrosteric stabilization represents a combination of electrostatic and steric stabilization (i.e., both, electrostatic repulsive forces and physical barrier)* [57], [64], [71], [82]–[92].

Nevertheless, system stability is steadily a struggle against time and basic laws of physics. Additionally, liquid formulations are less accepted by patients than solid dosage forms. Thus, it is a common procedure to transfer nano-suspensions into solid oral dosage forms [57], [82], [93], [94].

1.3. Transformation of nano-suspensions into solid products – state of the art

For the transformation of nano-suspensions into a dry product, well established unit-operations are applied. Frequently, nano-suspensions are transferred into a powder via freeze- and spray drying. The solid can be used as a powder for reconstitution or as a rapidly disintegrating dosage form (i.e., lyophilisate) or it is subsequently compressed into tablets or filled into capsules [82], [93], [95]–[100]. The most crucial quality criterion of these formulations is seen in a good reconstitution characteristic (i.e., reconversion into a nano-suspension during dissolution) in order to guarantee improved dissolution velocities. Thus, obtained dosage forms are required to show sufficient wetting and disintegration properties. For this, water-soluble sugars (e.g., mannitol, sucrose), mainly showing cryo-protective actions, are necessarily added as matrix formers prior to drying procedures [60], [82]. However, multi-step processes often hinder keeping nano-particles de-agglomerated until reaching the final dosage form, hampering improved dissolution behavior. Moreover, it has to be considered, that lyophilisates are very sensitive to moisture complicating handling and storage of the solid product.

Alternatively, nano-suspensions can either be layered onto an appropriate core material (e.g., lactose or microcrystalline cellulose) or beads via fluidized bed granulation or spray-layering. The obtained product can be compressed into tablets or filled into capsules [57], [101]–[103]. The already marketed product Rapamune® is commercially produced by direct layering of nano-suspensions onto tablets [57]. Again, multi-step processes are required, which are time consuming, cost-intensive, hard to control and to scale up and are therefore, unfavorable from an economic point of view.

Recently, inkjet and flexographic printing technologies have offered new opportunities for a flexible and continuous production of solid nano-formulations by printing nano-suspensions on substrates for (intra)oral administration [104]–[112]. However, this approach is often restricted to low-viscosity fluids and it is associated with problems concerning dosing precision. Moreover, the drug dose that can be applied on such substrates is limited, which makes this technology only an attractive alternative for low-dosed drugs [105], [110].

Nano-suspensions can also be incorporated into polymeric films via film casting methods [113], [114]. The disadvantageous issue is the subsequently required drying step, as well as the need of organic solvents.

In Table 1, examples for solidified nano-suspensions found in literature and the corresponding technological methods are listed. Currently, only a few products made it to the market (see Table 1). Possible reasons for this might be that many pharmaceutical companies either do not posses full in-house capabilities in terms of equipment and know-how or didn`t realize in time the full potential of nano-formulations [57], [115]. Apart from this, uneconomic multi-step processes, hard-to-reach final product quality/stability or limited dosing capabilities may be responsible for the small market share.

Table 1. *Examples for solidified nano-crystal suspensions found in literature (i.e., Ref.) (including marketed products).MM and HPH stand for the applied nano-sizing technology (MM = wet-media milling; HPH = high-pressure homogenization) and solidification for the applied approaches for transferring nano-suspensions into a solid product. To be continued.*

Nano-sizing	Solidification	Drug	Ref.
MM	Cooling	AZ68	[116]
MM	Freeze-drying	Danazol	[117]
MM	Freeze-drying	Itraconazole	[118]
MM	Freeze-drying	Loviride	[119]
MM	Freeze-drying	Itraconazole	[100]
MM	Freeze-drying	Naproxen	[99], [120]
MM	Freeze-drying and spray-drying	Cinnarizine, griseofulvin, indo-methacin, itraconazole, loviride, mebendazole, naproxen, phenylbutazone, phenytoin	[93]
MM	Spray-drying	Cilostazol	[98], [121]
MM	Spray-drying	Phenytoin	[122]
MM	Spray-layering (fluidized bed granulation)	Naproxen	[123]
MM	Spray-drying and pelletization of the dry powder in a high shear mixer	Ketoconazole	[124]
MM	Spray-drying, pelletization of the dry intermediate in a high shear mixer, compressed into tablets	Ketoconazole	[125]
MM	Spray-drying, compressed into tablets Spray-drying, roller compaction, granulation, compressed into tablets	Naproxen	[126]
MM	Spray –drying, blended with excipients, compressed into tablets	Candesartan cilexitil	[127]
MM	Spray-layering onto a water soluble carrier (via fluidized bed coating, solid intermediate = granules), compressed into tablets	Ketoconazole	[128]
MM	Spray-drying, film casting	Naproxen, cinnarizine	[129]
MM	Spray-drying, compressed into tablets	Undisclosed	[96]
MM	Flexographic printing	Indomethacin, itraconazole	[111]
MM	Film casting, drying	Griseofulvin, naproxen, fenofibrate	[114]

Continuation of Table 1.

Nano-sizing	Solidification	Drug	Ref.
MM	Film casting, drying	Griseofulvin	[130], [131]
MM	Film casting, drying	Fenofibrate, griseofulvin, naproxen, phenylbutazone, azodicarbonamide	[132]
MM	Spray-layering (spray-coating, fluidized bed coating) onto an inert tablet core	Sirolismus (Rapamune®)	[133]
MM	Spray-layering onto microcrystalline cellulose beads, filled into capsules (nine-step process)	Aprepitant (Emend®)	[134]
HPH	Freeze-drying	Azithromycin	[135]
HPH	Freeze-drying	Clofazimine	[136]
HPH	Freeze-drying	Oridonin	[137], [138]
HPH	Spray-drying	Amphotericin B	[139]
HPH	Spray-drying	Nifedipine	[140]
HPH	Spray-drying	Valsartan	[141]
HPH	Spray-coating on sugar spheres	Hydrocortisone Acetate	[103]
HPH	Spray-drying, blended with excipients, compressed into tablets	Celecoxib	[142]
HPH	Freeze-drying and spray-drying	Rutin	[143]
HPH	Inkjet printing	Folic acid	[104]
HPH	Film casting, drying	Herpetrione	[113], [144]
HPH	Film casting, drying	Quercetin	[145]
MM or HPH	Compressed into tablets or filled into capsules	Fenofibrate (Tricor®NP, Lipanthyl® Triglide®)	[146]

1.4. Objective

Efficient oral administration of lipophilic, poorly soluble drug molecules is challenging and becomes more relevant due to the frequently increasing number of poorly oral bioavailable APIs. To convert these complex molecules into effective medicines, various solubility enhancing strategies are applied. However, the final dosage forms often suffer from stability problems, are less accepted by patients and are produced via multi step processes.
In an attempt to provide a product, which exhibits

- improved dissolution characteristics,
- shelf-life stability,
- patient acceptance and
- economically efficient manufacturing,

two strategies were combined, i.e., nano-technology and HME, and the nano-extrusion (NANEX) process was developed [147], [148].
In an initial proof of concept study [147], a stabilized aqueous nano-suspension of the model substance titanium dioxide (TiO_2) was successfully transferred into a stable solid product via the NANEX process. Obtained nano-extrudates comprised de-agglomerated embedded nano-crystals (see Fig. 5).

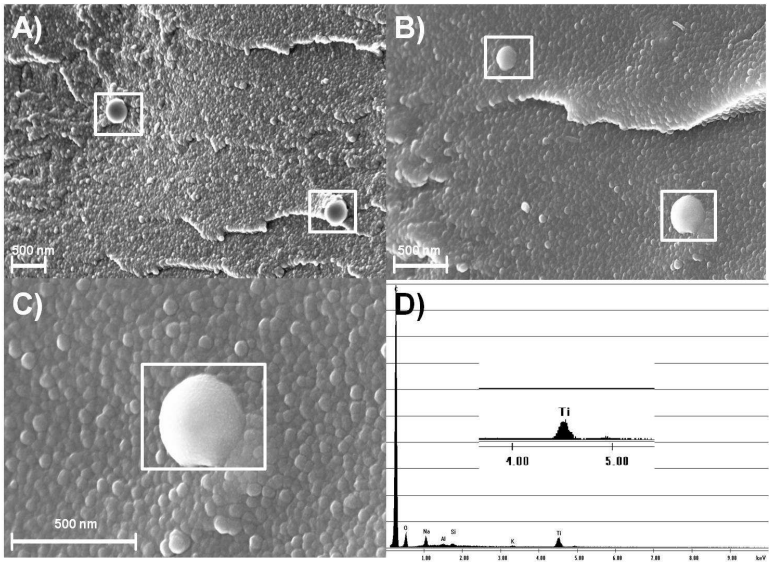

Fig. 5. *Scanning electron microscopic images of cross sections (A-C) of extrudates: A,B: 210-340 nm TiO_2 particles embedded in Soluplus® in de-aggregated form and C,D verification of a TiO_2 nano-particle (340 nm) via elemental analysis (energy-dispersive X-ray spectroscopy)* [147].

For this, the experimental set-up of the novel NANEX process was evolved (see Fig. 6). Analogous to traditional HME processes, the water soluble/miscible carrier system (i.e.,

Soluplus®) is fed gravimetrically into the extruder. Shear forces generated by the installed screw and applied barrel temperatures compress and soften the matrix while transporting it into the compression/melting zone. The innovation of the NANEX process is the subsequent addition of the nano-suspension to the molten mass via a flow controlled micro angular gear pump. By applying a vacuum in the degassing zone, the excess water stemming from the nano-suspension is eliminated (see Fig. 6).

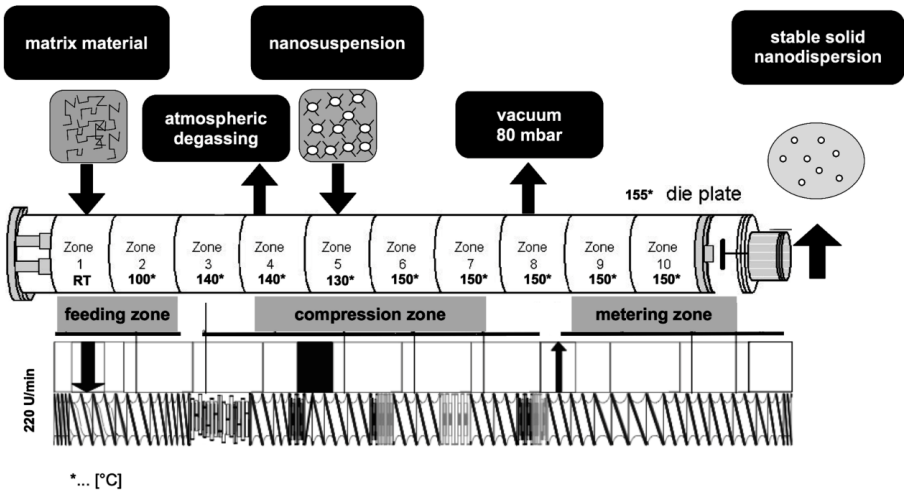

Fig.6. *Illustration of the extruder set-up, including the process temperatures of the barrel zones in degree Celsius and the screw configuration* [147].

In conclusion, the proof-of-concept study successfully demonstrated that nano-suspensions can be continuously transferred into stable solid products via the NANEX process. During this one-step process, nano-particle agglomeration is prevented and it can be expected that incorporated nano-crystals show improved dissolution velocities. Moreover, cost- and time-intensive process steps, such as freeze- and spray-drying, are circumvented [147], [148]. Additionally, the incorporation of crystalline drugs into polymeric carriers instead of metastable amorphous drugs improves shelf-life stability and product long-term quality (i.e., dissolution velocity).

On that account, during this thesis, the NANEX process was used for developing solid nano-formulations of a water-insoluble model drug in a single step. To this end, this work deals with

i) the design and characterization of a stable aqueous nano-suspension of a poorly soluble model API (i.e., phenytoin),

ii) the transformation of the nano-suspension into a stable solid product via the NANEX-process,
iii) the characterization of the obtained nano-extrudates and
iv) the optimization of the NANEX process (with respect to the process parameters and distinct polymer matrices).

First of all, bulk-phenytoin was physicochemically characterized and various non-ionic stabilizing agents were investigated with regard to their stabilizing efficacy (Chapter 2). Nano-suspensions were prepared via wet media milling and the most stable systems with the smallest particle sizes were studied regarding their in-vitro dissolution characteristics and permeability behavior.
In the next step, these nano-suspensions were transferred into a solid nano-formulation via the NANEX process using Soluplus® as matrix material (Chapter 3). The screw design was adapted to the physicochemical properties of Soluplus® (i.e., melting and glass transition temperature). The nano-suspensions were added to the matrix via liquid side feeding and the water (stemming from the nano-suspension) was removed via internal degassing. Obtained solid nano-formulations were physicochemically investigated to clarify whether the nano-crystalline API withstand the thermal as well as the mechanical forces during the NANEX process and remain de-agglomerated. After this, in-vitro drug release was studied.
Finally, this work encompasses a rational design and optimization of the NANEX process in order to reach high API loadings in the final nano-extrudates (Chapter 4). For this purpose, several polymers were investigated with regard to their maximum nano-suspension integration and water removal capacity considering such process parameters as throughput and screw speed.

1.5. References

[1] Newsletter, “Oral drug delivery,” *drugDel.com*, 2002.

[2] R. J. Mrsny, “Oral drug delivery research in Europe,” *J. Control. Release*, vol. 161, no. 2, pp. 247–253, 2012.

[3] E. N. Marieb and K. Hoehn, *Human Anatomy & Physiology*, 7th Editio. Pearson Benjamin Cummings, 2007.

[4] F. Gabor, C. Fillafer, L. Neutsch, G. Ratzinger, and M. Wirth, *Improving Oral Delivery*, vol. 197. 2010.

[5] H. Liu, P. Wang, X. Zhang, F. Shen, and C. G. Gogos, “Effects of extrusion process parameters on the dissolution behavior of indomethacin in Eudragit?? E PO solid dispersions,” *Int. J. Pharm.*, vol. 383, no. 1–2, pp. 161–169, 2010.

[6] G. L. Amidon, H. Lennernas, V. P. Shah, and J. R. Crison, “A theoretical basis for a biopharmaceutic drug classification: the correlation of in vitro drug product dissolution and in vivo bioavailability,” *Pharmaceutical Research*, vol. 12, no. 3. PLENUM PUBL CORP, pp. 413–420, 1995.

[7] H. Lennernäs and B. Abrahamsson, “The use of biopharmaceutic classification of drugs in drug discovery and development: current status and future extension.,” *J. Pharm. Pharmacol.*, vol. 57, no. 3, pp. 273–285, 2005.

[8] P. Langguth, G. Fricker, and H. Wunderli-Allenspach, *Biopharmazie*. Weinheim: Wiley, 2004.

[9] S. Sastry, J. Nyshadham, and J. Fix, “Recent technological advances in oral drug delivery - a review.,” *Pharm. Sci. Technolo. Today*, vol. 3, no. 4, pp. 138–145, Apr. 2000.

[10] S. K. Patil, K. S. Wagh, V. B. Parik, A. M. Akarte, and D. T. Baviskar, “Strategies for solubility enhancement of poorly soluble drugs,” *International Journal of Pharmaceutical Sciences Review and Research*, vol. 8, no. 2. pp. 74–80, 2011.

[11] J. E. Kipp, “The role of solid nanoparticle technology in the parenteral delivery of poorly water-soluble drugs.,” *Int J Pharm*, vol. 284, pp. 109–22, Oct. 2004.

[12] S. Shah, S. Maddineni, J. Lu, and M. A. Repka, “Melt extrusion with poorly soluble drugs.,” *Int J Pharm*, vol. 001, pp. 1–20, Nov. 2012.

[13] M. A. Repka, S. Majumdar, S. Kumar Battu, R. Srirangam, and S. B. Upadhye, “Applications of hot-melt extrusion for drug delivery.,” *Expert Opin. Drug Deliv.*, vol. 5, no. 12, pp. 1357–1376, 2008.

[14] H. Patil, R. V. Tiwari, and M. a. Repka, “Hot-Melt Extrusion: from Theory to Application in Pharmaceutical Formulation,” *AAPS PharmSciTech*, 2015.

[15] D. A. Miller, J. T. McConville, W. Yang, R. O. Williams, and J. W. McGinity, “Hot-melt extrusion for enhanced delivery of drug particles.,” *J. Pharm. Sci.*, vol. 96, no. 2, pp. 361–376, 2007.

[16] J. Breitenbach, “Melt extrusion: from process to drug delivery technology.,” *Eur. J. Pharm. Biopharm. Off. J. Arbeitsgemeinschaft fur Pharm. Verfahrenstechnik eV*, vol. 54, no. 2, pp. 107–117, 2002.

[17] M. A. Repka, S. K. Battu, S. B. Upadhye, S. Thumma, M. M. Crowley, F. Zhang, C. Martin, and J. W. McGinity, “Pharmaceutical applications of hot-melt extrusion: Part II.,” *Drug Dev. Ind. Pharm.*, vol. 33, no. 10, pp. 1043–1057, 2007.

[18] M. M. Crowley, F. Zhang, M. a. Repka, S. Thumma, S. B. Upadhye, S. Kumar Battu, J. W. McGinity, and C. Martin, “Pharmaceutical Applications of Hot-Melt Extrusion: Part I,” *Drug Dev. Ind. Pharm.*, vol. 33, no. 9, pp. 909–926, 2007.

[19] K. Kohlgrüber and W. Wiedmann, *Co-Rotating Twin-Screw Extruders - Fundamentals, Technology, and Applications*. Carl Hanser Verlag GmbH & CO. KG, 2008.

[20] D. Treffer, P. Wahl, D. Markl, G. Koscher, E. Roblegg, and J. G. Khinast, “Hot Melt Extrusion as a Continuous Pharmaceutical Manufacturing Process,” in *Melt Extrusion: Materials. Technoloy and Drug Product Design*, M. A. Repka, N. Langley, and J. C. Dinunzio, Eds. 2013, pp. 363–396.

[21] A. Rothen-Weinhold, N. Oudry, K. Schwach-Abdellaoui, S. Frutiger-Hughes, G. J. Hughes, D. Jeannerat, U. Burger, K. Besseghir, and R. Gurny, “Formation of peptide impurities in polyester matrices during implant manufacturing,” *Eur. J. Pharm. Biopharm.*, vol. 49, no. 3, pp. 253–257, 2000.

[22] Z. Ghalanbor, M. Körber, and R. Bodmeier, “Improved lysozyme stability and release properties of Poly(lactide-co- glycolide) implants prepared by hot-melt extrusion,” *Pharm. Res.*, vol. 27, no. 2, pp. 371–379, 2010.

[23] Z. Ghalanbor, M. Körber, and R. Bodmeier, “Protein release from poly(lactide-co-glycolide) implants prepared by hot-melt extrusion: Thioester formation as a reason for incomplete release,” *Int. J. Pharm.*, vol. 438, no. 1–2, pp. 302–306, 2012.

[24] D. Li, G. Guo, R. Fan, J. Liang, X. Deng, F. Luo, and Z. Qian, “PLA/F68/Dexamethasone implants prepared by hot-melt extrusion for controlled release of anti-inflammatory drug to implantable medical devices: I. Preparation, characterization and hydrolytic degradation study,” *Int. J. Pharm.*, vol. 441, no. 1–2, pp. 365–372, 2013.

[25] M. Stanković, J. Tomar, C. Hiemstra, R. Steendam, H. W. Frijlink, and W. L. J. Hinrichs, “Tailored protein release from biodegradable poly(ε-caprolactone-PEG)-b-poly(ε-caprolactone) multiblock-copolymer implants,” *Eur. J. Pharm. Biopharm.*, vol. 87, no. 2, pp. 329–337, 2014.

[26] M. A. Repka, T. G. Gerding, S. L. Repka, and J. W. McGinity, “Influence of plasticizers and drugs on the physical-mechanical properties of hydroxypropylcellulose films prepared by hot melt extrusion.,” *Drug Dev. Ind. Pharm.*, vol. 25, no. 5, pp. 625–633, 1999.

[27] M. A. Repka, K. Gutta, S. Prodduturi, M. Munjal, and S. P. Stodghill, “Characterization of cellulosic hot-melt extruded films containing lidocaine,” *Eur. J. Pharm. Biopharm.*, vol. 59, no. 1, pp. 189–196, 2005.

[28] P. K. Mididoddi and M. a. Repka, “Characterization of hot-melt extruded drug delivery systems for onychomycosis,” *Eur. J. Pharm. Biopharm.*, vol. 66, no. 1, pp. 95–105, 2007.

[29] A. Q. J. Low, J. Parmentier, Y. M. Khong, C. C. E. Chai, T. Y. Tun, J. E. Berania, X. Liu, R. Gokhale, and S. Y. Chan, “Effect of type and ratio of solubilising polymer on characteristics of hot-melt extruded orodispersible films,” *Int. J. Pharm.*, vol. 455, no. 1–2, pp. 138–147, 2013.

[30] C. R. Palem, S. Kumar Battu, S. Maddineni, R. Gannu, M. a. Repka, and M. R. Yamsani, “Oral transmucosal delivery of domperidone from immediate release films produced via hot-melt extrusion technology,” *Pharm. Dev. Technol.*, vol. 18, no. August 2011, pp. 1–10, 2012.

[31] M. Chen, J. Lu, W. Deng, A. Singh, N. N. Mohammed, M. a. Repka, and C. Wu, “Influence of Processing Parameters and Formulation Factors on the Bioadhesive, Temperature Stability and Drug Release Properties of Hot-Melt Extruded Films Containing Miconazole,” *AAPS PharmSciTech*, vol. 15, no. 3, pp. 522–529, 2014.

[32] D. A. Miller, J. C. DiNunzio, W. Yang, J. W. McGinity, and R. O. Williams, “Targeted intestinal delivery of supersaturated itraconazole for improved oral absorption,” *Pharm. Res.*, vol. 25, no. 6, pp. 1450–1459, 2008.

[33] C. M. Cassidy, M. M. Tunney, D. L. Caldwell, G. P. Andrews, and R. F. Donnelly, “Development of novel oral formulations prepared via hot melt extrusion for targeted delivery of photosensitizer to the colon,” *Photochem. Photobiol.*, vol. 87, no. 4, pp. 867–876, 2011.

[34] L. D. Bruce, N. H. Shah, a. Waseem Malick, M. H. Infeld, and J. W. McGinity, “Properties of hot-melt extruded tablet formulations for the colonic delivery of 5-aminosalicylic acid,” *Eur. J. Pharm. Biopharm.*, vol. 59, no. 1, pp. 85–97, 2005.

[35] A. Michalk, V. R. Kanikanti, H. J. Hamann, and P. Kleinebudde, “Controlled release of active as a consequence of the die diameter in solid lipid extrusion,” *J. Control. Release*, vol. 132, no. 1, pp. 35–41, 2008.

[36] N. Jedinger, J. Khinast, and E. Roblegg, “The design of controlled-release formulations resistant to alcohol-induced dose dumping - A review,” *Eur. J. Pharm. Biopharm.*, vol. 87, no. 2, pp. 217–226, 2014.

[37] N. Jedinger, S. Schrank, S. Mohr, a. Feichtinger, J. Khinast, and E. Roblegg, “Alcohol dose dumping: The influence of ethanol on hot-melt extruded pellets comprising solid lipids,” *Eur. J. Pharm. Biopharm.*, vol. 92, pp. 83–95, 2015.

[38] N. Jedinger, S. Schrank, J. M. Fischer, K. Breinhälter, J. Khinast, and E. Roblegg, “Development of an Abuse- and Alcohol-Resistant Formulation Based on Hot-Melt Extrusion and Film Coating,” *AAPS PharmSciTech*, no. 9, 2015.

[39] W. Roth, B. Setnik, M. Zietsch, a. Burst, J. Breitenbach, E. Sellers, and D. Brennan, “Ethanol effects on drug release from Verapamil Meltrex??, an innovative melt extruded formulation,” *Int. J. Pharm.*, vol. 368, no. 1–2, pp. 72–75, 2009.

[40] J. H. Bartholomaeus, E. Arkenau-Marić, and E. Galia, “Opioid extended-release tablets with improved tamper-resistant properties,” *Expert Opin. Drug Deliv.*, vol. 9, no. 8, pp. 879–891, 2012.

[41] A. Gryczke, S. Schminke, M. Maniruzzaman, J. Beck, and D. Douroumis, “Development and evaluation of orally disintegrating tablets (ODTs) containing Ibuprofen granules prepared by hot melt extrusion,” *Colloids Surfaces B Biointerfaces*, vol. 86, no. 2, pp. 275–284, 2011.

[42] R. Witzleb, V. R. Kanikanti, H. J. Hamann, and P. Kleinebudde, “Solid lipid extrusion with small die diameters - Electrostatic charging, taste masking and continuous production,” *Eur. J. Pharm. Biopharm.*, vol. 77, no. 1, pp. 170–177, 2011.

[43] J. Breitkreutz, F. El-Saleh, C. Kiera, P. Kleinebudde, and W. Wiedey, “Pediatric drug formulations of sodium benzoate: II. Coated granules with a lipophilic binder,” *Eur. J. Pharm. Biopharm.*, vol. 56, no. 2, pp. 255–260, 2003.

[44] J. Breitkreutz, M. Bornhöft, F. Wöll, and P. Kleinebudde, “Pediatric drug formulations of sodium benzoate: I. Coated granules with a hydrophilic binder,” *Eur. J. Pharm. Biopharm.*, vol. 56, no. 2, pp. 247–253, 2003.

[45] M. Maniruzzaman, J. S. Boateng, M. Bonnefille, A. Aranyos, J. C. Mitchell, and D. Douroumis, “Taste masking of paracetamol by hot-melt extrusion: An in vitro and in vivo evaluation,” *Eur. J. Pharm. Biopharm.*, vol. 80, no. 2, pp. 433–442, 2012.

[46] D. Douroumis, “Practical approaches of taste masking technologies in oral solid forms.,” *Expert Opin. Drug Deliv.*, vol. 4, no. 4, pp. 417–426, 2007.

[47] D. Douroumis, “Orally disintegrating dosage forms and taste-masking technologies; 2010.,” *Expert Opin. Drug Deliv.*, vol. 8, no. 5, pp. 665–675, 2011.

[48] J. T. Morott, M. Pimparade, J.-B. Park, C. P. Worley, S. Majumdar, Z. Lian, E. Pinto, Y. Bi, T. Durig, and M. a. Repka, “The Effects of Screw Configuration and Polymeric Carriers on Hot-Melt Extruded Taste-Masked Formulations Incorporated into Orally Disintegrating Tablets,” *J. Pharm. Sci.*, vol. 104, no. 1, pp. 124–134, 2015.

[49] S. Hülsmann, T. Backensfeld, S. Keitel, and R. Bodmeier, “Melt extrusion - An alternative method for enhancing the dissolution rate of 17β-estradiol hemihydrate,” *Eur. J. Pharm. Biopharm.*, vol. 49, no. 3, pp. 237–242, 2000.

[50] K. Nakamichi, T. Nakano, H. Yasuura, S. Izumi, and Y. Kawashima, “The role of the kneading paddle and the effects of screw revolution speed and water content on the preparation of solid dispersions using a twin-screw extruder.,” *Int J Pharm*, vol. 241, no. 2, pp. 203–11, Jul. 2002.

[51] H. He, R. Yang, and X. Tang, “In vitro and in vivo evaluation of fenofibrate solid dispersion prepared by hot-melt extrusion.,” *Drug Dev. Ind. Pharm.*, vol. 36, no. 6, pp. 681–687, 2010.

[52] S. K. Sathigari, V. K. Radhakrishnan, V. A. Davis, D. L. Parsons, and R. Jayachandra Babu, “Amorphous-State Characterization of Efavirenz - Polymer Hot-

Melt Extrusion Systems for Dissolution Enhancement," *Pharm. Technol.*, vol. 101, pp. 3456–3464, 2012.

[53] W. Wang, Q. Kang, N. Liu, Q. Zhang, Y. Zhang, H. Li, B. Zhao, Y. Chen, Y. Lan, Q. Ma, and Q. Wu, "Enhanced dissolution rate and oral bioavailability of Ginkgo biloba extract by preparing solid dispersion via hot-melt extrusion," *Fitoterapia*, vol. 102, pp. 189–197, 2015.

[54] S. M. Alshahrani, W. Lu, J.-B. Park, J. T. Morott, B. B. Alsulays, S. Majumdar, N. Langley, K. Kolter, A. Gryczke, and M. a. Repka, "Stability-enhanced Hot-melt Extruded Amorphous Solid Dispersions via Combinations of Soluplus® and HPMCAS-HF," *AAPS PharmSciTech*, no. 10, 2015.

[55] E. Mehuys, J. P. Remon, and C. Vervaet, "Production of enteric capsules by means of hot-melt extrusion," *Eur. J. Pharm. Sci.*, vol. 24, no. 2–3, pp. 207–212, 2005.

[56] E. Mehuys, C. Vervaet, and J. P. Remon, "Hot-melt extruded ethylcellulose cylinders containing a HPMC-Gelucire?? core for sustained drug delivery," *J. Control. Release*, vol. 94, no. 2–3, pp. 273–280, 2004.

[57] J. P. Möschwitzer, "Drug nanocrystals in the commercial pharmaceutical development process," *Int. J. Pharm.*, vol. 453, no. 1, pp. 142–156, 2013.

[58] P. Borm, F. C. Klaessig, T. D. Landry, B. Moudgil, J. Pauluhn, K. Thomas, R. Trottier, and S. Wood, "Research strategies for safety evaluation of nanomaterials, Part V: Role of dissolution in biological fate and effects of nanoscale particles," *Toxicol. Sci.*, vol. 90, no. 1, pp. 23–32, 2006.

[59] C. Galli, "Experimental determination of the diffusion boundary layer width of micron and submicron particles," *Int. J. Pharm.*, vol. 313, no. 1–2, pp. 114–122, 2006.

[60] F. Kesisoglou, S. Panmai, and Y. Wu, "Nanosizing-oral formulation development and biopharmaceutical evaluation.," *Adv. Drug Deliv. Rev. Drug Deliv Rev*, vol. 59, no. 7, pp. 631–44, Jul. 2007.

[61] A. A. Noyes and W. R. Whitney, "The rate of solution of solid substances in their own solutions," *J. Am. Chem. Soc.*, vol. 19, pp. 930–934, 1897.

[62] W. Nernst, "Theorie der Reaktionsgeschwindigkeit in heterogenen Systemen," *Zeitschrift für Phys. Chemie*, vol. 47, pp. 52–55, 1904.

[63] E. Brunner, "Theorie der Reaktionsgeschwindigkeit in heterogenen Systemen," *Zeitschrift für Phys. Chemie*, vol. 47, pp. 56–102, 1904.

[64] C. M. Keck and R. H. Müller, "Drug nanocrystals of poorly soluble drugs produced by high pressure homogenisation," *Eur. J. Pharm. Biopharm.*, vol. 62, no. 1, pp. 3–16, Jan. 2006.

[65] R. H. Müller and K. Peters, "Nanosuspensions for the formulation of poorly soluble drugs," *Int. J. Pharm.*, vol. 160, no. 2, pp. 229–237, 1998.

[66] R. Shegokar and R. H. Müller, "Nanocrystals: industrially feasible multifunctional formulation technology for poorly soluble actives.," *Int. J. Pharm.*, vol. 399, no. 1–2, pp. 129–39, 2010.

[67] A. Bhakay, M. Merwade, E. Bilgili, and R. N. Dave, “Novel aspects of wet milling for the production of microsuspensions and nanosuspensions of poorly water-soluble drugs.,” *Drug Dev. Ind. Pharm.*, vol. 37, no. 8, pp. 963–76, Aug. 2011.

[68] B. Van Eerdenbrugh, J. Vermant, J. A. Martens, L. Froyen, J. Van Humbeeck, P. Augustijns, and G. Van Den Mooter, “A screening study of surface stabilization during the production of drug nanocrystals,” *J. Pharm. Sci.*, vol. 98, no. 6, pp. 2091–2103, 2009.

[69] G. G. Liversidge and P. Conzentino, “Drug particle size reduction for decreasing gastric irritancy and enhancing absorption of naproxen in rats,” *Int. J. Pharm.*, vol. 125, no. 2, pp. 309–313, 1995.

[70] G. Liversidge and K. Cundy, “Surface modified drug nanoparticles,” *US Pat. 5145684*, 1992.

[71] G. G. Liversidge and K. C. Cundy, “Particle size reduction for improvement of oral bioavailability of hydrophobic drugs: I. Absolute oral bioavailability of nanocrystalline danazol in beagle dogs,” *Int. J. Pharm.*, vol. 125, no. 1, pp. 91–97, Oct. 1995.

[72] E. Merisko-Liversidge and G. G. Liversidge, “Nanosizing for oral and parenteral drug delivery: A perspective on formulating poorly-water soluble compounds using wet media milling technology,” *Adv. Drug Deliv. Rev.*, vol. 63, no. 6, pp. 427–440, 2011.

[73] M. J. Grau, O. Kayser, and R. H. Müller, “Nanosuspensions of poorly soluble drugs--reproducibility of small scale production.,” *Int. J. Pharm.*, vol. 196, no. 2, pp. 155–9, Mar. 2000.

[74] K. P. Krause and R. H. Müller, “Production and characterisation of highly concentrated nanosuspensions by high pressure homogenisation,” *Int. J. Pharm.*, vol. 214, no. 1–2, pp. 21–24, 2001.

[75] R. H. Müller and A. Akkar, “Drug nanocrystals of poorly soluble drugs,” *Encycl. Nanosci Nanotechnol.*, vol. 2, pp. 627–638, 2004.

[76] R. Müller and C. Jacobs, “Buparvaquone mucoadhesive nanosuspension: preparation, optimisation and long-term stability.,” *Int J Pharm*, vol. 237, no. 1–2, pp. 151–61, Apr. 2002.

[77] C. Jacobs and R. H. Müller, “Production and characterizatoin of a budesonide nanosuspension for pulmonary administration,” *Pharm. Res.*, vol. 19, no. 2, pp. 2–7, 2002.

[78] R. Müller, R. Becker, B. Kruss, and K. Peters, “Pharmaceutical nanosuspensions for medicament administration as systems with increased saturation solubility and rate of solution,” *US Pat. 5,858,410*, 1999.

[79] R. H. Müller et al., “Nanosuspensions: formulations for poorly soluble drugs with poor bioavailability,” *Pharm Ind*, vol. 61, no. 2, pp. 175–178.

[80] R. H. Müller, M. Radtke, and S. a Wissing, “Nanostructured lipid matrices for improved microencapsulation of drugs.,” *Int. J. Pharm.*, vol. 242, no. 1–2, pp. 121–8, Aug. 2002.

[81] F. Gonzáles-Caballero and de D. G. López-Durán, “Suspension formulation,” in *Nielloud, F., Marti-Mestres, G. (Eds.), Pharmaceutical Emulsions and Suspensions, Drugs and Pharmaceutical Sciences, vol.105. Marcel Dekker, Inc., New York*, 2000.

[82] B. Van Eerdenbrugh, G. Van den Mooter, and P. Augustijns, “Top-down production of drug nanocrystals: nanosuspension stabilization, miniaturization and transformation into solid products.,” *Int. J. Pharm.*, vol. 364, no. 1, pp. 64–75, Nov. 2008.

[83] B. E. Rabinow, “Nanosuspensions in drug delivery.,” *Nat. Rev. Drug Discov.*, vol. 3, no. 9, pp. 785–96, Sep. 2004.

[84] L. Gao, D. Zhang, and M. Chen, “Drug nanocrystals for the formulation of poorly soluble drugs and its application as a potential drug delivery system,” *J. Nanoparticle Res.*, vol. 10, no. 5, pp. 845–862, Mar. 2008.

[85] R. H. Müller, C. Jacobs, and O. Kayser, “Nanosuspensions as particulate drug formulations in therapy. Rationale for development and what we can expect for the future.,” *Adv. Drug Deliv. Rev.*, vol. 47, no. 1, pp. 3–19, Mar. 2001.

[86] E. Merisko-Liversidge, G. G. Liversidge, and E. R. Cooper, “Nanosizing: a formulation approach for poorly-water-soluble compounds.,” *Eur. J. Pharm. Sci.*, vol. 18, no. 2, pp. 113–20, Feb. 2003.

[87] B. V. Derjaguin and L. Landau, “Theory of the stability of strongly charged lyophobic sols and of the adhesion of strongly charged particles in solutions of electrolytes,” *Acta Physico-ChimicaSinica*, vol. 14, pp. 633–662, 1941.

[88] J. Israelachvili, “Intermolecular and Surface Forces, 2nd ed.,” *Academic Press, London*, 1992.

[89] C. J. van Oss, R. F. Giese, and P. M. Costanzo, “DLVA and non-DLVO interactions in hectorite,” *Clays Clay Min.*, vol. 38, pp. 151–159, 1990.

[90] J. D. G. Durán, M. C. Guindo, A. V. Delgado, and F. Gonzáles-Caballero, “Stability of monodisperse zinc sulfide colloidal dispersions,” *Langmuir*, vol. 11, pp. 3648–3655, 1995.

[91] E. J. W. Verwey and J. T. G. Overbeek, *Theory of the Stability of Lyophobic Colloids*. 1948.

[92] G. Cao and Y. Wang, “Nanostructures and Nanomaterials: Synthesis, Properties, and Applications,” in *World Scientific Series in Nanoscience and Nanotechnology*, Vol. 2., 2011, p. Chapter 2, 19 ff.

[93] B. Van Eerdenbrugh, L. Froyen, J. Van Humbeeck, J. a Martens, P. Augustijns, and G. Van den Mooter, “Drying of crystalline drug nanosuspensions-the importance of surface hydrophobicity on dissolution behavior upon redispersion.,” *Eur. J. Pharm. Sci.*, vol. 35, no. 1–2, pp. 127–35, 2008.

[94] L. Wu, J. Zhang, and W. Watanabe, “Physical and chemical stability of drug nanoparticles,” *Adv. Drug Deliv. Rev.*, vol. 63, no. 6, pp. 456–469, 2011.

[95] M. V. Chaubal and C. Popescu, “Conversion of nanosuspensions into dry powders by spray drying: A case study,” *Pharm. Res.*, vol. 25, no. 10, pp. 2302–2308, 2008.

[96] J. Lee, “Drug nano- and microparticles processed into solid dosage forms: Physical properties,” *J. Pharm. Sci.*, vol. 92, no. 10, pp. 2057–2068, 2003.

[97] Y. Gao, S. Qian, and J. Zhang, “Physicochemical and pharmacokinetic characterization of a spray-dried cefpoxodine proxetil nanosuspension,” *Chem. Pharm. Bull.*, vol. 414, no. 1–2, pp. 186–192, 2011.

[98] J. I. Jinno, N. Kamada, M. Miyake, K. Yamada, T. Mukai, M. Odomi, H. Toguchi, G. G. Liversidge, K. Higaki, and T. Kimura, “In vitro-in vivo correlation for wet-milled tablet of poorly water-soluble cilostazol,” *J. Control. Release*, vol. 130, no. 1, pp. 29–37, 2008.

[99] N. O. Chung, M. K. Lee, and J. Lee, “Mechanism of freeze-drying drug nanosuspensions,” *Int. J. Pharm.*, vol. 437, no. 1–2, pp. 42–50, 2012.

[100] M. Nakarani, A. K. Misra, J. K. Patel, and S. S. Vaghani, “Itraconazole Nanosuspension for Oral delivery: formulation, characterization and in vitro comparison with marketed formulation,” vol. 2, no. 1, pp. 162–171, 2010.

[101] P. Wang, Q. Luo, Y. Miao, L. Ying, H. He, C. Cai, and X. Tang, “Improved dissolution rate and bioavailability of fenofibrate pellets prepared by wet-milled-drug layering,” *Drug Dev. Ind. Pharm.*, vol. 38, no. 11, pp. 1344–1353, 2012.

[102] P. Kayaert, M. Anné, and G. Van Den Mooter, “Bead layering as a process to stabilize nanosuspensions: Influence of drug hydrophobicity on nanocrystal reagglomeration following in-vitro release from sugar beads,” *J. Pharm. Pharmacol.*, vol. 63, no. 11, pp. 1446–1453, 2011.

[103] J. Möschwitzer and R. H. Müller, “Spray coated pellets as carrier system for mucoadhesive drug nanocrystals.,” *Eur. J. Pharm. Biopharm.*, vol. 62, no. 3, pp. 282–7, Apr. 2006.

[104] J. Pardeike, D. M. Strohmeier, N. Schrödl, C. Voura, M. Gruber, J. G. Khinast, and A. Zimmer, “Nanosuspensions as advanced printing ink for accurate dosing of poorly soluble drugs in personalized medicines.,” *Int. J. Pharm.*, vol. 420, no. 1, pp. 93–100, 2011.

[105] M. Preis, J. Breitkreutz, and N. Sandler, “Perspective: Concepts of printing technologies for oral film formulations,” *Int. J. Pharm.*, vol. 494, no. 2, pp. 578–584, 2015.

[106] N. Genina, D. Fors, M. Palo, J. Peltonen, and N. Sandler, “Behavior of printable formulations of loperamide and caffeine on different substrates - Effect of print density in inkjet printing,” *Int. J. Pharm.*, vol. 453, no. 2, pp. 488–497, 2013.

[107] D. Raijada, N. Genina, D. Fors, E. Wisaeus, J. Peltonen, J. Rantanen, and N. Sandler, “A Step Toward Development of Printable Dosage Forms for Poorly Soluble Drugs,” *J. Pharm. Sci.*, vol. 102, pp. 3694–3704, 2013.

[108] N. Genina, E. M. Janßen, A. Breitenbach, J. Breitkreutz, and N. Sandler, “Evaluation of different substrates for inkjet printing of rasagiline mesylate,” *Eur. J. Pharm. Biopharm.*, vol. 85, pp. 1075–1083, 2013.

[109] N. Sandler, A. Määttänen, P. Ihalainen, L. Kronberg, A. Meierjohann, T. Viitala, and J. Peltonen, “Inkjet Printing of Drug Substances and Use of Porous Substrates-Towards Individualized Dosing,” *J. Pharm. Sci.*, vol. 100, no. 8, pp. 3386–3395, 2011.

[110] N. Genina, D. Fors, H. Vakili, P. Ihalainen, L. Pohjala, H. Ehlers, I. Kassamakov, E. Haeggström, P. Vuorela, J. Peltonen, and N. Sandler, “Tailoring controlled-release oral dosage forms by combining inkjet and flexographic printing techniques,” *Eur. J. Pharm. Sci.*, vol. 47, no. 3, pp. 615–623, 2012.

[111] M. Palo, R. Kolakovic, T. Laaksonen, A. Määttänen, N. Genina, J. Salonen, J. Peltonen, and N. Sandler, “Fabrication of drug-loaded edible carrier substrates from nanosuspensions by flexographic printing,” *Int. J. Pharm.*, pp. 1–8, 2015.

[112] C. Planchette, H. Pichler, M. Wimmer-teubenbacher, M. Gruber, and J. Khinast, “Printing medicines as orodispersible dosage forms : Effect of substrate on the printed micro-structure,” *Int. J. Pharm.*, p. in press, 2015.

[113] B. Shen, C. Shen, X. Yuan, J. Bai, Q. Lv, H. Xu, L. Dai, C. Yu, J. Han, and H. Yuan, “Development and characterization of an orodispersible film containing drug nanoparticles.,” *Eur. J. Pharm. Biopharm.*, vol. 85, no. 3 Pt B, pp. 1348–56, Nov. 2013.

[114] L. Sievens-Figueroa, A. Bhakay, J. I. Jerez-Rozo, N. Pandya, R. J. Romañach, B. Michniak-Kohn, Z. Iqbal, E. Bilgili, and R. N. Davé, “Preparation and characterization of hydroxypropyl methyl cellulose films containing stable BCS Class II drug nanoparticles for pharmaceutical applications,” *Int. J. Pharm.*, vol. 423, no. 2, pp. 496–508, 2012.

[115] E. R. Cooper, “Nanoparticles: A personal experience for formulating poorly water soluble drugs,” *J. Control. Release*, vol. 141, no. 3, pp. 300–302, 2010.

[116] K. Sigfridsson, S. Forssén, P. Holländer, U. Skantze, and J. de Verdier, “A formulation comparison, using a solution and different nanosuspensions of a poorly soluble compound,” *Eur. J. Pharm. Biopharm.*, vol. 67, no. 2, pp. 540–547, 2007.

[117] G. C. Liversidge, C. P. Phillips, and K. C. Cundy, “Method to reduce particle size growth during lyophilization,” 5,302,401, 1994.

[118] B. Van Eerdenbrugh, S. Vercruysse, J. A. Martens, J. Vermant, L. Froyen, J. Van Humbeeck, G. Van Den Mooter, and P. Augustijns, “Microcrystalline cellulose, a useful alternative for sucrose as a matrix former during freeze-drying of drug nanosuspensions - A case study with itraconazole,” *Eur. J. Pharm. Biopharm.*, vol. 70, no. 2, pp. 590–596, 2008.

[119] B. Van Eerdenbrugh, L. Froyen, J. a Martens, N. Blaton, P. Augustijns, M. Brewster, and G. Van den Mooter, “Characterization of physico-chemical properties and pharmaceutical performance of sucrose co-freeze-dried solid nanoparticulate powders of the anti-HIV agent loviride prepared by media milling.,” *Int. J. Pharm.*, vol. 338, no. 1–2, pp. 198–206, Jun. 2007.

[120] A. Ain-Ai and P. K. Gupta, “Effect of arginine hydrochloride and hydroxypropyl cellulose as stabilizers on the physical stability of high drug loading nanosuspensions of a poorly soluble compound,” *Int. J. Pharm.*, vol. 351, no. 1–2, pp. 282–288, 2008.

[121] J. I. Jinno, N. Kamada, M. Miyake, K. Yamada, T. Mukai, M. Odomi, H. Toguchi, G. G. Liversidge, K. Higaki, and T. Kimura, “Effect of particle size reduction on dissolution and oral absorption of a poorly water-soluble drug, cilostazol, in beagle dogs,” *J. Control. Release*, vol. 111, no. 1–2, pp. 56–64, 2006.

[122] T. Niwa, S. Miura, and K. Danjo, “Design of dry nanosuspension with highly spontaneous dispersible characteristics to develop solubilized formulation for poorly water-soluble drugs,” *Pharm. Res.*, vol. 28, no. 9, pp. 2339–2349, 2011.

[123] C. E. Figueroa and S. Bose, “Spray granulation: Importance of process parameters on in vitro and in vivo behavior of dried nanosuspensions,” *Eur. J. Pharm. Biopharm.*, vol. 85, no. 3 PART B, pp. 1046–1055, 2013.

[124] G. J. Vergote, C. Vervaet, I. Van Driessche, S. Hoste, S. De Smedt, J. Demeester, R. a. Jain, S. Ruddy, and J. P. Remon, “An oral controlled release matrix pellet formulation containing nanocrystalline ketoprofen,” *Int. J. Pharm.*, vol. 219, no. 1–2, pp. 81–87, 2001.

[125] G. J. Vergote, C. Vervaet, I. Van Driessche, S. Hoste, S. De Smedt, J. Demeester, R. a. Jain, S. Ruddy, and J. P. Remon, “In vivo evaluation of matrix pellets containing nanocrystalline ketoprofen,” *Int. J. Pharm.*, vol. 240, no. 1–2, pp. 79–84, 2002.

[126] G. G. Liversidge, W. M. Eickhoff, S. B. Ruddy, K. R. Mueller, M. E. Roberts, and D. A. Engers, “Formulations of nanoparticle naproxen tablets,” WO 98/35666, 1998.

[127] V. Nekkanti, R. Pillai, V. Venkateshwarlu, and T. Harisudhan, “Development and characterization of solid oral dosage form incorporating candesartan nanoparticles.,” *Pharm. Dev. Technol.*, vol. 14, no. 3, pp. 290–298, 2009.

[128] S. Basa, T. Muniyappan, P. Karatgi, R. Prabhu, and R. Pillai, “Production and in vitro characterization of solid dosage form incorporating drug nanoparticles.,” *Drug Dev. Ind. Pharm.*, vol. 34, no. 11, pp. 1209–1218, 2008.

[129] P. Kayaert and G. Van den Mooter, “Is the amorphous fraction of a dried nanosuspension caused by milling or by drying? A case study with Naproxen and Cinnarizine.,” *Eur. J. Pharm. Biopharm.*, vol. 81, no. 3, pp. 650–6, 2012.

[130] R. Susarla, L. Sievens-Figueroa, A. Bhakay, Y. Shen, J. I. Jerez-Rozo, W. Engen, B. Khusid, E. Bilgili, R. J. Romañach, K. R. Morris, B. Michniak-Kohn, and R. N. Davé, “Fast drying of biocompatible polymer films loaded with poorly water-soluble drug nano-particles via low temperature forced convection,” *Int. J. Pharm.*, vol. 455, no. 1–2, pp. 93–103, 2013.

[131] R. Susarla, A. Afolabi, D. Patel, E. Bilgili, and R. N. Davé, “Novel use of superdisintegrants as viscosity enhancing agents in biocompatible polymer films containing griseofulvin nanoparticles,” *Powder Technol.*, 2015.

[132] S. M. Krull, R. Susarla, A. Afolabi, M. Li, Y. Ying, Z. Iqbal, E. Bilgili, and R. N. Davé, “Polymer strip films as a robust, surfactant-free platform for delivery of BCS Class II drug nanoparticles,” *Int. J. Pharm.*, vol. 489, no. 1–2, pp. 45–57, 2015.

[133] P. Raheja, A. Kaushik, R. Gandhi, R. B. Singh, and R. S. Mathur, “Sirolismus having specific particle size and pharmaceutical compositions thereof,” US 2009/0068266 A1, 2009.

[134] “Aprepitant FDA Advisory Committee Background Package,” pp. 1–165, 2003.

[135] D. Zhang, T. Tan, L. Gao, W. Zhao, and P. Wang, “Preparation of azithromycin nanosuspensions by high pressure homogenization and its physicochemical characteristics studies.,” *Drug Dev. Ind. Pharm.*, vol. 33, no. 5, pp. 569–75, May 2007.

[136] K. Peters, S. Leitzke, J. E. Diederichs, K. Borner, H. Hahn, and S. Ehlers, “Preparation of a clofazimine nanosuspension for intravenous use and evaluation of its therapeutic efficacy in murine,” pp. 77–83, 2000.

[137] L. Gao, D. Zhang, M. Chen, C. Duan, W. Dai, L. Jia, and W. Zhao, “Studies on pharmacokinetics and tissue distribution of oridonin nanosuspensions.,” *Int. J. Pharm.*, vol. 355, no. 1–2, pp. 321–7, May 2008.

[138] L. Gao, D. Zhang, M. Chen, T. Zheng, and S. Wang, “Preparation and characterization of an oridonin nanosuspension for solubility and dissolution velocity enhancement.,” *Drug Dev. Ind. Pharm.*, vol. 33, no. 12, pp. 1332–9, Dec. 2007.

[139] R. H. Müller, J. Möschwitzer, and F. N. Bushrab, “Manufacturing of nanoparticles by milling and homogenization techniques,” in *Nanoparticle Technology for Drug Delivery, Drugs and Pharmaceutical Sciencies*, vol.159 ed., R. B. Gupta and U. B. Kompella, Eds. New York: Taylor & Francis Group, LLC, 2006, pp. 21–51.

[140] J. Hecq, M. Deleers, D. Fanara, H. Vranckx, and K. Amighi, “Preparation and characterization of nanocrystals for solubility and dissolution rate enhancement of nifedipine.,” *Int. J. Pharm.*, vol. 299, no. 1–2, pp. 167–77, Aug. 2005.

[141] Q. Ma, H. Sun, E. Che, X. Zheng, T. Jiang, C. Sun, and S. Wang, “Uniform nano-sized valsartan for dissolution and bioavailability enhancement: Influence of particle size and crystalline state,” *Int. J. Pharm.*, vol. 441, no. 1–2, pp. 75–81, 2013.

[142] A. Dolenc, J. Kristl, S. Baumgartner, and O. Planinšek, “Advantages of celecoxib nanosuspension formulation and transformation into tablets,” *Int. J. Pharm.*, vol. 376, no. 1–2, pp. 204–212, 2009.

[143] R. Mauludin, R. H. Müller, and C. M. Keck, “Kinetic solubility and dissolution velocity of rutin nanocrystals,” *Eur. J. Pharm. Sci.*, vol. 36, no. 4–5, pp. 502–510, 2009.

[144] C. Shen, B. Shen, H. Xu, J. Bai, L. Dai, Q. Lv, J. Han, and H. Yuan, “Formulation and optimization of a novel oral fast dissolving film containing drug nanoparticles by Box-Behnken design-response surface methodology.,” *Drug Dev. Ind. Pharm.*, vol. 40, no. 5, pp. 649–56, 2014.

[145] F. Lai, I. Franceschini, F. Corrias, M. C. Sala, F. Cilurzo, C. Sinico, and E. Pini, “Maltodextrin fast dissolving films for quercetin nanocrystal delivery. A feasibility study,” *Carbohydr. Polym.*, vol. 121, pp. 217–223, 2015.

[146] V. Weissig, T. Pettinger, and N. Murdock, “Nanopharmaceuticals (part 1): products on the market,” *Int. J. Nanomedicine*, p. 4357, 2014.

[147] J. G. Khinast, R. Baumgartner, and E. Roblegg, “Nano-extrusion: a one-step process for manufacturing of solid nanoparticle formulations directly from the liquid phase.,” *AAPS Pharm. Sci. Technol.*, vol. 14, no. 2, pp. 601–4, Jun. 2013.

[148] R. Baumgartner, G. Koscher, T. Klein, E. Roblegg, and J. Khinast, “System for producing a solid preparation from a suspension - GB 2503710,” 2012.

2. Rational design and characterization of a nanosuspension for intraoral administration considering physiological conditions

Ramona Baumgartner [a], Birgit J. Teubl [b], Carolin Tetyczka [b], Eva Roblegg [a,b,*]

[a] *Research Center Pharmaceutical Engineering GmbH, Inffeldgasse 13, 8010 Graz, Austria*

[b] *Institute of Pharmaceutical Sciences, Department of Pharmaceutical Technology, Karl-Franzens University Graz, Universitätsplatz 1, 8010 Graz, Austria*

* Corresponding author at: Institute of Pharmaceutical Sciences, Department of Pharmaceutical Technology, Karl-Franzens University Graz, Universitätsplatz 1, 8010 Graz, Austria. Tel.: +43 316 380 8888.

Published in: Journal of Pharmaceutical Sciences
DOI: 10.1016/j.xphs.2015.10.021

Abstract

The oral cavity displays an attractive route in drug administration that is not associated with gastric transit and hepatic first-pass metabolism. However, limiting factors for an efficient transit of drugs through the oral mucosa are poor water solubility and permeability. Hence, various strategies exist to enhance solubility. Specifically, nanotechnology has attracted much research interest in the past decade. This study aimed at developing a stable nanosuspension of the model compound phenytoin via wet media milling. The nanosuspensions were carefully characterized regarding hydrodynamic particle sizes, crystallinity, and dissolution characteristics under nonphysiological or physiological (salivary) conditions. The permeability of bulk phenytoin and nanophenytoin through a buccal *in vitro a*nd *ex vivo* model was investigated, and the apparent permeability coefficients were determined. Moreover, cytotoxicity studies were conducted. The addition of Tween® 80 as stabilizer resulted in a stable crystalline nanosuspension (330 nm). The solubility characteristics significantly increased under salivary conditions, which further impacted the permeability, as the steady state appearance rate of nanosized phenytoin was 1.4-fold higher. Cytotoxicity studies demonstrated that bulk-/nano-phenytoin exhibited no harmful effects. It can be concluded that the salivary environment (i.e., ionic strength, pH) strongly impacts the solubility and consequently the permeability of crystalline nanosuspensions across the buccal mucosa.

Keywords

Physicochemical properties; solubility; dissolution rate; milling; nanoparticles; stability; *in vitro* models; permeability; transmucosal drug delivery; toxicology

1. Introduction

Oral administration of drugs with intestinal absorption is the traditionally preferred route of drug delivery. However, it faces serious obstacles including pH changes, enzymatic degradation of the active pharmaceutical ingredient (API), and hepatic first-pass metabolism, making this route a considerable challenge for molecules.[1, 2, 3] Hence, alternative sites for drug administration, which avoid these obstacles, are increasingly sought.

The oral cavity displays an attractive route for drug administration that is not associated with this phenomenon. However, it is equipped with distinct protective barriers, such as saliva, which acts as lubricant but also is likely to impact the solubility and permeability behavior of certain drug candidates. The lining mucosa (i.e., buccal, sublingual) represents the largest surface area in the oral cavity and comprises a nonkeratinized stratified squamous epithelium, which consists of 40-50 cell layers with a thickness of approximately 500-600 µm.[4] It is formed from 4 different morphological layers, namely the basal layer, the prickle cell layer, the intermediate layer, and the superficial layer. Once cells leave the basal layer, they enter differentiation and become large and flat. Moreover, the prickle cells contain membrane-coating granules. These cytosolic granules fuse with the cell membrane and extrude lipids into the intercellular spaces. Thereby, they constitute a strong barrier and limit the penetration of drugs specifically in the top third region of the epithelium.[3, 5] Apart from anatomic and physiological barriers, permeation of substances is also impacted by the drug's physicochemical properties (i.e., solubility, ionization, lipophilicity, molecular weight).[3, 4] The majority of drugs are transported passively through the buccal mucosa,[3] either via the paracellular (i.e., in between epithelial cells) or via the transcellular route (i.e., through epithelial cells).[6, 7, 8, 9] The former pathway is predominantly available for hydrophilic molecules having small molecular sizes.

The latter one is the preferred route for lipophilic drugs, which interact with the lipophilic cell membrane.[2, 10, 11]

However, because of the increasing number of drugs that show poor solubility and/or permeability, diffusion through oral mucosae is often hindered. Hence, different strategies have been used to enhance drug transport through buccal tissues. These strategies include permeation enhancers and vehicles and cosolvents.[2, 10, 11] Permeation enhancers, such as bile salts, surfactants, and fatty acids, are applied to change the mucus rheology, increase the fluidity of the lipid bilayer membrane, solubilize the intercellular lipids (to facilitate paracellular transport), or increase the flux of the drug by increasing the thermodynamic activity.[2, 12, 13, 14, 15] However, the exact mechanism is often not well understood, and knowledge of possible adverse effects of penetration enhancers on biological tissues is lacking.[16]

Another alternative for overcoming insufficient transport across buccal tissue is to enhance the solubility of poorly soluble drugs. Particle size reduction to the nanoscale is a promising strategy and can be achieved either by top-down approaches (i.e., breakage of large particles into nanocrystals) or by bottom-up approaches (e.g., nanoparticles are built up from molecules via precipitation).[17, 18, 19, 20, 21, 22, 23] The former one results in nanosuspensions, which are carrier-free-submicron colloidal dispersions of drug particles in an aqueous medium, stabilized by polymers and/or surfactants. These stabilizing agents are used to prevent agglomeration, caused by the higher surface energy of the nanomaterial.[21, 24, 25, 26, 27, 28 , 29] Moreover, sedimentation and/or crystal growth might occur[30 , 31]; thus, for applicability in the oral cavity, nanosuspensions need to be further processed into solid orodispersible formulations, including oral lyophilisates, orodispersible tablets, orodispersible granules, and orodispersible films.[32] This facilitates easier handling, shipping, and storage of the delivery form and improves efficacy, safety, and stability.[26, 33 , 34] Most commonly, freeze drying, spray drying, and vacuum drying are conducted to result in a nanopowder, which can be further incorporated into tablets, granules, and films.[35, 36 , 37] More importantly, nanosuspensions can be transferred into the desired dosage directly from the liquid phase using casting methods,[38, 39 , 40] printing technologies,[41 , 42] or the recently developed continuous nanoextrusion process.[43 , 44]

Although it is known that nanoformulations can improve drug delivery, the understanding of how they interact with the anatomic and physiological barriers in the oral cavity is lacking. In this study, we aimed at investigating whether the salivary environment, such as ionic strength and pH, impacts the solubility behavior of a nanosuspension and as a further consequence the permeability of the drug across the buccal mucosa. To this end, phenytoin (5,5-diphenylhydantoin), which is an antiepileptic and antiarrhythmic drug45showing poor solubility (11.5 ± 0.5 µg/mL[44]) and a slow rate of absorption after oral intestinal administration,[12, 46, 47] was used as model drug. A stable aqueous nanosuspension of the model compound was prepared via 1-step wet media milling. Various stabilizers were tested, and the nanosuspensions were carefully characterized regarding hydrodynamic particle sizes, crystallinity, and dissolution characteristics. The most stable and promising nanosuspension was identified, and the particle behavior in terms of solubility was recorded under salivary conditions (i.e., mimicking the pH and the ionic strength). Moreover, permeability studies were conducted. For this, human buccal TR 146 cells were used and cultured on Transwells to evaluate the transport mechanism involved. Additionally, permeability studies of the bulk suspensions and nanosuspensions were conducted using a standardized porcine *ex vivo* model. [48,49, 50] Because it is known that by reducing the particle size from the microscale to the nanoscale, the specific nano-

material changes its properties, which might result in adverse effects, [34, 49, 51, 52, 53, 54, 55, 56, 57, 58 , 59] cytotoxicity studies were conducted as safety feature.

2. Materials and Methods

2.1. Materials

Phenytoin (5,5-diphenylhydantoin) from Sigma–Aldrich (Munich, Germany) was used as model API. The stabilizers Tween 20 (P20), Tween 80 (P80), and methanol (CHROMASOLV®, for high-performance liquid chromatography [HPLC], ≥99.9%) were purchased from Simga–Aldrich. Kolliphor EL (KEL), Kolliphor RH40 (KRH40), Kolliphor P188 (KP188), and Kolliphor P407 (KP407) were donated by the manufacturer BASF (BASF SE, Ludwigshafen, Germany). Ultrapurified water (i.e., Milli-Q-water [MQ-water], Millipore S.A.S., Molsheim, France) was used for all experiments. For cell culture tests, Dulbecco's Modified Eagle's medium (DMEM; Gibco, Life Technologies Corporation, Paisley, UK), DMEM with 10% of fetal bovine serum (FBS; Sigma–Aldrich), and Hank's buffered salt solution (HBSS; Gibco, Life Technologies Corporation) were used. For *ex vivo* studies, PBS (Gibco, Life Technologies Corporation) and Krebs Buffer (Krebs–Ringer Bicarbonate Buffer with 1.8 mg/L glucose, without $CaCl_2$ and $NaHCO_3$; Sigma–Aldrich) were applied.

2.2. Methods

2.2.1. Nanosuspension Preparation

Contact Angle

Contact angle measurements were conducted using the sessile drop method (Easy Drop; Krüss, Hamburg, Germany) to obtain preliminary indications of the most appropriate stabilizer for wetting the newly generated drug surface. For this, phenytoin powder compacts (500 mg) were prepared. A drop of 10 µL of water and stabilizer solutions (5% [w/w] stabilizer diluted with MQ-water) was dispensed onto the sample surface, and images were captured by camera (Stingray F046B; Allied Vision Technologies). The contact angle was calculated by the instrument (DSA1 “drop shape analysis,” Krüss) by fitting a mathematical expression to the shape of the drop and then calculating the slope of the tangent to the drop at the liquid-solid-vapor interface line. The experiments were carried out in triplicate, and average values and standard deviations were calculated. All measurements were performed in air under ambient conditions.

Surface Tension of the Stabilizer Solutions

For determining the surface tension of the various stabilizer solutions, the Easy Drop System (Krüss) was used. The surface tension was calculated using the L-Y method considering the densities of stabilizer solutions. The solution densities were determined via sound velocity measurements using a DSA 5000M (Anton Paar GmbH, Graz, Austria) at 20°C.

Wet Media Milling

Phenytoin nanocrystals were prepared by wet media milling using various stabilizers (i.e., P80, P20, KEL, KRH 40, KP188, KP407) as described previously by Baumgartner et al..[44] After diluting 10 g of the stabilizer with 200 mL MQ-water, 40 g phenytoin was dispersed in this aqueous stabilizer solution. Yttrium-stabilized zirconium beads (600 g, 0.5 mm in diameter) were used as a milling agent. Milling was performed with a planetary ball mill (Retsch PM 100; Retsch GmbH, Haan, Germany) equipped with a zirconium oxide grinding bowl (500 mL) at 250 rpm for 24 h. The experiments were carried out at ambient temperature. After milling, the grinding beads were separated from the nanocrystals by sieving.

2.2.2. Nanosuspension Characterization

Particle Size and Zeta Potential Analyses

The prepared nanosuspensions were investigated by photon correlation spectroscopy (PCS) using a Zetasizer Nano ZS (Malvern Instruments, Malvern, UK) equipped with a 532-nm laser. PCS yields the mean diameter as a light intensity weighted size of the bulk population (z-average) and the polydispersity index (PdI) as a measure for the width of the particle size distribution.[60] To prevent nanoparticle dissolution during measurements, nanosuspensions were diluted in a saturated phenytoin–water solution.[61, 62] The measurements were performed at 25°C at a measurement angle of 173° (backscattering).

The zeta potential was determined via laser-Doppler-Micro-Electrophorese (scattering angle of 173°) coupled with PCS (Zetasizer Nano ZS; Malvern Instruments) and calculated according to the Helmholtz–Smoluchovski equation. For measurements, nanosuspensions were dispersed in zeta water (i.e., distilled water adjusted with 0.9% [w/v] sodium chloride solution to a conductivity of 50 µS/cm and a pH of 5.5-6.0) at 25°C to obtain information on the surface charge.

Samples were stored in a refrigerator (i.e., 5 ± 3°C) and investigated on a weekly basis for 4 weeks to assess the physical stability of the nanocrystal suspensions. All measurements

were carried out in triplicate, and the average values and the standard deviations were calculated.

Structure Analysis Using Small- and Wide-Angle X-Ray Scattering (SWAXS)

SWAXS (HECUS S3-MICRO; Bruker AXS, Karlsruhe, Germany) was used to study the crystal structure and morphology of pure and nanocrystalline phenytoin. The SWAXS (SAXS and WAXS) system was equipped with a high-flux laboratory SWAXS camera S3-Micro (Bruker AXS), a high-brilliance microbeam delivery system with point-focus optics (FOX3D; Xenocs, Grenoble, France) and with a 1D or 2D detection system. Samples were filled into glass capillaries (2 mm in diameter) that were sealed with wax and placed into the SpinCap. For X-ray, a wavelength of 1.54 Å was used, and the SAXS and WAXS curves (scattering intensities as a function of the scattering angle 2 Θ) were recorded by 2 independent 1D detectors (PSD-50; Hecus X-ray Systems, Graz, Austria) in the angular ranges of $0.06° < 2\,\Theta < 8°$ and $18° < 2\,\Theta < 27°$. Duration of exposure was 600 s.

Thermal Analysis

The thermal properties of untreated and nanocrystalline phenytoin were analyzed using a differential scanning calorimeter (DSC; 204F1 Phoenix; Netzsch GmbH, Selb, Germany). Samples were placed into an aluminum crucible, which was sealed, pierced, and purged with pure nitrogen, and an empty aluminum crucible served as reference. The heating rate was 10 K/min from 20°C to 350°C, and pure nitrogen at a flow rate of 20 mL/min was used for purging the DSC cell. The DSC data were analyzed with Proteus Thermal Analysis software (Netzsch GmbH, Selb, Germany). Each experiment was carried out in triplicate, and average values and their standard deviations were calculated.

Saturation Solubility and Dissolution Studies

Saturation solubility of bulk and nanocrystalline phenytoin was determined in an aqueous P80 solution (5% [w/w]). An excess of each sample was added to 50 mL of dissolution media and agitated at 250 rpm for 3 days at 25°C. Subsequently, an aliquot was withdrawn and filtered through 0.02-µm filters (Anotop 25 Plus; Whatman, Maidstine, UK) and analyzed via HPLC. Each experiment was performed in triplicate, and the average values and the standard deviations were calculated.

In vitro dissolution studies were performed according to the official monograph of phenytoin described in the United States Pharmacopeia (USP) using USP dissolution Apparatus II (100 rpm) under sink conditions. For this, 27 mg of bulk phenytoin and an aliquot of the

nanosuspension corresponding to a phenytoin dose of 27 mg were transferred into 900 mL of 0.05-M Tris buffer (i.e., 36.3 g of tris[hydroxymethyl] aminomethane and 60 g of sodium lauryl sulfate in 6 L of water, adjusted with hydrochloric acid to a pH of 7.5 ± 0.05). The dissolution media was maintained at 37 ± 0.5°C, and samples (1 mL) were withdrawn after 5, 10, 20, 30, 40, 50, and 60 min without media replacement. Prior to HPLC analyses, samples were filtered through 0.02-µm filters (Anotop 25 Plus; Whatman). Each experiment was performed in triplicate, and the average values and the standard deviations were calculated.

2.2.3. Permeability and Cytotoxicity Studies

Particle Size Analysis and Saturation Solubility of Nanosuspensions in Relevant Media

To study the cytotoxicity and permeability of (nano)phenytoin under physiological conditions, dispersions with a final phenytoin concentration of 1600, 800, and 160 µg/mL were prepared in DMEM, HBSS, and PBS. Since the ionic strength of the dispersion media is likely to influence the physical stability of the nanosuspension, particle sizes were determined.

Prior to particle size analysis via PCS (Zetasizer Nano ZS; Malvern Instruments), samples were ultrasonicated for 20 min. The measurements were conducted at 25°C at a measurement angle of 173° (backscattering). All measurements were carried out in triplicate, and the average values and the standard deviations were calculated.

Moreover, saturation solubility of bulk and nanophenytoin in HBSS and PBS was determined. Again, an excess of bulk and nanomaterial was added to 50 mL media and agitated for 3 days at 250 rpm at 37°C. Subsequently, 1 mL was withdrawn and filtered through 0.02-µm filters (Anotop 25 Plus; Whatman) and analyzed via HPLC. Each experiment was performed in triplicate, and the average values and the standard deviations were calculated.

In Vitro Cell Culture Model

Human buccal epithelial TR 146 cells (Imperial Cancer Research Technology, London, UK), grown in DMEM with supplements of 10% FBS, 200-µM l-glutamine, 100 IU/mL penicillin, and 100 µg/mL streptomycin were used for investigating permeability and cytotoxicity of (nano)phenytoin.[49, 63, 64] The culture conditions with a temperature of 37°C and a

humidity of 98% (5% CO_2/95% air) were kept constant, and subcultivation (0.25% trypsin-EDTA) was performed at about 70% confluence.

For cell viability and cytotoxicity studies, TR 146 cells were seeded in 96-well plates and cultured for 24 h. The medium was replaced after 24 h by bulk phenytoin and nanophenytoin, respectively, dispersed in DMEM with concentrations of 1600, 800, and 160 µg/mL and incubated for 4 h.

To determine cell viability, CellTiter 96 Aqueous Non-Radioactive Cell Proliferation Assay (Promega; Formazan Bioreduction Assay) was performed by adding 20 µL of an MTS/PMS solution to each well, and the absorbance was measured at 490 nm (VIS-plate reader, FLUOstar Optima, BMG, Labortechnik) after 4-h incubation time. Out of the experiments (n = 6), average values and their standard deviations were calculated.

Possible effects on membrane integrity were evaluated by determining the lactate dehydrogenase (LDH) release using a CytoTox-ONE Homogenous Membrane Integrity Assay (Promega). For this, 25 µL of the CytoTox-ONE reagent were added to 25 µL of the supernatant and incubated for 10 min (room temperature). To stop the reaction, 12.5 µL of the stop solution were applied. Subsequently, fluorescence was measured (FLUOstar Optima, BMG, Labortechnik) at 560 nm excitation wavelength and 590 nm emission wavelength. The LDH release was normalized to cells treated with 2 µL of lysis solution. Average values and their standard deviations were calculated (n = 6).

For *in vitro* permeability tests, cells were cultured on 1.131 cm^2 permeable Corning Costar 12-well inserts equipped with polycarbonate filters (pore size of 3.0 µm; Szabo Scandic, Vienna, Austria). Cells were seeded with a density of 2.4 × 104 cells/cm^2 and incubated for 30 days. The transepithelial electrical resistance (TEER) was measured with an Endohm culture cup connected to an EVOM voltohmmeter (World Precision Instruments) during the time of cultivating to control the confluency.[50]

Permeability tests were carried out at 37°C by adding 0.5 mL of phenytoin and nanophenytoin, respectively, dispersed in HBSS with concentrations of 1600, 800, and 160 µg/mL to the apical compartment and 1.5-mL HBSS buffer to the basolateral compartment. After 10, 30, and 45 min and 1, 2, 3, and 4 h, an aliquot of 200 µL was withdrawn (and replaced with fresh HBSS) from the basolateral side, and the amount of the transported phenytoin was evaluated via HPLC. Average values and their standard deviations were calculated (n = 6).

The apparent permeability coefficient (P_{app}, cm/s) was calculated using Equation 1, where dQ/dt is the slope of the cumulative drug transported versus time curve (µg/s), A(cm^2) is the surface area of the well inserts (i.e., 1.131 cm^2), and c_0 is the initial drug concentration in the donor compartment (µg/mL). Slope values were evaluated from the linear portion of the cumulative amount of drug permeated (µg) versus time (s) profile in each case.

Equation(1)

$$P_{app} = \frac{dQ}{dt} \times \frac{1}{A} \times \frac{1}{c_0}$$

To study potential cellular uptake of the nanocrystals, *in vitro* permeability studies were combined with a visualization tool (i.e., confocal laser scanning microscopy [CLSM]). On that account, TR 146 cells were cultivated on chamber slides (BD Biosciences, Schwechat, Austria), and phenytoin nanocrystals were labeled with Alizarin Red S (Sigma-Aldrich, Munich, Germany). For this purpose, Alizarin red S was dissolved in HBSS to a final concentration of 0.9 mM followed by the addition of the phenytoin nanocrystals. The obtained dispersion was ultrasonificated, centrifuged, and washed with fresh HBSS to remove the unbound dye. The labeled nanocrystals were diluted with HBSS to a final phenytoin concentration of 1600 µg/mL.[65, 66] For cell culture studies, the monolayers were rinsed once with PBS. After equilibration, cells were incubated with the labeled nanocrystal dispersions at 37°C for 4 h. Integrity (i.e., TEER) was measured before and after the experiment. After the incubation period, the particle dispersion was removed and nonadhered nanocrystals were washed off with PBS (n = 3). Before cutting and mounting on glass slides, imaging inserts were also washed thrice with PBS for CLSM investigations. At the same time, cytoskeleton of the TR 146 cells was stained with Alexa Fluor 488 Phalloidin (Life Technologies Corporation), and nuclei were counterstained with Hoechst 33342 (Life Technologies Corporation). Slides were investigated with CLSM (Zeiss LSM 510 META) equipped with LSM510 software package. Alexa Fluor 488 Phalloidin–dyed cytoskeleton was detected at 488 nm excitation wavelength using a BP 505/550 nm bandpass detection for the green channel. Hoechst 33342–stained cell nuclei were visualized at an excitation wavelength of 405 nm in conjunction with BP 420/480. Red-labeled nanocrystals were visualized at 543 nm excitation wavelength using a LP 560 nm bandpass detection for the red spectral region. Images of randomly chosen areas of the cell monolayers were captured via CLSM. To record 3-dimensional data set, images were taken with z stack.

Ex Vivo Porcine Buccal Model

Permeability studies of bulk and nanocrystalline phenytoin through excised fresh porcine buccal mucosa were performed using static Franz diffusion cells (PermeGear, Hellertown) according to Roblegg et al.[48, 50, 67] Porcine tissues, which were obtained from freshly sacrificed pigs (age, <6 months; Karnerta Slaughter House, Graz, Austria), were transported to the laboratory in 4°C Krebs Buffer. After the careful removal of the underlying tissue, via-

bility and integrity of the buccal mucosa were evaluated.[49, 50] The excised buccal mucosa was mounted between the donor compartment (charged with 1-mL PBS buffer, 37°C) and the receptor compartment (charged with 8.0-mL PBS buffer, 37°C). After equilibrating the buccal mucosa to 37°C with PBS buffer for 30 min, the buffer of the donor compartment was replaced by phenytoin and nanophenytoin, respectively, dispersed in PBS buffer (i.e., 1600, 800, and 160 µg/mL, 37°C). After 10, 30, and 45 min and 1, 2, 3, and 4 h incubation time, an aliquot of 200 µL was withdrawn (and replaced by fresh PBS) from the donor compartment. The amount of permeated phenytoin was quantitatively analyzed via HPLC. The apparent permeability coefficient (Papp; cm/s) was calculated using Equation 2. Average values and their standard deviations were calculated (n = 6).

Quantitative Assays via HPLC

Quantitative determination of phenytoin was performed on a Merck-Hitachi LaChrom HPLC system equipped with a pump L-7100, an autosampler L-7200, a column oven L-7300, a UV-VIS detector L-7420, and a Merck-Hitachi interface L-7000 (Hitachi High Technologies Corporation, Tokyo, Japan) using a C18 column (300 Extend-C18, 4.6 × 100 mm, 3.5 µm, 300 Å, Agilent Technologies Austria GmbH, Vienna, Austria) with a matching precolumn according to van Eerdenbrugh et al..[62] The mobile phase (a mixture of 50% MQ-water and 50% methanol [v/v%]) was introduced at a flow rate of 1 mL/min. The injection volume per sample was 20 µL. The UV spectrum was recorded at a wavelength of 225 nm. Quantification of the compounds was carried out by measuring the peak areas in relation to those of the standards (i.e., 0.5-100 µg/mL) chromatographed under the same conditions with an evaluated limit of detection of 0.1 µg/mL and a limit of quantification of 0.5 µg/mL.

3. Results and Discussion

3.1. Preparation and Characterization of Phenytoin Nanosuspensions

Particle size reduction causes a significant increase in the specific surface area and the interfacial tension.[24] Thus, nanoparticles tend to agglomerate, resulting in instable suspensions. To counter this phenomenon, surface-active agents (approved for oral application) can be added to act as physical barriers.[19, 26] The mechanisms of stabilizer adsorption on the drug surface (i.e., hindering of ionic interactions, hydrogen bonding, van der Waals forces, non-dipole interactions, or hydrophobic effects) are dependent on the given drug properties.[68]

Phenytoin is a highly crystalline compound with strong intermolecular hydrogen bonding and poor water solubility (i.e., 11.5 ± 0.5 µg/mL).[44] The calculated log *p* value is 2.95 ± 0.05, [44] and the contact angle in water is 79.5 ± 2.7°, indicating a lipophilic nature. Particle size characterization of the bulk material was performed with laser diffraction and yielded a d (0.1) of 7.9 µm, a d (0.5) of 14.4 µm, and a d (0.9) of 25.3 µm. To prevent agglomeration of the drug particles P20, P80, KEL, KRH40, KP188, and KP407 (5% [w/w]) were used as nonionic stabilizers. [62, 69, 70] The affinity of a stabilizer to the particle surface can be evaluated by measuring the wettability via contact angle measurements. In general, a small contact angle (i.e., <90°) between the API surface and the stabilizer is a good predictor for the stabilizing efficacy. [71, 72] All tested stabilizers yielded smaller contact angles compared to water (Table 1). Highest wettability was obtained for P20, whereas KP407 showed comparatively larger contact angles. Moreover, surface tensions of stabilizer solutions were evaluated because a low surface tension associated with a high surface activity was found to be advantageous when stabilizing nanosuspensions (Table 1).[62] The tested surfactants showed lower surface tensions than water (i.e., 72.8 ± 0.2 mN/m). Lowest values were found for P20 and highest for K188, which is in agreement with the results of contact angle measurements.

Table 1.: *Contact Angles and Surface Tension of Aqueous Stabilizer Solutions (5%, w/w)*

Stabilizer	Contact Angle ± SD (°)	Surface Tension ± SD (mN/m)
P20	23.6 ± 4.0	36.61 ± 0.04
P80	34.2 ± 1.7	40.81 ± 0.15
KEL	30.2 ± 2.2	40.01 ± 0.03
KRH40	33.1 ± 2.8	43.03 ± 0.06
KP188	33.3 ± 2.2	45.89 ± 0.09
KP407	36.0 ± 6.9	36.80 ± 0.05

For the production of the phenytoin nanosuspensions, wet media milling was applied as previously described.[44] During this top-down approach, impaction of the milling medium (containing milling beads and stabilizer solution) with the drug generates high energy and shear forces, providing the necessary energy input for breaking microparticulate drug particles into nanocrystals. For this, process conditions including size and number of the installed milling beads, milling speed, time, and temperature are key parameters that need to be adapted for a successful particle size reduction.[20, 21, 28] Apart from process condi-

tions, drug loading is of paramount importance. Commonly used drug loadings range from 2% to 30% (w/w).[19] In our study, preliminary investigations showed that a maximum drug loading of 16% (w/w) yielded smallest particle sizes associated with suitable milling times. Because a large number of small milling beads is more likely to create the compulsory number of contact points and hence, high kinetic energy, 600 g of milling beads (i.e., 50% of the volume of the presuspension) with a size of 0.5 mm were added to 210 g of the stabilizer solution. To prevent physical modifications of phenytoin during milling due to additional thermal stresses, all experiments were carried out at ambient temperatures by applying a milling speed of 250 rpm. Because phenytoin is a highly crystalline compound with strong intermolecular hydrogen bonding, it was necessary to grind the suspension for 24 h to achieve a sufficient particle size reduction.[44]

For characterization of phenytoin nanosuspensions, we recorded the mean hydrodynamic particle sizes, zeta potentials, and PdI values to quantify the size distribution (Table 2). PdI values ≤0.5 show reliability of the measurements, whereas high PdIs indicate invalid results (i.e., broad size distribution of indefinite shape).[60]

Table 2.: *Mean Z-Average, PdI, and Zeta Potential of Phenytoin Nanosuspensions With the Addition of Various Stabilizers on the Day of the Production and 28 Days Later*

	Z-Average ± SD (d.nm)	**PdI ± SD**	**Zeta Potential ± SD (mV)**
Stabilizer	**Day 0/Day 28**	**Day 0/Day 28**	**Day 0/Day 28**
P20	6347 ± 2037/N.D.	0.62 ± 0.33/N.D.	N.D.
P80	335 ± 6/429 ± 5	0.31 ± 0.01/0.41 ± 0.01	−18.3 ± 0.4/−26.4 ± 0.3
KEL	377 ± 4/N.D.	0.31 ± 0.03/N.D.	−12.5 ± 0.6/N.D.
KRH40	1333 ± 122/1375 ± 52	0.43 ± 0.01/0.39 ± 0.01	−14.7 ± 0.4/−11.6 ± 0.4
KP188	1224 ± 18/N.D.	0.39 ± 0.01/N.D.	−8.6 ± 0.3/N.D.
KP407	538 ± 22/N.D.	0.36 ± 0.06/N.D.	−10.7 ± 0.1/N.D.

N.D., non-determinable due to agglomeration and/or phase separation.

The addition of P20 resulted in suspensions showing large particle sizes (i.e., 6347 ± 2037 nm) and highest PdI values (i.e., 0.62 ± 0.33) with high standard deviations and nondeterminable zeta potentials. This was due to the fact that during the wet media milling process, significant foaming occurred; thus, the impact forces between the grinding balls and the API crystals were decreased resulting in an insufficient size reduction. In contrast, P80-stabilized suspensions yielded smallest particle sizes (i.e., 335 ± 6 nm) with a suffi-

cient PdI (i.e., 0.31 ± 0.01) and high zeta potential values (i.e., −18.3 ± 0.4 mV). The zeta potential was evaluated to allow a prediction of the stability of the nanocrystals. However, the zeta potential only gives information about the electrostatic stabilization. P80 and all other tested stabilizers are nonionic stabilizers, which theoretically hinder interparticle interactions by steric stabilization. They adsorb to the surface of the nanocrystals and thus protect the diffuse layer against removal during the movement in the electrical field and shift the shear plane further away from the particle surface.[72,73] It was shown by Jacobs et al.[74] that for nonionic stabilizers, values of approximately ±20 mV are sufficient for obtaining physically stable systems, which is in agreement with our studies.

The addition of KEL resulted in nanosuspensions with slightly higher mean hydrodynamic particle sizes (i.e, 377 ± 4 nm; PdI, 0.31 ± 0.03). The zeta potential was −12.5 ± 0.6 mV, indicating a reduced steric stabilization and/or a diminished diffuse layer leading to a closer interparticle contact and thus, a higher agglomeration tendency.[73] Similar results were found for KRH40-, KP188-, and KP407-stabilized nanosuspensions. Because the principle quality criterion for further processing steps is a stable system, nanosuspensions were stored in a refrigerator at 5 ± 3°C for at least 4 weeks, and sedimentation and particle growth were evaluated. The results showed that sufficiently stable nanosuspensions were only obtained with the stabilizer P80. Measured particle sizes remained nearly constant, and the zeta potential values slightly increased but were still in the appropriate range (i.e., 26.4 ± 0.3 mV). Thus, stabilized P80 nanosuspensions exhibited the required features and were used for further investigations.

Nanoization of drug crystals is always coupled with high mechanical forces and thermal stress (due to increased process temperature), which might affect the crystalline structure of an API (e.g., amorphization). Although amorphous compounds might exhibit improved dissolution characteristics, they always suffer from thermodynamic instabilities. Hence, SWAXS and DSC measurements of nanophenytoin were carried out, and results were compared to the bulk material.

Bulk phenytoin displayed crystallinity Bragg peaks in the angular WAXS region at 4.88, 4.60, 4.42, 4.37, 3.98, 3.91, 3.47, 3.43, and 3.34 Å. Because the nanosuspension showed the same positions of the Bragg peaks, it can be concluded that no changes in crystallinity or amorphization of the drug occurred during the nanosizing process (Fig. 1).

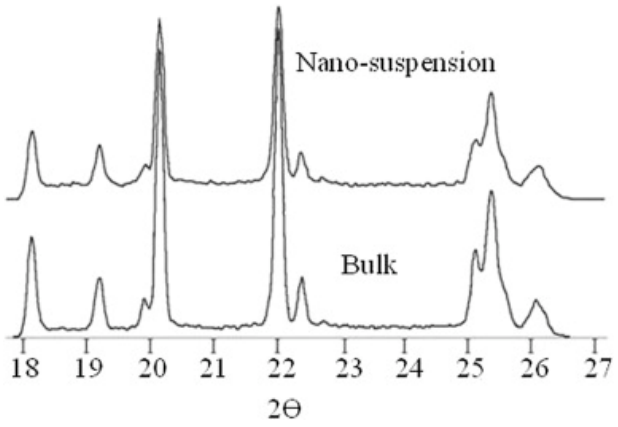

Figure 1. *: WAXS spectra of bulk phenytoin and air-dried nanosuspension.*

To verify these results, the thermal characteristics of the bulk material and the nanosuspension were explored using DSC (Fig. 2) because shifting of the melting endotherm or the appearance of additional thermal events would indicate changes in the crystal structure.

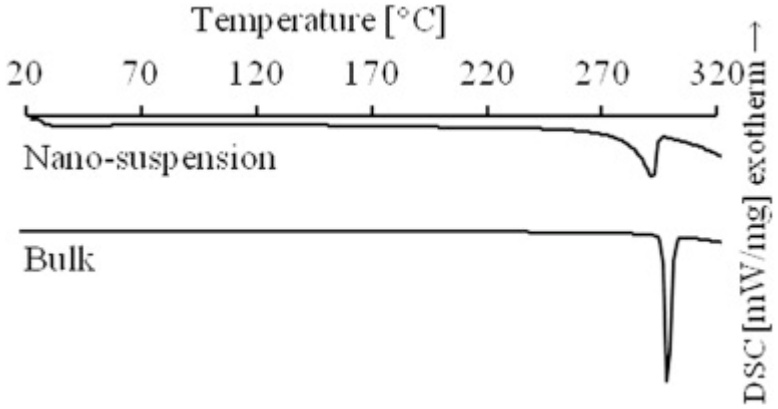

Figure 2. *: DSC thermograms of bulk phenytoin and air-dried nanosuspension.*

Untreated phenytoin exhibited a sharp melting endotherm at 298.6 ± 0.4°C (onset at 296.3 ± 0.1°C), indicating the crystalline nature of the drug. After melting and further heating up, degradation of phenytoin occurred (degradation peak in the thermogram). The DSC curve of nanophenytoin showed a melting point at 291.7 ± 0.4°C (onset at 283.2 ± 0.9°C), which was slightly lower than that of bulk phenytoin. However, the marginal shifting of the melting endotherm of the nanosuspension is presumably caused by the P80 coating, which was verified in our previous investigations via energy-filtered transmission electron microscopy.[44] After melting, a similar degradation peak was seen in the thermogram.

Furthermore, the saturation solubilities of bulk and nanophenytoin were determined. Given the fact that the surfactant P80 was applied to the nanosuspension as stabilizing agent (also likely affecting the solubility), an aqueous P80 solution (i.e., 5%, w/w) was used for the bulk material to assure comparable conditions.[72]

Nanocrystals exhibited a 1.4-fold higher solubility (i.e., 77.7 ± 3.2 µg/mL) compared to the bulk material (i.e., 53.9 ± 0.5 µg/mL). Because of the increased ratio between the surface area and the volume, which specifically accounts for particles below 2 µm, surface interaction between solute and solvent is enhanced, resulting in a higher saturation solubility.[75, 76, 77] However, this higher saturation solubility is actually a "kinetic" solubility, which is higher than the "thermodynamic" equilibrium solubility of the untreated bulk material and stems from the increased dissolution pressure of smaller particles with augmented curvature (Kelvin and Ostwald–Freundlich equation).[29, 78]

To determine the time-dependent dissolution, *in vitro* studies were conducted as recommended by the USP (official monograph of phenytoin). The dissolution profiles of both samples were recorded over a period of 60 min (Fig. 3) taking into account sink conditions (i.e., saturation solubility of bulk phenytoin in 0.05-M Tris buffer [100.6 ± 0.9 µg/mL]). Again, the effect of the stabilizer P80 on the dissolution kinetics of nanophenytoin was compensated by the addition of 1% (w/v) sodium lauryl sulfate.

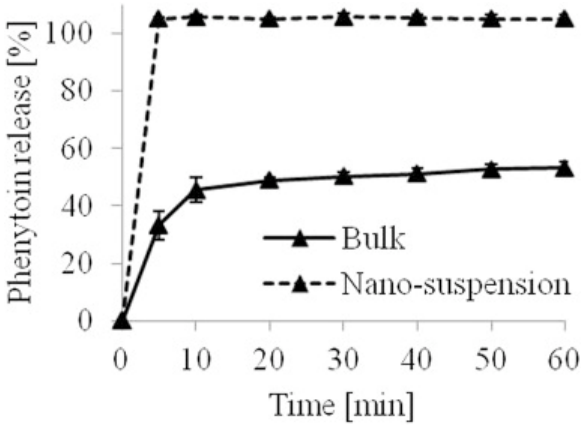

Figure 3. *: Dissolution profiles of bulk phenytoin and nanophenytoin in 0.05-M Tris buffer (pH 7.5; 1 h). Mean values ± SD (n = 3).*

The dissolution profile of the bulk material demonstrated that 45.6 ± 4.3% of the applied dose was released after 10 min, which was only slightly enhanced to 53.3 ± 2.2% after 60 min. In contrast, for nanocrystalline phenytoin, the entire drug was dissolved within 5 min.

These results corroborate that the (kinetic) solubility and the dissolution rate of phenytoin can be significantly improved by reducing the particle size to the nanometer range because of the increase in the specific surface area.

3.2. Permeability and Cytotoxicity Studies

To evaluate whether the improved dissolution characteristics of nanophenytoin change under more physiological conditions and enhance permeation across buccal tissues without causing adverse side effects, bulk phenytoin and the phenytoin nanosuspension were tested using 2 well-established buccal models.[48, 49, 50, 67 , 79] *In vitro* permeability and cytotoxicity studies were conducted with TR 146 cells, which originate from a squamous human cell carcinoma of the buccal mucosa. [80 , 81] *Ex vivo* permeability studies were performed with static Franz Diffusion cells, using excised porcine buccal mucosa, which highly recapitulates the anatomy and the physiology of the human buccal mucosa. [3, 9 , 82] It was shown in prior investigations [48, 49 , 50] that the viability and integrity of excised porcine tissue can only be maintained for 4 h. This is of paramount importance because the permeation barriers, which finally determine whether a drug can penetrate or permeate across the biological barrier, are only active in the viable state. Thus, to be able to compare the *ex vivo* investigations with the *in vitro* data, the cell monolayers and the porcine tissues were incubated for 4 h with the respective particle dispersions. Dependent on the investigations performed, distinct physiological media were used to mimic salivary conditions (i.e., pH and ionic strength) without affecting the viability and membrane integrity of the excised tissues and cells during the experiments. For *ex vivo* and *in vitro* studies, bulk and nanophenytoin were dispersed in PBS (pH 7.4; ionic strength of 162.7 mM) and HBSS (pH 7.4; ionic strength of 167.3 mM), respectively. Cytotoxicity studies were performed with DMEM. [48, 50, 67 , 79]

Generally, the steady state flux of a drug across a barrier is proportional to its applied concentration, as stated by the Fick's law of diffusion (Eq. 2). More precisely, the mass of a solute transported per unit time (d*m*/d*t*) through an area *A* is controlled by the concentration gradient d*C*/d*x* with *D* as the solute diffusion coefficient. [83]

Equation(2)

$$\frac{1}{A} \times \frac{dm}{dt} = -D\frac{dC}{dx}$$

The problem encountered referred to low-soluble drugs is that the concentration is often too low to maintain a sufficient driving force necessary for an efficient drug transport. Hence, in our study, the solution in the donor compartment was kept saturated.[83 , 84] On

that account, the saturation solubility of bulk and nanophenytoin in HBSS and PBS was determined after 72 h. In HBSS, a saturated concentration of 39.7 ± 2.6 µg/mL was obtained for bulk phenytoin, whereas nanophenytoin yielded a 2.9-fold higher maximum concentration (113.3 ± 13.7 µg/mL). In PBS, bulk phenytoin showed a maximum solubility of 17.0 ± 1.3 µg/mL and nanophenytoin exhibited a saturation concentration of 103.6 ± 2.0 µg/mL. Comparing these results with the solubility data obtained in the aqueous P80 solution, it is obvious that the ionic strength and the pH of the dispersion media significantly decreased the maximum solubility of bulk phenytoin (because of increased particle agglomeration) while increasing the maximum solubility of nanophenytoin 1.3- to 1.5-fold (because of minor agglomeration).

Based on the obtained data, bulk and nanophenytoin were dispersed in HBSS, PBS, and DMEM to a final phenytoin concentration of 1600, 800, and 160 µg/mL, to ensure driving forces.

Moreover, the mean hydrodynamic diameter (z-average, d.nm) and the PdI values of the various nanosuspension dilutions were once more determined via PCS.

The mean PdI values of nanocrystals were >0.5 in all tested media, indicating a broad particle size distribution. In the Q0-recorded spectra (Figs. 4 a,c,e), nanoparticles dispersed in DMEM exhibited one peak at 200 nm (90%-99%) and a second one at 800-1000 nm (1%-10%). In PBS and HBSS, dispersion of nanocrystals yielded a monomodal distribution with a peak at 100 nm. However, the Q3-recorded spectra (Figs. 4 b,d,f) displayed one large peak at 240-260 nm (DMEM) and 140 nm (HBSS and PBS), respectively, a second peak at >1000 nm and a third peak in the micrometer range. P80-stabilized phenytoin nanocrystals dispersed in zeta water yielded zeta potential values of −18.3 ± 0.4 to −26.4 ± 0.3 (1600-160 µg/mL) indicating a negative surface charge of the phenytoin nanocrystals. Because all tested physiological media exhibited high concentrations of monovalent (Na^+ and K^+) and divalent cations (Mg^{2+} and Ca^{2+}; more pronounced in HBSS and DMEM), the electric double layer surrounding the surface of the charged nanocrystals was diminished. Thus, the electrostatic repulsive forces were weaker than the attractive van der Waals forces, resulting in agglomeration of the nanocrystals.[22, 60, 73] However, a significant amount of smaller particles was still present in the nanorange.

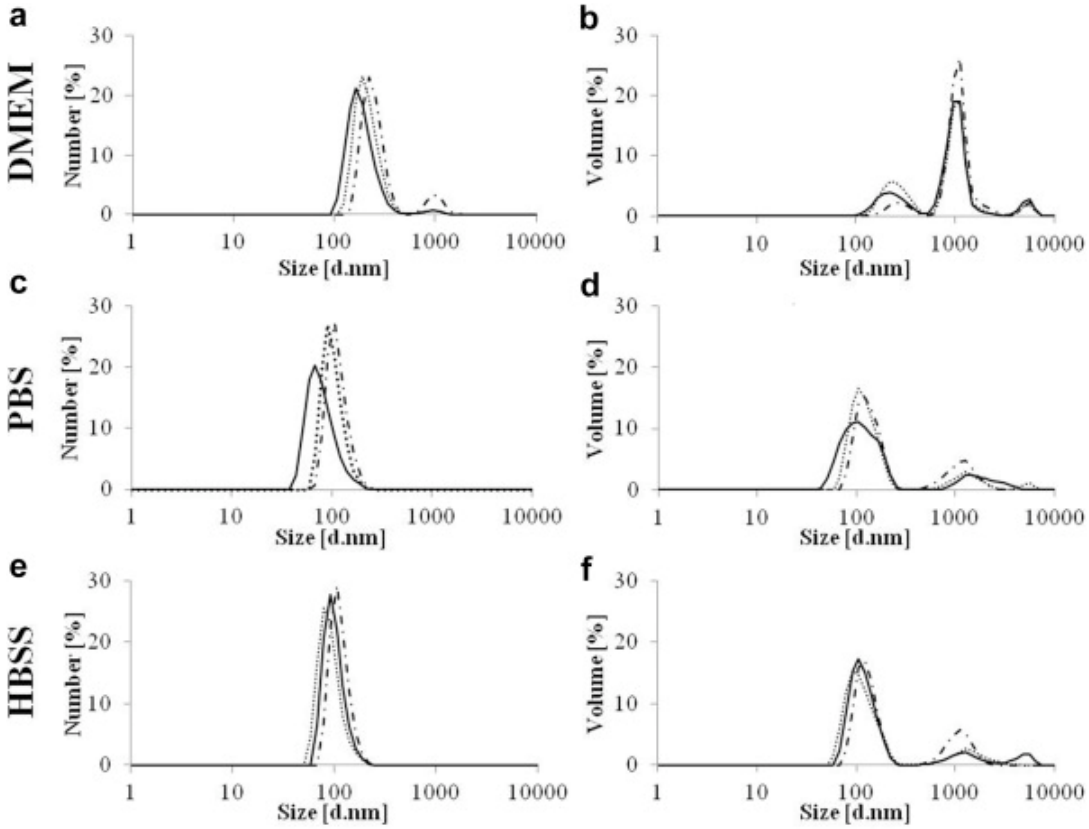

Figure 4. ***:*** *Particle size distribution Q0 (a, c, and e) and Q3 (b, d, and f) of phenytoin nanocrystals dispersed in DMEM, PBS, and HBSS. The solid line indicates the dispersion with a final phenytoin concentration of 1600 µg/mL, the dotted line shows the PSD of 800 µg/mL phenytoin, and the dashed line presents 160 µg/mL phenytoin in the corresponding medium.*

3.3. Permeability Studies

For *in vitro* and *ex vivo* permeability studies, the apparent permeability coefficients per unit membrane surface area (P_{app} [cm/s]) of bulk and nanophenytoin and the steady state appearance rate of (nano)phenytoin to the basolateral side (d*Q*/d*t* [µg/s]) were calculated (Table 3).

Table 3.: *Apparent Permeability Coefficients (Papp, ×10−6 cm/s) and dQ/dt (×10−3 µg/s) From Cell Culture Model (TR 146 cell line) and Porcine Buccal Mucosa (Franz diffusion cells) of Bulk and Nanocrystal Phenytoin at 3 Different Concentrations (1600, 800, and 160 µg/mL)*

	Bulk				**Nanosuspension**			
	TR 146 (*C*s = 39.7 ± 2.6 µg/mL)		**Porcine Mucosa** (*C*s = 17.0 ± 1.3 µg/mL)		**TR 146** (*C*s = 113.3 ± 13.7 µg/mL)		**Porcine Mucosa** (*C*s = 103.6 ± 2.0 µg/mL)	
Phenytoin Concentration (µg/mL)	d*Q*/d*t* × 10^{-3}(µg/s)	P_{app} × 10^{-6}(cm/s)	d*Q*/d*t* × 10^{-3}(µg/s)	P_{app} × 10^{-6}(cm/s)	d*Q*/d*t* × 10^{-3}(µg/s)	P_{app} × 10^{-6}(cm/s)	d*Q*/d*t* × 10^{-3}(µg/s)	P_{app} × 10^{-6}(cm/s)
1600		1.71 ± 0.13	N.D.	N.D.		1.90 ± 0.00		0.17 ± 0.05
800	2.58 ± 0.19	3.09 ± 0.00	N.D.	N.D.	3.62 ± 0.12	3.70 ± 0.10	0.30 ± 0.06	0.37 ± 0.00
160		13.70 ± 0.82	N.D.	N.D.		19.80 ± 1.1		2.11 ± 0.43

All values are presented as mean values (*n* = 6) ± SD. The respective values for the saturation solubility of bulk and nanosuspension in HBSS (*in vitro* studies) and PBS (*ex vivo* studies) at 37°C are stated.
N.D., nondeterminable: amount of permeated phenytoin was under the limit of quantification.

To ensure high barrier properties of the TR 146 cell monolayer cultured on Transwells, the integrity was confirmed prior to the permeability experiments by measuring and calculating the transepithelial electrical resistance (TEER 52-60 Ωcm^2).

The calculated steady state appearance rates were 2.58 ± 0.19 × 10−3 µg/s for bulk phenytoin and 1- to 1.4-fold higher (i.e., 3.62 ± 0.12 × 10−3 µg/s) for nanophenytoin, independent of the applied dose. Considering the distinct concentrations used (i.e., 1600, 800, and 160 µg/mL), the calculated *P*app values ranged from 1.90 to 19.80 × 10−6cm/s for nanophenytoin and from 1.71 to 13.70 × 10−6 cm/s for bulk phenytoin.

It is known that nanoparticles are small enough to penetrate or permeate epithelial barriers and are internalized by the buccal cells.[48, 49, 50, 79, 85 , 86] Thus, to investigate whether the enhanced permeability of nanophenytoin was due to not only the increased solubility behavior but also cellular uptake (acting as “depot” for nanocrystals), TR 146 cells were treated with fluorescently labeled nanosamples, rinsed with buffer, and histochemical investigations were performed (Fig. 5). The CLSM images showed that most of the particles were removed by the washing step, and only isolated particles were occasionally visible in the intercellular spaces. Because of the negative surface charge of the phenytoin nanocrystals, electrostatic repulsion from anionic sites of the plasma membrane occurred

and cellular uptake was inhibited. This suggests that the enhanced permeability behavior is determined by the increased solubility of nanophenytoin in the physiological liquid.

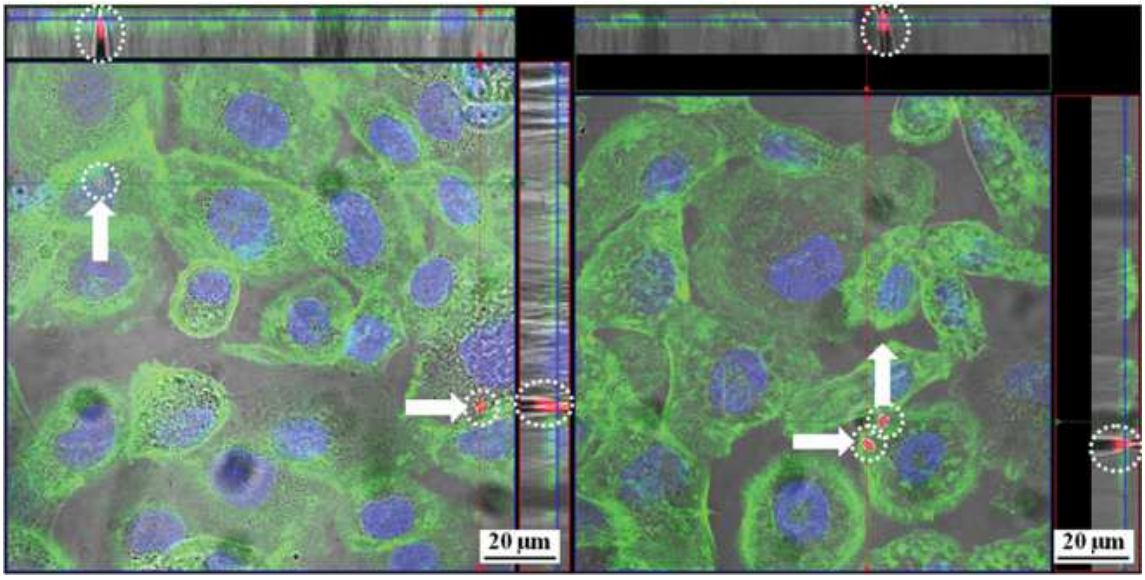

Figure 5. *: CLSM images (z stack) of TR 146 monolayers incubated with Alizarin Red S labeled phenytoin nanocrystals (red). Cell nuclei were stained with Hoechst (blue) and the cell membrane was stained with Alexa Fluor 488 Phalloidin (green). The circles and arrows indicate nanocrystals.*

The *ex vivo* studies showed that the permeated amount of bulk phenytoin through freshly excised porcine mucosa was lower than the limit of quantification, and thus, quantification was not possible. However, the steady state appearance rate of nanophenytoin was 0.30 ± 0.06 × 10−3 µg/s (independent of the applied initial dose) and the P_{app} were 0.17 ± 0.05 × 10−6 for the highest initial concentrations (1600 µg/mL) and 2.11 ± 0.43 × 10−6 cm/s for lower concentrations (160 µg/mL).

Comparing the results from the *ex vivo* with the *in vitro* investigations, P_{app} values were 10 times lower. This is due to the fact that the barrier thickness also plays a dominant role in drug permeability. Porcine (and also human) buccal mucosa is 13-18 times thicker compared to the *in vitro* cell monolayer. [87] To circumvent this obstacle, we carefully characterized both biological membranes and calculated the transference (*T*, µg/s/cm), which is the product of the membrane thickness *l* (cm) and the solute flux *J*sat(µg/s/cm^2)[83] (Eq. 3).

Equation(3)
$$T = \frac{l}{A} \times \left(\frac{dQ}{dt}\right) = J_{sat} \times l$$

The calculated *T* values showed that the *ex vivo* data (1.5 × 10−5-2.1 × 10−5 µg/s/cm) were well in accordance with the *in vitro* data (1.0 × 10−5-1.9 × 10−5 µg/s/cm).

3.4. Cytotoxicity

Because nanosystems might interfere with physiological functions, thus affecting cellular homeostasis, potential cytotoxic events were assessed. On that account, the cell viability was examined by a Formazan Bioreduction (MTS) Assay, and the membrane integrity was evaluated by measuring the LDH release after incubation of TR 146 cells with the particle suspensions (4 h; Fig. 6).

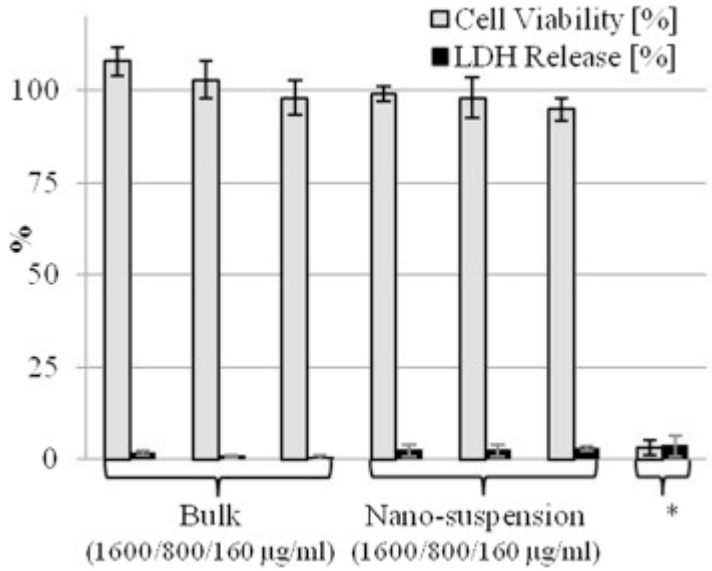

Figure 6. ***:*** *Cell viability (%) and LDH release (%) of human buccal epithelial TR 146 cells treated with dispersions of bulk phenytoin [PHT_1600-160 µg/mL] and nanosuspension [NS_1600-160 µg/mL] in DMEM. ⁎Control: formazan bioreduction assay; control wells were treated with lysis solution to generate 100% cell death; LDH release studies: control wells without the treatment of phenytoin bulk or nanodispersion.*

The results showed only small variances in the cell viability within the tested phenytoin concentration of 1600-160 µg/mL for both the bulk and the nanocrystalline phenytoin (control = 3 ± 2% viability). After 4 h of incubation time, cell viability was at least 98 ± 5% for bulk phenytoin (160 µg/mL) and 95 ± 3% for nano phenytoin (160 µg/mL). Moreover, no significant LDH release was observed within 4 h of incubation. Hence, neither bulk nor nanophenytoin caused harmful effects on buccal cells.

4. Conclusions

This study focused on enhancing drug permeation of phenytoin, a poorly soluble drug, across the buccal mucosa by increasing the drug solubility via particle size reduction. For this, a stable aqueous phenytoin nanosuspension was prepared via media milling, carefully characterized and tested considering the physiological conditions in the oral cavity.

The addition of the stabilizer P80 resulted in a stable crystalline nanosuspension with a mean hydrodynamic particle size of 330 nm. An enhanced saturated solubility and increased dissolution rate of phenytoin nanocrystals were observed in nonphysiological media. However, adapting the test media to salivary conditions, the solubility of the nanosuspension significantly increased. *In vitro* permeability studies revealed a 1.4-fold higher steady state appearance rate of nanophenytoin and a 1- to 1.4-fold higher P_{app} because of an improved saturated solubility of nanophenytoin. Additionally, *ex vivo* permeability studies showed that nanophenytoin permeated across the buccal epithelium more efficiently (dQ/dt = 0.30 ± 0.06 × 10−3 µg/s and P_{app} = 0.17 ± 0.05-2.11 ± 0.43 × 10−6 cm/s) than bulk phenytoin. Considering the membrane thickness, the *ex vivo* results were well in accordance with the *in vitro* data. No impact on the cell viability was observed despite size reduction. Since the nanocrystals did not interfere with the cells, the increased permeability can be attributed to the enhanced solubility of nanophenytoin in saliva.

This study clearly demonstrates that crystalline nanosuspensions are (1) a promising tool for enhancing the solubility of poorly soluble drugs and (2) are appropriate for safe intraoral drug administration. Moreover, it was shown that it is of paramount importance to consider the physiological conditions in the oral cavity because the salivary environment (i.e., ionic strength, pH) strongly impacts not only the stability but also the solubility and as a consequence the permeability of the compound across the buccal mucosa.

Acknowledgments

This work was funded through the Austrian COMET Program by the Austrian Federal Ministry of Transport, Innovation and Technology (BMVIT), the Austrian Federal Ministry of Economy, Family and Youth (BMWFJ) and by the State of Styria (Styrian Funding Agency SFG).

The authors acknowledge Bruker (Bruker AXS, Karlsruhe, Germany) for support with the SWAXS measurement system and Markus Absenger-Novak (Center for Medical Research, Medical University of Graz, BioTechMed-Graz, Austria) and Christa Schimpel (Department of Pharmaceutical Technology, Institute of Pharmaceutical Sciences, NAWI Graz, University of Graz, Austria) for conducting confocal laser scanning microscopy investigations.

References

1. Harris D, Robinson JR (1992) Drug delivery via the mucous membranes of the oral cavity. J. Pharm. Sci. 81:1–10.

2. Shojaei A, Chang R, Guo X, Burnside B, Couch R (2001) Systemic drug delivery via the buccal mucosal route. J. Pharm. Technol. 25:70–81.

3. Sattar M, Sayed OM, Lane ME (2014) Oral transmucosal drug delivery--current status and future prospects. Int. J. Pharm. 471:498–506.

4. Gandhi RB, Robinson JR (1994) Oral cavity as a site for bioadhesive drug delivery. Adv. Drug Deliv. Rev. 13:43–74.

5. Dawson D V, Drake DR, Hill JR, Brogden KA, Fischer CL, Wertz PW (2013) Organization, barrier function and antimicrobial lipids of the oral mucosa. Int. J. Cosmet. Sci. 35:220–3.

6. Deneer VHM, Drese GB, Roemelé PEH, Verhoef JC, Lie-A-Huen L, Kingma JH, Brouwers JRBJ, Junginger HE (2002) Buccal transport of flecainide and sotalol: Effect of a bile salt and ionization state. Int. J. Pharm. 241:127–134.

7. Nicolazzo JA, Reed BL, Finnin BC (2003) The Effect of Various in Vitro Conditions on the Permeability Characteristics of the Buccal Mucosa. J. Pharm. Sci. 92:2399–2410.

8. Nicolazzo J a, Reed BL, Finnin BC (2004) Modification of buccal drug delivery following pretreatment with skin penetration enhancers. J. Pharm. Sci. 93:2054–63.

9. Lesch CA, Squier CA, Cruchley A, Williams DM, Speight P (1989) The permeability of human oral mucosa and skin to water. J. Dent. Res. 68:1345–1349.

10. Wertz PM, Squier CA (1991) Cellular and molecular basis of barrier function in oral epithelium. Crit. Rev. Ther. Drug Carrier Syst. 8:237–269.

11. Shojaei AH, Berner B, Xiaoling L (1998) Tansbuccal delivery of acyclovir: I. In vitro determination of routes of buccal transport. Pharm. Res. 15:1182–1188.

12. Chinna Reddy P, Chaitanya KSC, Madhusudan Rao Y (2011) A review on bioadhesive buccal drug delivery systems: current status of formulation and evaluation methods. DARU J. Pharm. Sci. 19:385–403.

13. Shojaei AH, Khan M, Lim G, Khosravan R (1999) Transbuccal permeation of a nucleoside analog, dideoxycytidine: Effects of menthol as a permeation enhancer. Int. J. Pharm. 192:139–146.

14. Siegel I, Gordon H (1985) Surfactant-induced increases of permeability of rat oral mucosa to non-electrolytes in vivo. Arch. Oral Biol. 30:43–47.

15. Aungst BJ, Rogers NJ (1989) Comparison of the effects of various transmucosal absorption promoters on buccal insulin delivery. Int. J. Pharm. 53:227–235.

16. Shen B, Shen C, Yuan X, Bai J, Lv Q, Xu H, Dai L, Yu C, Han J, Yuan H (2013) Development and characterization of an orodispersible film containing drug nanoparticles. Eur. J. Pharm. Biopharm. 85:1348–56.

17. Sarkari M, Brown J, Chen X, Swinnea S, Williams RO, Johnston KP (2002) Enhanced drug dissolution using evaporative precipitation into aqueous solution. Int. J. Pharm. 243:17–31.

18. Chen X, Young TJ, Sarkari M, Williams RO, Johnston KP (2002) Preparation of cyclosporine A nanoparticles by evaporative precipitation into aqueous solution. Internaitonal J. Pharm. 242:3–14.

19. Peltonen L, Hirvonen J (2010) Pharmaceutical nanocrystals by nanomilling: critical process parameters, particle fracturing and stabilization methods. J. Pharm. Pharmacol. 62:1569–79.

20. Liversidge GG, Conzentino P (1995) Drug particle size reduction for decreasing gastric irritancy and enhancing absorption of naproxen in rats. Int. J. Pharm. 125:309–313.

21. Merisko-Liversidge E, Liversidge GG, Cooper ER (2003) Nanosizing: a formulation approach for poorly-water-soluble compounds. Eur. J. Pharm. Sci. 18:113–20.

22. Müller RH, Peters K (1998) Nanosuspensions for the formulation of poorly soluble drugs. Int. J. Pharm. 160:229–237.

23. Krause KP, Müller RH (2001) Production and characterisation of highly concentrated nanosuspensions by high pressure homogenisation. Int. J. Pharm. 214:21–4.

24. Rabinow BE (2004) Nanosuspensions in drug delivery. Nat. Rev. Drug Discov. 3:785–96.

25. Gao L, Zhang D, Chen M (2008) Drug nanocrystals for the formulation of poorly soluble drugs and its application as a potential drug delivery system. J. Nanoparticle Res. 10:845–862.

26. Van Eerdenbrugh B, Van den Mooter G, Augustijns P (2008) Top-down production of drug nanocrystals: nanosuspension stabilization, miniaturization and transformation into solid products. Int. J. Pharm. 364:64–75.

27. Müller RH, Jacobs C, Kayser O (2001) Nanosuspensions as particulate drug formulations in therapy. Rationale for development and what we can expect for the future. Adv. Drug Deliv. Rev. 47:3–19.

28. Liversidge GG, Cundy KC (1995) Particle size reduction for improvement of oral bioavailability of hydrophobic drugs: I. Absolute oral bioavailability of nanocrystalline danazol in beagle dogs. Int. J. Pharm. 125:91–97.

29. Keck CM, Müller RH (2006) Drug nanocrystals of poorly soluble drugs produced by high pressure homogenisation. Eur. J. Pharm. Biopharm. 62:3–16.

30. Van Eerdenbrugh B, Froyen L, Van Humbeeck J, Martens J a, Augustijns P, Van den Mooter G (2008) Drying of crystalline drug nanosuspensions-the importance of surface hydrophobicity on dissolution behavior upon redispersion. Eur. J. Pharm. Sci. 35:127–35.

31. Wu L, Zhang J, Watanabe W (2011) Physical and chemical stability of drug nanoparticles. Adv. Drug Deliv. Rev. 63:456–469.

32. Slavkova M, Breitkreutz J (2015) Orodispersible drug formulations for children and elderly. Eur. J. Pharm. Sci. 75:2–9.

33. Kesisoglou F, Panmai S, Wu Y (2007) Nanosizing-oral formulation development and biopharmaceutical evaluation. Adv. Drug Deliv. Rev. Drug Deliv Rev 59:631–44.

34. Shegokar R, Müller RH (2010) Nanocrystals: industrially feasible multifunctional formulation technology for poorly soluble actives. Int. J. Pharm. 399:129–39.

35. Ohshima H, Miyagishima A, Kurita T, Makino Y, Iwao Y, Sonobe T, Itai S (2009) Freeze-dried nifedipine-lipid nanoparticles with long-term nano-dispersion stability after reconstitution. Int. J. Pharm. 377:180–184.

36. Chaubal M V., Popescu C (2008) Conversion of nanosuspensions into dry powders by spray drying: A case study. Pharm. Res. 25:2302–2308.

37. Abdelwahed W, Degobert G, Stainmesse S, Fessi H (2006) Freeze-drying of nanoparticles: Formulation, process and storage considerations. Adv. Drug Deliv. Rev. 58:1688–1713.

38. Rana P, Murthy RSR (2013) Formulation and evaluation of mucoadhesive buccal films impregnated with carvedilol nanosuspension: a potential approach for delivery of drugs having high first-pass metabolism. Drug Deliv. 20:224–35.

39. Rao S, Song Y, Peddie F, Evans AM (2011) Particle size reduction to the nanometer range: a promising approach to improve buccal absorption of poorly water-soluble drugs. Int. J. Nanomedicine 6:1245–1251.

40. Hoffmann EM, Breitenbach A, Breitkreutz J (2011) Advances in orodispersible films for drug delivery. Expert Opin. Drug Deliv. 8:299–316.

41. Pardeike J, Strohmeier DM, Schrödl N, Voura C, Gruber M, Khinast JG, Zimmer A (2011) Nanosuspensions as advanced printing ink for accurate dosing of poorly soluble drugs in personalized medicines. Int. J. Pharm. 420:93–100.

42. Preis M, Breitkreutz J, Sandler N (2015) Perspective: Concepts of printing technologies for oral film formulations. Int. J. Pharm.:in press.

43. Khinast J, Baumgartner R, Roblegg E (2013) Nano-extrusion: a one-step process for manufacturing of solid nanoparticle formulations directly from the liquid phase. AAPS Pharm. Sci. Technol. 14:601–4.

44. Baumgartner R, Eitzlmayr A, Matsko N, Tetyczka C, Khinast J, Roblegg E (2014) Nano-extrusion: A promising tool for continuous manufacturing of solid nano-formulations. Int. J. Pharm. 477:1–11.

45. Tunnicliff G (1996) Basis of the antiseizure action of phenytoin. Gen Pharmacol 27:1091–1097.

46. Suzuki T, Saitoh Y, Nishihara K (1970) Kinetics of diphenylhydantoin disposition in man. Chem. Pharm. Bull. 18:405–411.

47. Arnold K, Gerber N, Levy G (1970) Absorption and dissolution studies on sodium diphenylhydantoin capsules. Can. J. Pharm. Sci. 5:89–92.

48. Roblegg E, Fröhlich E, Meindl C, Teubl B, Zaversky M, Zimmer A (2012) Evaluation of a physiological in vitro system to study the transport of nanoparticles through the buccal mucosa. Nanotoxicology 6:399–413.

49. Teubl BJ, Leitinger G, Schneider M, Lehr CM, Fröhlich E, Zimmer A, Roblegg E (2014) The buccal mucosa as a route for TiO2 nanoparticle uptake. Nanotoxicology:1–9.

50. Teubl BJ, Absenger M, Fröhlich E, Leitinger G, Zimmer A, Roblegg E (2013) The oral cavity as a biological barrier system: design of an advanced buccal in vitro permeability model. Eur. J. Pharm. Biopharm. 84:386–93.

51. Oberdörster G, Stone V, Donaldson K (2007) Toxicology of nanoparticles: A historical perspective. Nanotoxicology 1:2–25.

52. Gupta VK, Karar PK, Ramesh S, Misra SP, Gupta A (2010) Nanoparticle Formulation for Hydrophilic & Hydrophobic Drugs. Int. J. Res. Pharm. Sci. 1:163–169.

53. Krug HF, Wick P (2011) Nanotoxicology: an interdisciplinary challenge. Angew. Chem. Int. Ed. Engl. 50:1260–78.

54. Boczkowski J, Hoet P (2010) What's new in nanotoxicology? Implications for public health from a brief review of the 2008 literature. Nanotoxicology 4:1–14.

55. Jiang J, Oberdörster G, Biswas P (2008) Characterization of size, surface charge, and agglomeration state of nanoparticle dispersions for toxicological studies. J. Nanoparticle Res. 11:77–89.

56. Nel A, Xia T, Mädler L, Li N (2006) Toxic potential of materials at the nanolevel. Science 311:622–627.

57. Brown DM, Donaldson K, Borm PJ, Schins RPF, Dehnhardt M, Gilmour PS, Jimenez L a, Stone V (2004) Calcium and ROS-mediated activation of transcription factors and TNF-α cytokine gene expression in macrophages exposed to ultrafine particles. Am. J. Pyhsiology. Lung Cell. Mol. Physiol. 286:344–353.

58. Borm PJ a (2002) Particle toxicology: from coal mining to nanotechnology. Inhal. Toxicol. 14:311–324.

59. Borm P, Klaessig FC, Landry TD, Moudgil B, Pauluhn J, Thomas K, Trottier R, Wood S (2006) Research strategies for safety evaluation of nanomaterials, Part V: Role of dissolution in biological fate and effects of nanoscale particles. Toxicol. Sci. 90:23–32.

60. Müller R, Schuhmann R Teilchengrößenbestimmung in der Laborpraxis. In: Wissenschaftliche Verlagsgesellschaft mbH Stuttgart, editor. ; 1996.

61. Kayaert P, Van den Mooter G (2012) Is the amorphous fraction of a dried nanosuspension caused by milling or by drying? A case study with Naproxen and Cinnarizine. Eur. J. Pharm. Biopharm. 81:650–6.

62. Van Eerdenbrugh B, Vermant J, Martens JA, Froyen L, Van Humbeeck J, Augustijns P, Van Den Mooter G (2009) A screening study of surface stabilization during the production of drug nanocrystals. J. Pharm. Sci. 98:2091–2103.

63. Jacobsen J, van Deurs B, Pedersen M, Rassing MR (1995) TR146 cells grown on filters as a model for human buccal epithelium: I. Morphology, growth, barrier properties, and permeability. Int. J. Pharm. 125:165–184.

64. Nielsen HM, Rassing MR (2000) TR146 cells grown on filters as a model of human buccal epithelium: IV. Permeability of water, mannitol, testosterone and beta-adrenoceptor antagonists. Comparison to human, monkey and porcine buccal mucosa. Int. J. Pharm. 194:155–67.

65. Wang D, Bradford S a., Harvey RW, Gao B, Cang L, Zhou D (2012) Humic acid facilitates the transport of ARS-labeled hydroxyapatite nanoparticles in iron oxyhydroxide-coated sand. Environ. Sci. Technol. 46:2738–2745.

66. Vukomanović M, Zavašnik-Bergant T, Bračko I, Škapin SD, Ignjatović N, Radmilović V, Uskoković D (2011) Poly(d,l-lactide-co-glycolide)/hydroxyapatite core–shell nanospheres. Part 3: Properties of hydroxyapatite nano-rods and investigation of a distribution of the drug within the composite. Colloids Surfaces B Biointerfaces 87:226–235.

67. Fröhlich E, Roblegg E (2012) Models for oral uptake of nanoparticles in consumer products. Toxicology 291:10–7.

68. Law SL, Kayes JP (1983) Adsorption of non-ionic water-soluble cellulose polymers at the solid-water interface and their effect on suspension stability. Int. J. Pharm. 15:251–260.

69. Lee J, Lee S-J, Choi J-Y, Yoo JY, Ahn C-H (2005) Amphiphilic amino acid copolymers as stabilizers for the preparation of nanocrystal dispersion. Eur. J. Pharm. Sci. 24:441–9.

70. Palla B, Shah D (2002) Stabilization of high ionic strength slurries using surfactant mixtures: molecular factors that determine optimal stability. J. Colloid Interface Sci. 152:143–152.

71. Cerdeira AM, Mazzotti M, Gander B (2010) Miconazole nanosuspensions: Influence of formulation variables on particle size reduction and physical stability. Int. J. Pharm. 396:210–8.

72. Pardeike J, Müller RH (2010) Nanosuspensions: a promising formulation for the new phospholipase A2 inhibitor PX-18. Int. J. Pharm. 391:322–329.

73. Müller R Zetapotential und Partikelladung in der Laborpraxis. (Wissenschaftliche Verlagsgesellschaft mbH Stuttgart, editor.).; 1996.

74. Jacobs C, Müller RH (2002) Production and characterizatoin of a budesonide nanosuspension for pulmonary administration. Pharm. Res. 19:2–7.

75. Nyström C, Bisrat M (1988) Physicochemical aspects of drug release. VIII. The relation between particle size and surface specific dissolution rate in agitated suspensions. Int. J. Pharm. 47:223–231.

76. Torrado G, Fraile S, Torrado S, Torrado S (1998) Process-induced crystallite size and dissolution changes elucidated by a variety of analytical methods. Int. J. Pharm. 166:65–73.

77. Beckman KB, Ames BN (1998) The free radical theory of aging matures. Physiol. Rev 78:547–81.

78. Müller RH, Akkar A (2004) Drug nanocrystals of poorly soluble drugs. Encycl. Nanosci Nanotechnol. 2:627–638.

79. Teubl BJ, Meindl C, Eitzlmayr A, Zimmer A, Fröhlich E, Roblegg E (2013) In-vitro permeability of neutral polystyrene particles via buccal mucosa. Small 9:457–66.

80. Nielsen HM, Verhoef JC, Ponec M, Rassing MR (1999) TR146 cells grown on filters as a model of human buccal epithelium: permeability of fluorescein isothiocyanate-labelled dextrans in the presence of sodium glycocholate. J. Control. Release 60:223–233.

81. Jacobsen J, Nielsen EB, Brøndum-Nielsen K, Christensen ME, Olin HB, Tommerup N, Rassing MR (1999) Filter-grown TR146 cells as an in vitro model of human buccal epithelial permeability. Eur. J. Oral Sci. 107:138–146.

82. Heaney TG, Jones RS (1978) Histological investigation of the influence of adult porcine alveolar mucosal connective tissues on epithelial differentiation. Arch. Oral Biol. 23:713–717.

83. Theeuwes F, Gale RM, Baker RW (1976) Transference: a comprehensive parameter governing permeation of solutes through membranes. J. Memb. Sci. 1:3–16.

84. Kokate A, Li X, Singh P, Jasti BR (2008) Effect of thermodynamic activities of the unionized and ionized species on drug flux across buccal mucosa. J. Pharm. Sci. 97:4294–4306.

85. Schimpel C, Teubl B, Absenger M (2014) Development of an Advanced Intestinal in Vitro Triple Culture Permeability Model To Study Transport of Nanoparticles. Mol. Pharm.

86. Schimpel C, Werzer O, Fröhlich E, Leitinger G, Absenger-Novak M, Teubl B, Zimmer A, Roblegg E (2015) Atomic force microscopy as analytical tool to study physico-mechanical properties of intestinal cells. Beilstein J. Nanotechnol. 6:1457–1466.

87. Nielsen HM Chapter 18: In vitro models of the human buccal epithelium: the TR146 cell culture model and the porcine in vitro model. In: Cell culture models of biological barriers: in-vitro test systems for drug absorption and delivery. ; 2002.

3. Nano-extrusion: A promising tool for continuous manufacturing of solid nano-formulations

Ramona Baumgartner [a], Andreas Eitzlmayr [a,b], Nadejda Matsko [c], Carolin Tetyczka [d], Johannes Khinast [a,b], Eva Roblegg [a,d,*]

[a] *Research Center Pharmaceutical Engineering GmbH, Inffeldgasse 13, 8010 Graz, Austria*

[b] *Institute for Process and Particle Engineering, Graz University of Technology, Inffeldgasse 13, 8010 Graz, Austria*

[c] *Graz Center for Electron Microscopy (ZFE), Steyrergasse 17, 8010 Graz, Austria*

[d] *Institute of Pharmaceutical Sciences, Department of Pharmaceutical Technology, Karl-Franzens University Graz, Universitätsplatz 1, 8010 Graz, Austria*

* Corresponding author at: Institute of Pharmaceutical Sciences, Department of Pharmaceutical Technology, Karl-Franzens University Graz, Universitätsplatz 1, 8010 Graz, Austria. Tel.: +43 316 380 8888.

Published in: International Journal of Pharmaceutics 477 (2014) 1-11.
DOI: 10.1016/j.ijpharm.2014.10.008

Abstract

Since more than 40% of today's drugs have low stability, poor solubility and/or limited ability to cross certain biological barriers, new platform technologies are required to address these challenges. This paper describes a novel continuous process that converts a stabilized aqueous nano-suspension into a solid oral formulation in a single step (i.e., the NANEX process) in order to improve the solubility of a model drug (phenytoin). Phenytoin nano-suspensions were prepared via media milling using different stabilizers. A stable nano-suspension was obtained using Tween® 80 as a stabilizer. The matrix material (Soluplus®) was gravimetrically fed into the hot melt extruder. The suspension was introduced through a side feeding device and mixed with the molten polymer to immediately devolatilize the water in the nano-suspension. Phenytoin nano-crystals were dispersed and embedded in the molten polymer. Investigation of the nano-extrudates via transmission electron microscopy and atomic force microscopy showed that the nano-crystals were embedded de-aggregated in the extrudates. Furthermore, no changes in the crystallinity (due to the mechanical and thermal stress) occurred. The dissolution studies confirmed that the prepared nano-extrudates increased the solubility of nano-crystalline phenytoin, regardless of the polymer. Our work demonstrates that NANEX represents a promising new platform technology in the design of novel drug delivery systems to improve drug performance.

Graphical abstract

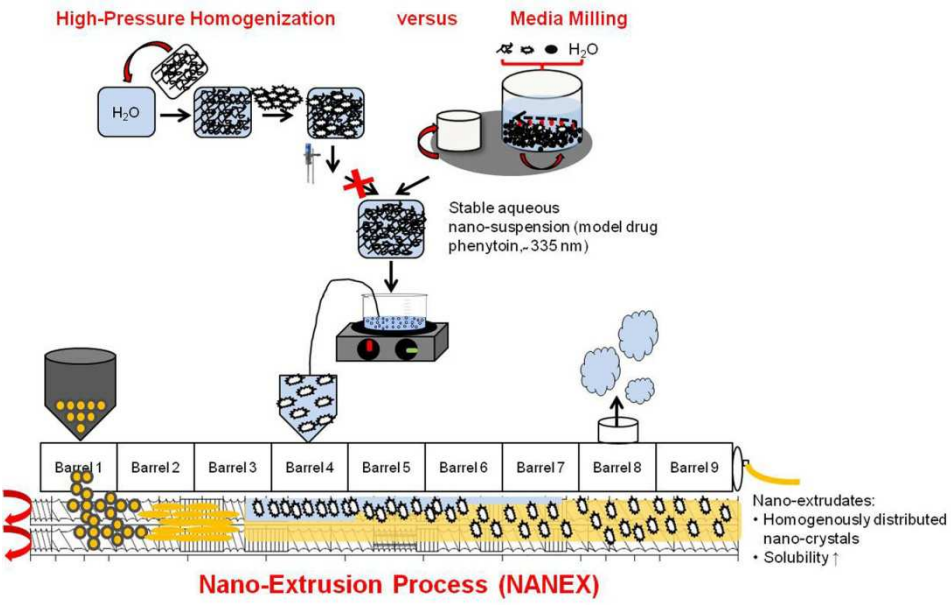

Keywords

Phenytoin nano-suspension; Hot melt extrusion; One-step continuous process; Solid nano-formulation; Nano-extrusion (NANEX)

1. Introduction

Oral administration of drugs is traditionally preferred by the patients and remains the most convenient and industrially relevant delivery form. However, many newly-developed chemical entities (NCE) have poor water solubility, which poses a great challenge since drug solubility is frequently a rate-limiting step in the intestinal drug absorption, negatively affecting bioavailability (Fasano, 1998). To overcome this problem and to improve drug efficacy and safety, innovative formulation platforms and strategies for novel oral drug delivery technologies are increasingly developed (Verma and Garg, 2001).

An ample body of research exists in this area, focusing on salt- or co-crystal formation, amorphous solid dispersions, or other solubility enhancement strategies (Crowley et al., 2007, Fasano, 1998, Pardeike et al., 2011, Patil and Wagh, 2011, Patravale et al., 2004,Paudel et al., 2013, Roblegg et al., 2011, Shah et al., 2012 and Verma and Garg, 2001). Another strategy in this rapidly emerging field is the development of nano-systems (Van Eerdenbrugh et al., 2008), where solubility enhancement is achieved by making use of the high surface-to-volume ratio and the associated increase in energy levels and (apparent) solubility (Müller et al., 2001 and Müller and Peters, 1998).

The range of nano-systems in the oral drug delivery area includes polymeric nano-particles, solid lipid nano-particles and nano-crystals (<500 nm), which are obtained (for example) via specialized milling techniques, such as the Elan Nano-crystal® technology (Chingunpituk, 2011, Liversidge and Cundy, 1992 and Van Eerdenbrugh et al., 2008) or by high-pressure homogenization (DissoCubes®, SkyePharma PLC (Müller et al., 1999a)). Typically, nano-crystals exhibit stability issues caused by the agglomeration (Kesisoglou et al., 2007, Rabinow, 2004, Van Eerdenbrugh et al., 2009 and Verma and Garg, 2001), which can be of both physical (e.g., Ostwald ripening and agglomeration) and chemical (e.g., hydrolysis) nature (Möschwitzer et al., 2004). Thus, specific stabilizers are added that inhibit particle agglomeration.

Currently, five oral solid nano-products (i.e., Rapamune®, Emend®, TriCor®, Megace®ES and Triglide™) (Chingunpituk, 2011 and Van Eerdenbrugh et al., 2008) are available on the market, four of which are produced via the media milling technique and one (Triglide™) via high-pressure homogenization. However, the manufacturing process of converting a nano-suspension into a solid powder (Müller et al., 1999b) and further compacting it into tablets or filling it into capsules requires several intricate steps, including freeze drying, spray drying, spray coating, pelletization or granulation. These complex

processes are time-consuming, cost-intensive, and hard to control and to scale-up. Moreover, they cannot be easily integrated in a continuous manufacturing environment. Thus, new technologies are required that enable a continuous transformation of nano-suspensions into a solid formulation. This allows to (i) precisely control the product quality, (ii) increase the manufacturing capacity, and (iii) to produce a range of drug doses in an efficient manufacturing environment.

In our initial proof-of-concept study we reported on a one-step nano-extrusion process (NANEX) (Khinast et al., 2013), in which a model nano-suspension (titanium dioxide nano-particles) was fed directly into a hot melt extruder. The solvent was removed from the extruder by devolatilization, and the nano-particles were embedded de-agglomerated in a molten polymer (Soluplus®).

In the current study we present the use of the NANEX process for developing solid nano-formulations of the water-insoluble model drug phenytoin in a single step. First, the physicochemical characteristics of the bulk material were evaluated, and nano-suspensions were prepared via media milling (by selecting and adding appropriate stabilizers). The nano-suspensions were characterized and the most stable systems were selected for the NANEX development. The polymer (Soluplus®) was fed gravimetrically into the extruder and the aqueous nano-suspension was added through liquid side feeding. Screw optimization was performed to render a stable, reproducible and well-controlled process. Next, the extruded material was studied via electron-microscopic analysis and atomic force microscopy to verify the presence of de-agglomerated distributed phenytoin nano-crystals in the matrix system. Finally, dissolution profiles of the obtained nano-extrudates were measured to determine the release characteristics of phenytoin nano-crystals in the extrudates.

2. Materials and methods

2.1. Materials

As a model active pharmaceutical ingredient (API), phenytoin (5,5-diphenylhydantoin) from Sigma–Aldrich (Sigma–Aldrich®, Munich, Germany) was used. The stabilizers Tween® 20 (P20) and Tween® 80 (P80), as well as methanol (CHROMASOLV®, for HPLC, ≥ 99.9%) were purchased from Sigma–Aldrich (Sigma–Aldrich®, Munich, Germany). Soluplus®, Kolliphor® P188 (KP188), and Kollicoat® IR (KIR) were donated by the manufacturer BASF (BASF SE, Ludwigshafen, Germany). Ultrapurified water (i.e., Milli-Q®-water (MQ-water), Millipore S.A.S., Molsheim, France) was used for all experiments.

2.2. Methods

2.2.1. Characterization of bulk phenytoin

2.2.1.1. Sample preparation for transmission electron microscopy (TEM) and atomic force microscopy (AFM)

Samples for TEM and AFM were prepared by placing a small droplet of the sample onto plastic paraffin films. Next, samples were covered by a holey carbon coated copper electron microscopy (EM) grid for a few seconds. The grids were padded with filter paper to remove excess material and left to dry.

2.2.1.2. Determination of morphology, size and shape of bulk phenytoin via transmission electron microscopy (TEM)

TEM analysis was performed using a Philips CM 20 microscope (FEI, Eindhoven) equipped with a Gatan imaging filter (GIF) and operated at a high voltage of 200 kV with LaB6 cathode. Energy-dispersive X-ray spectroscopy (EDXS) experiments were conducted with scanning transmission electron microscopy (STEM) mode with a probe current of 20 nA and a beam diameter of 100 nm. Data processing was carried out with the Digital Micrograph software (Gatan, USA). All EDX spectra and TEM micrographs were recorded without prior staining.

2.2.1.3. Crystalline structure of bulk phenytoin via small- and wide-angle X-ray scattering (SWAXS)

Crystal structure and morphology were investigated using a SWAXS System (HECUS S3-MICRO, Bruker AXS, Karlsruhe, Germany) with automated data evaluation software. The SWAXS (SAXS and WAXS) system is equipped with a high-flux laboratory SWAXS camera S3-Micro (Bruker AXS, Karlsruhe, Germany), a high-brillance microbeam delivery system with point-focus optics (FOX3D, Xenocs, Grenoble, France) and with a 1D- or 2D-detection system. For sample preparation, material was filled into glass capillaries (2 mm in diameter) that were sealed with wax and placed into the SpinCap. For X-ray a wavelength λ of 1.54 Å was used and the SAXS and WAXS curves (scattering intensities as a function of the scattering angle 2θ) were recorded by two independent 1D detectors (PSD-50, Hecus X-ray Systems, Graz, Austria) in the angular ranges of $0.06° < 2\theta < 8°$ and $18° < 2\theta < 27°$. Duration of exposure was 600 s.

2.2.1.4. Thermal behavior of bulk phenytoin via differential scanning calorimetry (DSC)

The thermal properties of phenytoin were investigated using DSC (204F1 Phoenix, Netzsch GmbH, Selb, Germany). Phenytoin was placed into an aluminum crucible, which was sealed, pierced and purged with pure nitrogen (20 ml/min). The heating rate was 10 K/min from 20 to 350 °C. After cooling (10 K/min) to 40 °C, a second run was performed, with an empty aluminum crucible as a reference. The DSC data were analyzed

with Proteus Thermal Analysis software (Netzsch GmbH, Selb, Germany). Each experiment was carried out in triplicate, and average values and their standard deviations were calculated.

2.2.1.5. Aqueous solubility of bulk phenytoin

The aqueous solubility of bulk phenytoin in MQ-water was calculated at room temperature. For this purpose, an excess of the bulk material was transferred into glass vessels. Subsequently, 50 ml of media (i.e., MQ-water) were added and samples were placed in a horizontal shaker (IKA yellow line RS 10 control, IKA®-Werke GmbH & Co., KG, Staufen, Germany) operating at 200 rpm for 24 h and 96 h. (room temperature at 25 ± 1 °C). 1 ml was withdrawn and the samples were centrifuged (5 min, 20817.16 g; room temperature) and analyzed via high performance liquid chromatography (HPLC). Each experiment was performed in triplicate, and the average values and the standard deviations were calculated.

2.2.1.6. In vitro drug release studies

The release profile of phenytoin was obtained using dissolution apparatus II (paddle) according to the official monograph of phenytoin described in the United States Pharmacopeia (USP). Analyses were carried with 27 mg of phenytoin in 900 ml of 0.05 M Tris buffer (i.e., 36.3 g of tris(hydroxymethyl) aminomethane and 60 g of sodium lauryl sulfate in 6 l of water, adjusted with hydrochloric acid to a pH of 7.5 ± 0.05). The dissolution medium was maintained at 37 ± 0.5 °C and agitated with a rotational speed of 100 rpm. At predetermined time intervals (i.e., 5, 10, 20, 30, 40, 50 and 60 min) samples of 1 ml were taken and filtered through 0.02 µm filters (Anotop 25 Plus, Whatman, Maidstine, UK). Dissolution experiments were carried out in triplicate and all samples were analyzed via high performance liquid chromatography (HPLC).

2.2.1.7. Quantitative assays via high performance liquid chromatography (HPLC)

Quantitative determination of phenytoin was performed on a Merck–Hitachi LaChrom HPLC system equipped with a pump L-7100, an autosampler L-7200, a column oven L-7300, a UV–vis detector L-7420 and a Merck–Hitachi interface L-7000 (Hitachi High Technologies Corporation, Tokyo, Japan) using a C18 column (300 Extend-C18, 4.6 × 100 mm, 3.5 µm, 300 Å, Agilent Technologies Austria GmbH, Vienna, Austria) with a matching pre-column after Van Eerdenbrugh et al. (2009). The mobile phase (a mixture of 50% MilliQ-water and 50% methanol (v/v%)) was introduced at a flow rate of 1 ml/min. The injection volume per sample was 20 µl. The UV spectrum was recorded at a wavelength of 225 nm. Quantification of the compounds was carried out by measuring the peak areas in relation to those of the standards (i.e., 0.5–100 µg/ml) chromatographed under

the same conditions with an evaluated limit of detection (LOD) of 0.1 µg/ml and a limit of quantification (LOQ) of 0.5 µg/ml.

2.2.2. Preparation and characterization of the nano-suspensions

2.2.2.1. Media milling (MM)

For the production of nano-suspensions via MM, a stabilized aqueous suspension at the ratio 4:20:1 (drug:water:stabilizer in w/w) was prepared. Yttrium-stabilized zirconium beads of 0.5 mm in diameter were used as a milling agent with a weight ratio of 2.4:1 for milling beads to starting suspension. Milling was performed with a planetary ball mill (Retsch PM 100, Retsch GmbH, Haan, Germany) equipped with a zirconium oxide grinding bowl (500 ml) at 250 rpm for 24 h. The experiments were carried out at room temperature (25 ± 1 °C). Each batch had a mass of 250 g, and the API concentration of the nano-suspension was 16% (w/w).

2.2.2.2. Z-average and polydispersity index (PdI) via photon correlation spectroscopy (PCS) and zeta potential via laser-doppler-micro-electrophorese

Z-average and PdI of the prepared nano-suspensions were analyzed via photon correlation spectroscopy (PCS) using a Zetasizer Nano ZS (Malvern Instruments, Malvern, UK) equipped with a 532 nm laser. Prior to the measurements, nano-suspensions were diluted in a saturated phenytoin-water solution (i.e., concentration of 11.5 µg/ml) to result in an appropriate particle concentration and to prevent the dissolution of particles during measurements (Kayaert and Van den Mooter, 2012 and Van Eerdenbrugh et al., 2009). The measurements were performed at 25 °C. Equilibration time was 30 s, and the measurement angle was 173° (backscattering). The measurements were carried out in triplicate, and the average values and the standard deviations were calculated.

The zeta potential was evaluated via Laser-Doppler-Micro-Electrophorese (scattering angle of 173°) coupled with PCS (Zetasizer Nano ZS, Malvern Instruments, Malvern, UK) and calculated according to the Helmholtz–Smoluchovski equation. The measurements were performed in Zeta-water (i.e., distilled water adjusted with 0.9% (w/v) sodium chloride solution to a conductivity of 50 Scm^{-1} and a pH of 5.5–6.0) at 25 °C to obtain information on the surface charge. The measurements were carried out in triplicate and the average values as well as the standard deviations were calculated.

2.2.2.3. Stability studies

Physical stability of the nano-suspensions was investigated by storing samples in a refrigerator (i.e., 5 ± 3 °C) for four weeks and measuring the Z-average and zeta potential of the formulations weekly via PCS and LDME.

2.2.2.4. Characterization of the nano-suspension

Nano-suspensions were characterized and analyzed via HPLC with respect to their crystalline structure (SWAXS, air dried suspension), thermal behavior (DSC, air dried suspension), particle size (TEM), aqueous saturation solubility and dissolution profile. For determination of the aqueous solubility an excess of the nano-suspension was used. For in-vitro dissolution studies an aliquot of the nano-suspension corresponding to a phenytoin-dose of 27 mg was transferred into the glass vessels and samples were treated equally as the bulk material.

2.2.3. Preparation and characterization of the nano-extrudates

2.2.3.1. The continuous nano-extrusion process (NANEX)

Extrusion was performed with the MICRO 27 GL twin-screw extruder (Leistritz Extrusionstechnik GmbH, Nürnberg, Germany) through a die with two identical 1 mm holes. The barrel had nine sections (8 temperature-controlled barrel zones), which were individually heated with electric heaters or cooled with water. The temperatures of the individual barrels were in the range of 100–150 °C, and the screw-speed was 200 rpm (Fig. 1). Soluplus® (i.e., the matrix material) was fed gravimetrically into zone 1 (i.e., 2.0 kg/h) via a K-Tron twin-screw feeder K-CL-SFS-KT20 (K-Tron LLC, Switzerland). The nano-suspension (i.e., 0.6 kg/h) was added into zone 4 by using a flow-controlled micro-angular gear pump mzr7205 G (HNP Microsystems GmbH, Germany), and water vapor was eliminated via devolatilization (200 mbar) in barrel zone 8. Thus, the whole process can be run continuously.

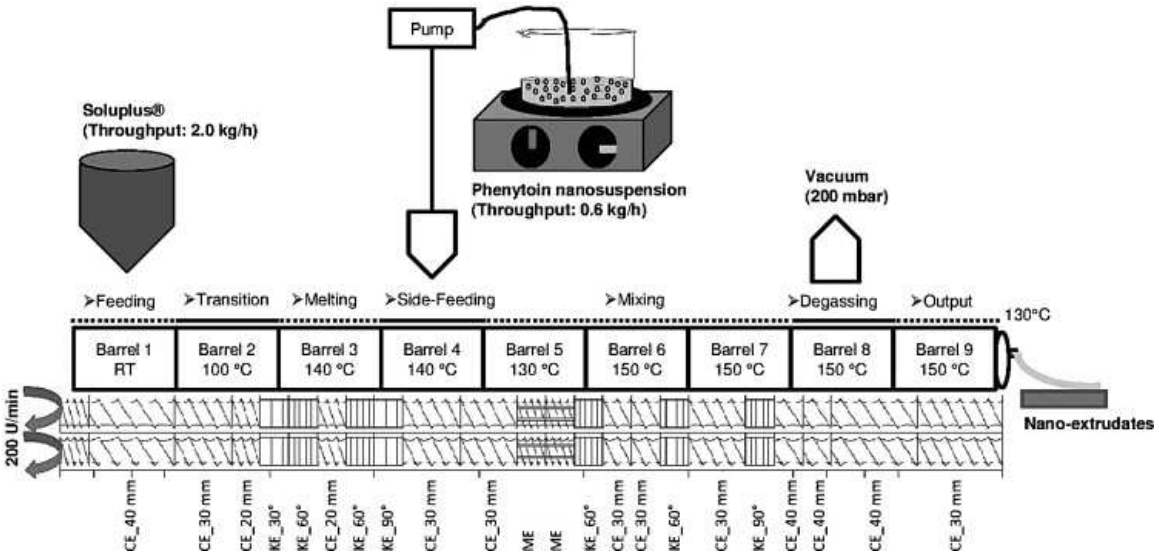

Fig.1. *Schematic illustration of the extruder setup, including the process temperatures of the barrel zones in °C, the screw configuration and speed [U/min] and the throughput of the feeder in barrel 1 and the liquid side-feeding device (barrel 4). (Legend for screw elements: CE = conveying element; KE = kneading element; ME = mixing element; 40, 30, 20 mm = pitch of conveying elements; 30°, 60°, 90° = offset angles of kneading elements.)*

Combined with a suitable downstream processing step, such as calandering or hot-die cutting (Radl et al., 2010; Treffer et al., 2013 and Treffer et al., 2014) this process can be used to produce a final drug product in one processing step.

The screw-configuration was adapted to the process requirements. For that purpose, the screw in the feeding section (barrel 1) had powder conveying elements with a large pitch of 40 mm. The pitch of the screw elements decreased in the transition zone (barrel 2) (i.e., from 30 mm to 20 mm). In the melting zone (barrel 3), kneading elements with 30° and 60° offset angles were used in the front part, followed by a conveying element with a 20 mm pitch and the second section of kneading elements with 60° and 90° offset angles. The screw in the side feeding zone (barrel 4, where the nano-suspension was added) had partially-filled conveying elements. The mixing zone (i.e., barrel 5–7) contained various mixing, kneading and conveying elements. Two mixing elements were used initially (barrel 5), and three kneading elements with 60° and 90° offset angles with conveying elements followed each kneading element. The degassing zone (barrel 8) had conveying elements with a large pitch of 40 mm. The screw in the rear of the extruder (barrel 9) had a conveying element.

For comparison purposes, bulk extrudates were prepared by extruding a premix comprising 95.4% (w/w) Soluplus® and 4.6% (w/w) untreated phenytoin (bulk material) with the MICRO 27 GL twin-screw extruder (Leistritz Extrusionstechnik GmbH, Nürnberg, Germany). The process parameters, screw configuration and barrel temperatures were identical to the NANEX settings.

2.2.3.2. Characterization of the nano-extrudates

The nano- and bulk-extrudates were characterized in terms of thermal behavior as described for bulk-phenytoin. For DSC measurements, extrudates were cut into pellets. Experiments were performed at 10 K/min (20 ml/min nitrogen; from 20 °C to 320 °C). Furthermore, the distribution of the (nano-) crystals in the extrudates was studied and verified via TEM and atomic force microscopy (AFM). For the purposes of TEM and AFM studies, the original phenytoin (nano-) extrudate materials were mounted on special holders that fit in the microtome and could be used to examine the block face via AFM. Since Soluplus® is a water soluble substance, the sections (50–70 nm) were cut in a water-free environment using a Leica Ultracut E microtome (Leica, Austria) equipped with a diamond knife (Diatome, Switzerland). The sections for TEM analysis were collected on holey carbon coated 400-mesh copper TEM grids. For AFM studies, after ultramicrotomy the block faces of the specimens were investigated at ambient conditions using a Dimension 3100 AFM/SPM (Veeco, USA) atomic force microscope. AFM images were collected in a “hard-

tapping" mode using the silicon nitride cantilevers with natural frequencies in the 300 kHz range (force constant 20 N/m, tip radius 10 nm (NT-MDT, Russia). AFM image processing was performed using the Nanoscope v720 software (Veeco, USA). The aqueous solubility and the in-vitro dissolution studies of the extrudates were performed as described for the bulk and the nano-suspension.

3. Results and discussion

3.1. Rational selection of the matrix material and of the model drug

In general, thermoplastic polymers applied in hot-melt extrusion must have suitable physico-chemical properties. Extrudability is primarily determined by the glass transition temperature (T_g) and/or the melting temperature (T_m), as well as the melt viscosity and/or stickiness. Polymers with a low T_g and a low T_m (50–180 °C) are typically selected to prevent the degradation of thermo-sensitive APIs (Kolter et al., 2012). Furthermore, physiological compatibility (i.e., GRAS – generally recognized as safe – status) and, if possible, low hygroscopicity are required. In addition, to achieve a homogeneous distribution of the aqueous nano-suspension in a matrix, the polymer has to be miscible with or swell in water during the NANEX process.

For these reasons, amphiphilic Soluplus®, a polyvinylcaprolactam–polyvinyl acetate–polyethylene glycol graft co-polymer, was selected as the matrix material. It is miscible with water, has a low T_g (70 °C) and is thermally stable up to 293 °C (Terife et al., 2012). It acts as solubilizer for poorly soluble APIs and has an instant release profile (Kolter et al., 2012).

The physicochemical characteristics to make an API suitable for the NANEX process include thermal and mechanical stability and poor solubility. Thus, phenytoin (5,5-diphenylimidazolidine-2,4-dione) which is an anticonvulsive, antiepileptic and anti-arrhythmic drug was used. It is poorly soluble (i.e., 11.5 ± 0.5 μg/ml) and lipophilic (i.e., log P = 2.95 ± 0.05; contact angle with water = 79.5 ± 2.7°). Moreover, phenytoin is a highly crystalline compound with a T_m of 298.6 ± 0.4 °C, which does not decompose prior to its melting point (see Fig. 4) (Nokhodchi et al., 2003 and Thakur and Gupta, 2006).

3.2. Preparation and characterization of the nano-suspensions

For the production of the nano-suspension media milling (MM) was applied. During the MM-process, the most important process parameters are number and size of the milling pearls, the milling speed, time and temperatures, and the drug loading (Merisko-Liversidge et al., 2003). Clearly, a high number of small milling pearls generated the re-

quired number of contact points and, therefore, the required kinetic energy. Typically, the size of nano-milling pearls is 0.5 mm and the amount of pearls is quite high (10–50% of the weight/volume of the pre-suspension (Peltonen and Hirvonen, 2010)). In this study, a 500 ml milling bowl was used (Retsch GmbH, Haan, Germany); 60% of the bowl volume was filled with milling pearls and one-third with the suspension (i.e., 2.4:1 (w/w)). A milling speed of 250 rpm was applied and a milling time of 24 h was chosen. All experiments were carried out at ambient temperatures to prevent physical modifications of the API due to thermal stresses. Concerning the API-load of the nano-suspensions, in the literature the typical amount of the drug in the milling chamber ranges from 2 to 30% (w/w) (Peltonen and Hirvonen, 2010). Preliminary studies (data not shown) indicated that 16% (w/w) of phenytoin (i.e., nano-suspension formulation of 4:20:1 of API:water:stabilizer) was most appropriate, resulting in smallest particles and suitable milling times.

All obtained nano-suspensions were characterized with regard to their Z-average, PdI, zeta potential, and physical long-term stability. Additionally, electron microscopic investigations, SWAXS- and DSC-studies were conducted in order to establish differences in the nano-crystal formation and chemical composition of the formulations. Nano-suspensions were classified as stable when their Z-average was constant after four weeks of storage. Therefore, no agglomeration followed by sedimentation and phase separation was expected to occur during the stability studies. The results of the characterization are shown in Table 1.

Table 1. *Z-average [d.nm], PdI, zeta potential [mV] and physical stability of nano-suspensions.*

Formulation	Z-average [d.nm]	PdI	Zeta potential [mV]	Stability
MM_KIR	624 ± 6	0.34 ± 0.05	−7.8 ± 0.2	Stable; 854 ± 29 nm after 4 weeks of storage
MM_P20	6347 ± 2037	0.62 ± 0.33	−N.D.[a]	Unstable immediately after production
MM_P80	335 ± 6	0.31 ± 0.01	−18.3 ± 0.4	Stable; 429 ± 5 nm after 4 weeks of storage
MM_KP188	1224 ± 18	0.39 ± 0.01	−8.6 ± 0.3	Unstable after 2 days of storage

[a] Non-determinable

The smallest particle size was obtained for nano-suspensions stabilized with P80 (Z-average = 335 ± 6 nm). To quantify the size distribution, the PdI values were measured.

According to the literature, PdI values ≤0.5 indicate reliability of the measurements, whereas a high PdI (1 being the maximum) indicates invalid results with a broad size distribution of indefinite shape (Müller and Schuhmann, 1996). As can be seen in Table 1all suspensions had PdI values ≤0.5, except MM_P20. During the MM process, significant foaming occurred and a broad particle size distribution was obtained. The particles agglomerated, resulting in high PdI values.

The zeta potential of all obtained nano-suspensions stabilized with the different stabilizers was analyzed in bi-distilled water with an adjusted conductivity of 50 µS/cm to minimize ionic effects and to measure potential differences in the surface charge of nano-particles (Müller, 1996). In general, the zeta potential depends on the class and concentration of the stabilizer. According to the literature (Müller and Jacobs, 2002 and Müller, 1996), a zeta potential of at least ± 20 mV is required for a stable system. Nano-suspensions stabilized via P80 generated the best results (−18.3 ± 0.4 mV).

The principle quality criterion for processing-related considerations is that the system is stable for at least four weeks without sedimentation and/or significant particle growth due to agglomeration (see Table 1). Thus, samples were stored in a refrigerator for four weeks at 5 ± 3 °C and characterized via PCS and LDME (data not shown) on a weekly basis. Sufficient stability was only achieved in the case of nano-suspensions stabilized with P80 and KIR. The MM-prepared P80-stabilized particles showed the lowest Z-average (i.e., 335 ± 6 nm to 429 ± 5 nm after 4 weeks) with a PdI of 0.31 ± 0.01, and a relatively high zeta potential of −18.3 ± 0.4 mV, and were thus used for the nano-extrusion experiments.

3.3. Crystalline structure of bulk phenytoin versus the nano-suspensions

Since the crystalline structure of a drug may be affected by milling, SWAXS measurements were conducted, and Bragg peaks of bulk phenytoin as well as air-dried nano-suspensions were examined (Fig. 2). Bulk phenytoin had crystallinity Bragg peaks in the angular WAXS region at 4.88, 4.60, 4.42, 4.37, 3.98, 3.91, 3.47, 3.43, and 3.34 Å. Bragg peaks of the bulk material and of the air-dried nano-suspension had the same peak positions, indicating that no changes in crystallinity, amorphization or degradation of the API occurred during nano-sizing.

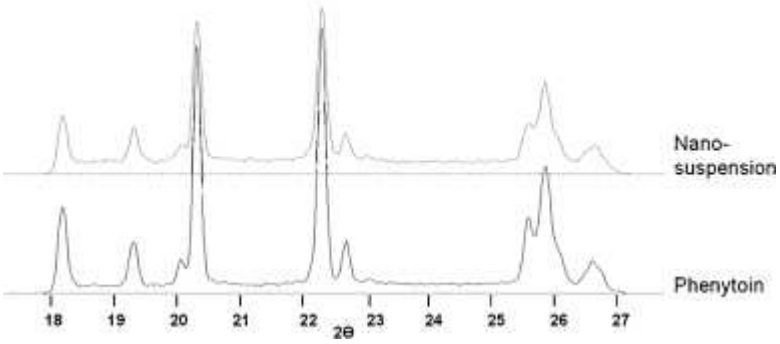

Fig. 2. *WAXS spectra of bulk-phenytoin and air-dried nano-suspension.*

TEM and analytical TEM (ATEM) measurements were performed to obtain a comprehensive chemical and morphological description of bulk-phenytoin, the phenytoin nano-suspension and solid phenytoin nano-extrudates. The bulk material resulted in two distinct shapes, (i) hexagons and (ii) ellipsoids (Fig. 3A and B). The nano-sized phenytoin crystals stabilized by P80 showed a distinct hexagonal shape with a tendency to extend along one axis. It was found that nitrogen and silicium were present in the crystals and oxygen mostly in the periphery (Fig. 4). Thus, it can be assumed that oxygen corresponds to the P80 ($C_{64}H_{124}O_{26}$) coating of the phenytoin nano-crystals. Moreover EDXS spectra were recorded to have a reference for verifying nano-crystals within the polymeric matrix and to identify/verify the full set of chemical elements of phenytoin and nano-phenytoin (see Fig. 3C and F), mainly consisting of carbon (CK) and oxygen (OK). Since the energy resolution of the EDX detector (HPGe detector with a solid angle of 0.13 sr) is not sufficient enough to resolve N peak between C and O, N and C peaks were visible as one (independently of C and N concentration).

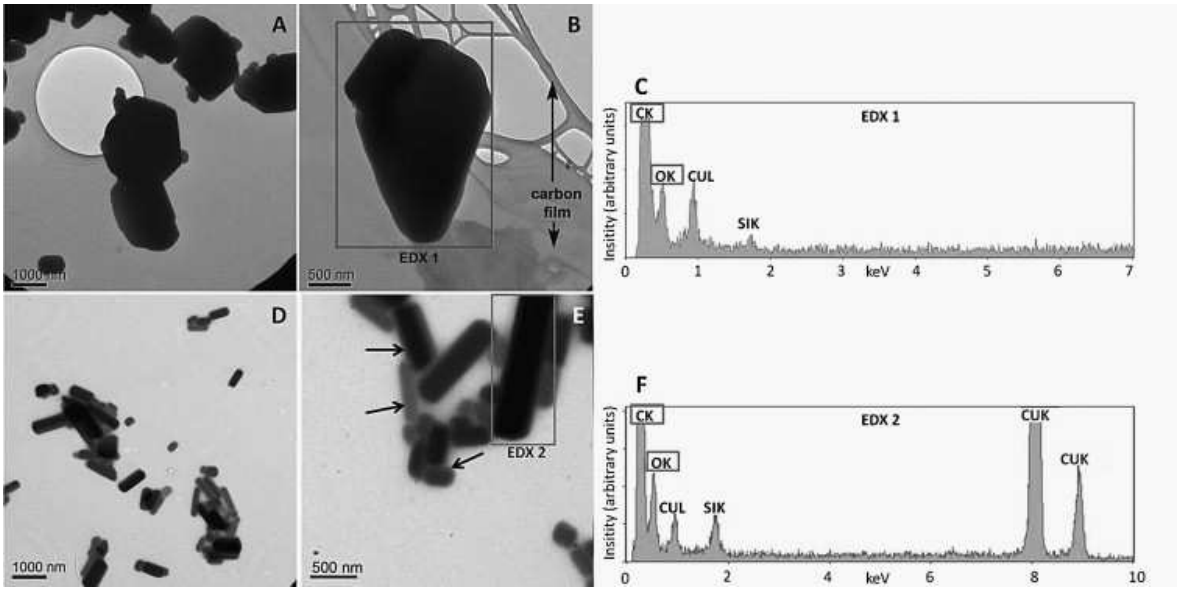

Fig. 3. *Analytical TEM images of the bulk-phenytoin crystals (A and B) and the nano-suspension (D and E). Arrows in image E indicate dense coating of the nano-crystals with the stabilizer P80. Images (C) and (F) show EDXS spectra obtained from the EDX 1 and 2 areas (marked as frames in B and E). Carbon (CK) and oxygen (OK) present the main chemical elements of the drug; copper (CUL, CUK) and silicium (SIK) originate from sample preparation.*

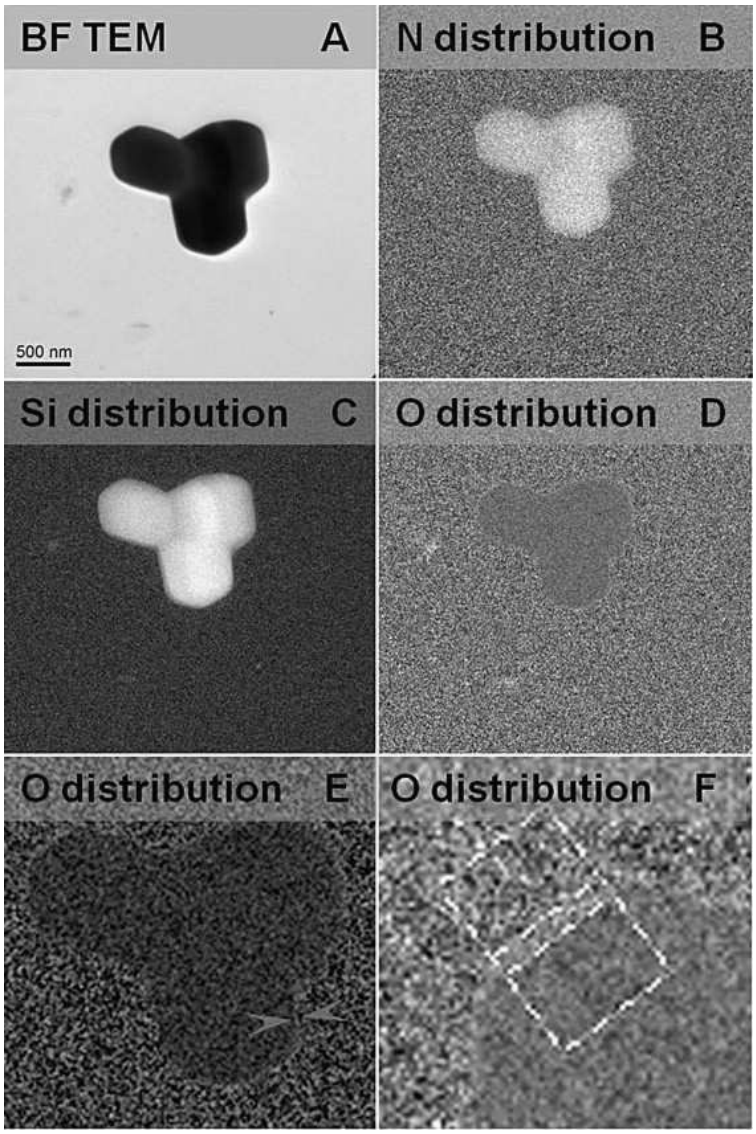

Fig. 4. *Image (A) is a bright field (BF) TEM image of the nano-crystals and images (B–F) are chemical analyses of the visualized nano-crystals via energy filtered TEM (EFTEM): (B) nitrogen- (N), (C) silicium- (Si) and (D–F) oxygen (O)-distribution. (E) Arrows indicate oxygen-rich regions. Image (F) is a magnification of (D) and (E).*

3.4. Preparation and characterization of nano-extrudates

The basic concept of the NANEX process is to produce continuously solid nano-formulations in a single step by embedding stabilized nano-crystals homogeneously in a molten matrix. These solid nano-formulations should have an increased dissolution rate due to an increase in the effective particle surface area. Most importantly, the NANEX process reduces time and costs both in process development and manufacturing.

In previous work, experiments were performed in a ZSK Mc18 modular co-rotating twin-screw extruder with a screw diameter of 18 mm (Coperion GmbH, Stuttgart, Germany). Titanium dioxide nano-particles were embedded in a de-aggregated form in the matrix material (Soluplus®) (Khinast et al., 2013). In this work, organic APIs were used and a

larger, industrial-scale extruder was chosen, i.e., experiments were performed in the MICRO 27 GL modular twin-screw extruder (Leistritz Extrusionstechnik GmbH, Nürnberg, Germany) with a screw diameter of 27 mm. This required scale up of the feeders for solid materials (i.e., the matrix) and for the nano-suspension.

The scale-up factor of $3 = (27/18)^2 \times 1020/764$ was calculated by assuming that the throughput was proportional to the free volume of the extruder (i.e., proportional to the square of the screw diameter D^2 and the length L), resulting in a throughput of approximately 1.7 kg/h for feeder 1 and 0.25 kg/h for feeder 2. Based on these calculations, we used 2 kg/h for feeder 1 while applying the same screw speed of 200 rpm. In order to increase the nanoparticle content in the extrudate, we increased the relative amount of the nano-suspension by a factor of 2 and used a feed rate of 0.6 kg/h.

Furthermore, the screw-configuration was modified and designed to yield a stable and robust process (see Fig. 1). In particular, in the feeding section (barrel 1), Soluplus®powder was transferred from a hopper directly into the extruder. The feeding section of the screw had powder conveying elements with a large pitch of 40 mm, which provided the sufficient free volume in order to take in and convey the powder at a desired rate. As shown in Fig. 1, the pitch of the screw elements decreased in the transition zone (barrel 2), which led to a stepwise compaction of the fed matrix material and partial melting in the 100 °C-hot barrel. In the melting zone (barrel 3), kneading elements were used, which provided the required energy input for melting. To generate pressure and to overrun the second section of kneading elements with 60° and 90° offset angles, a conveying element with 20 mm pitch was installed between the kneading elements. As a result, a completely molten matrix material reached the section where the nano-suspension was added via a liquid side feeding device (barrel 4). In the side-feeding zone, the screw had partially filled conveying elements that provided enough free volume to feed the required amount of aqueous API nano-suspensions into the molten mass. It can be expected that the water of the nano-suspension immediately evaporates after entering the 140 °C hot barrel and being in contact with barrel wall and melt. Upon evaporation, the phenytoin nano-crystals remain on the surface of the molten Soluplus®. In the mixing zone (barrels 5–7), various mixing, kneading and conveying elements facilitate a homogenous distribution of the phenytoin nano-crystals in the molten matrix material. In the front (barrel 5), two mixing elements were used that were shaped as conveying elements but had periodical grooves in their flights, allowing more backflow and exchange between adjacent screw channels (i.e., division and merging of material) (Kohlgrüber and Wiedmann, 2008). These were followed by three kneading elements with 60° and 90° offset angle, which enhanced mixing due to dividing and merging (Kohlgrüber and Wiedmann, 2008) and, in the case of the non-conveying 90° element, a pile-up. Between the kneading elements, conveying

elements were arranged to reduce the energy input and to decrease the melt temperature. The pile-up generated by the 90° kneading element also separated the mixing zone from the subsequent degassing (devolatilization) zone. By applying a vacuum of 200 mbar, the water vapor was eliminated (barrel 8). To create a large surface of the conveyed melt for transfer of water vapor and other volatile components into the gas phase, conveying elements with a large pitch of 40 mm were used. Since the filling ratio of these elements was low, the specific surface was increased. In the end section of the extruder (barrel 9), the screw had a conveying element that transported the molten and mixed mass to the outlet and generated the required die pressure. At the outlet, the extrudate solidified, was collected and analyzed in terms of the residual moisture content, the crystalline structure, (nano-) API distribution, aqueous solubility and dissolution characteristics.

The mean residual moisture content of the pure extrudates and the NANEX formulations was determined by Karl Fischer titration. Bulk-extrudates (i.e., no additional water was added) showed a mean residual moisture content of 1.9 ± 0.1% and the nano-extrudates showed a mean residual moisture content of 1.6 ± 0.1%. This demonstrates that the entire water, which was added during the process, was removed.

Since X-ray diffraction cannot detect less than 5–10% of a crystalline content and may fail to detect small-size crystals even if their concentration in the sample is above the limit of detection (Leuner and Dressman, 2000 and Munson, 2009), DSC measurements were conducted to elucidate possible post-extrusion changes in the morphology of phenytoin. In addition, the thermal properties of Soluplus® (i.e., bulk material; 10 K/min, 20 ml/min, 20–350 °C) were investigated. The DSC thermograms of the drug, the matrix material, the nano-suspension and the extrudates are presented in Fig. 5. Pure phenytoin showed sharp melting endotherms at 298.6 ± 0.4 °C with an onset at 296.3 ± 0.1 °C, indicating the crystalline nature of the drug. The DSC curves of pure untreated Soluplus® showed a softening region starting at around 50 °C. In the case of further heating up, a peak that indicates degradation occurred at 317.7 ± 0.1 °C (onset 306.4 ± 0.3 °C). The melting point of the nano-suspension was slightly lower than that of the untreated phenytoin, i.e., 291.7 ± 0.4 °C with an onset at 283.2 ± 0.9 °C. The obtained thermograms of the melt-extruded strands (i.e., bulk- and nano-extrudates) appeared as a sum of the characteristic peaks of the individual components. The softening region starting at around 50 °C, referring to amorphous Soluplus®, was visible in both thermograms. Furthermore, melting endotherms with low intensities (onset at 295.1 ± 0.6 °C for bulk-extrudate and at 291.2 ± 0.2 °C for nano-extrudate) originating from crystalline phenytoin were observed. This implies that the drug remained in its crystalline state. At temperatures above 300 °C, degradation of Soluplus® was observed.

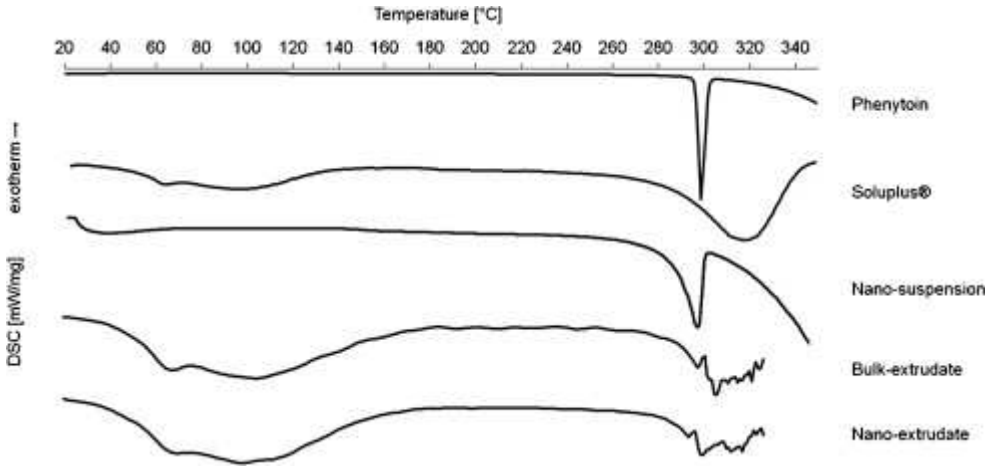

Fig. 5. *DSC thermograms of pure untreated phenytoin and Soluplus®, nano-suspensions and bulk- and nano-extrudates*.

For the analysis of the distribution of phenytoin (nano-) crystals embedded in the Soluplus® matrix two analytical techniques, i.e., TEM and AFM, were used. When applying TEM, the image contrast is formed by sufficiently scattering structures that are present in the 50–70 nm thick area of the section. Since both the phenytoin (nano-) crystals and the Soluplus® matrix mainly consist of the same light elements (C, H, O) that scatter the incident electrons rather weakly, the TEM contrast between them was not specific enough to ensure proper identification. However, the TEM images of both phenytoin extrudates (Fig. 6 A and 6 D) showed that the bulk- as well as the nano-crystals were embedded in a de-aggregated manner. Clearly, the particle sizes differed significantly. For bulk phenytoin a mean particle size of 2.5 µm and for the nano-crystals a mean size of 400 nm was observed. This is in correlation with the primary particle size analyses. The EDXS spectra confirmed that no inorganic impurities were observed (Fig. 6).

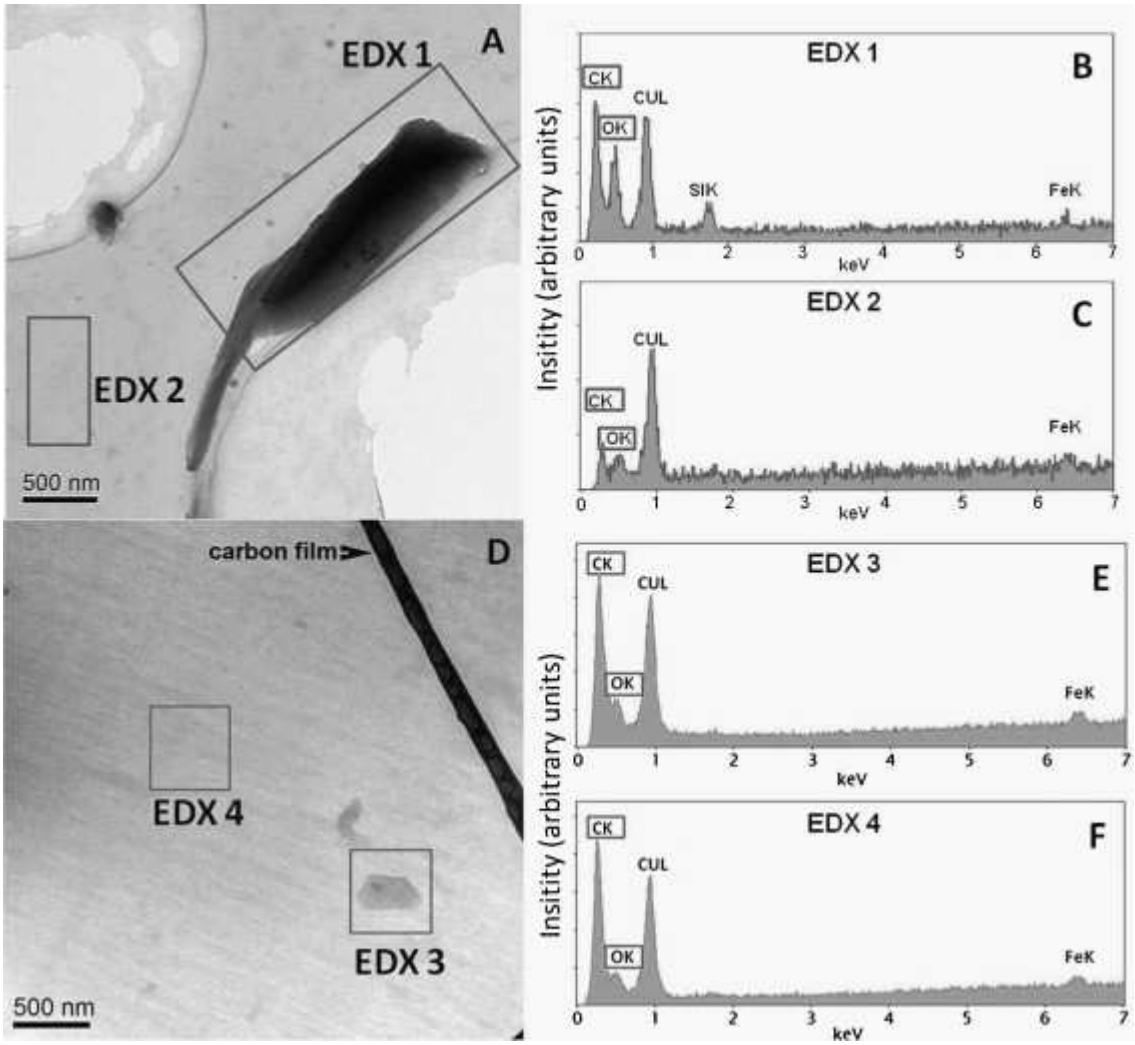

Fig. 6. *Analytical TEM characterization of the solid phenytoin bulk extrudate (A) and nano-extrudate (D). Images (A and D) are zero-loss filtered bright field TEM images of a thin section of the phenytoin/Soluplus® extrudates. Images (B) and (C) show EDXS spectra obtained from the areas EDX 1 (phenytoin crystal) and EDX 2 (Soluplus® matrix), respectively. Images (E) and (F) show EDXS spectra obtained from the areas EDX 3 (phenytoin nano-crystal) and EDX 4 (Soluplus® matrix). (Legend for EDXS spectra (B, C, E and F): CK = carbon, OK = oxygen; CUL = copper and FeK = iron originate from sample preparation)*

Additionally, AFM was applied to investigate nano-extrudates. On the investigated block face surface, macromolecules created a pronounced topographical contrast due to the relaxation of the tension inside the polymer block during or immediately after the sectioning process (see Fig 7). AFM also detects phase shifts, which can be attributed to the different density, hardness and elastic modulus of the materials. Fig. 7A and B reveal that there were denser particles (phenytoin) distributed in the less dense matrix (polymer). Since particles seem to have a hexagonal shape (Fig. 7B) and a chemical composition similar to phenytoin, they can be identified as phenytoin nano-crystals embedded in the Soluplus® matrix. Only a few particles were seen in both images because only small parts of the samples can be imaged by AFM and TEM. In addition, the crystal sizes in the AFM

image differed from the TEM micrographs, which was due to the fact that the nano-crystals (in the matrix) showed a random orientation and that the microtome knife split the crystals into smaller fragments. However, both methods confirmed the presence of nano-phenytoin in the polymer indicating that the API was not solubilized in the matrix.

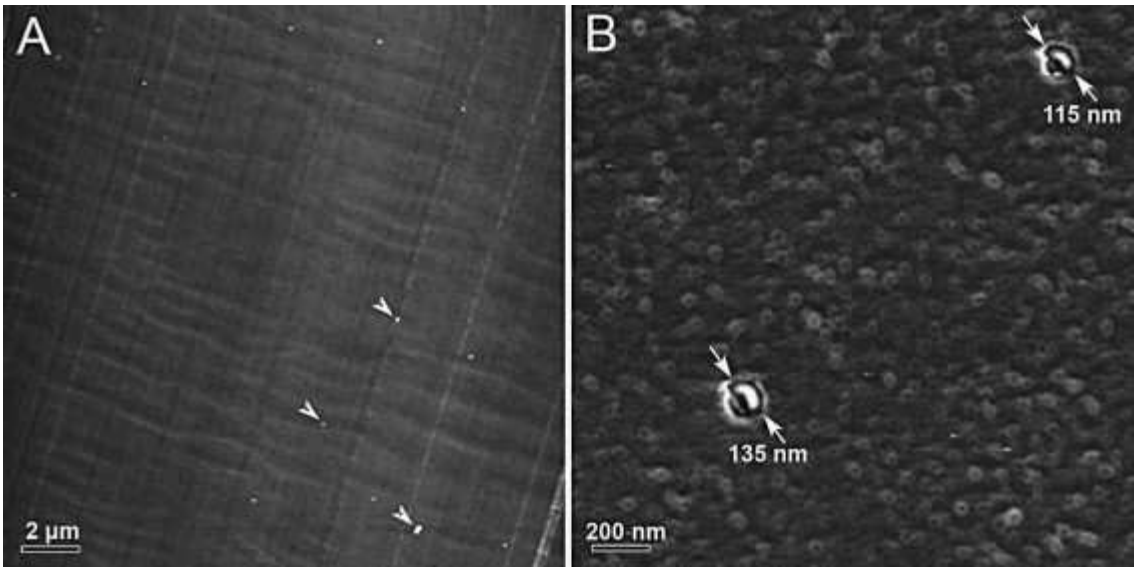

Fig. 7. *AFM characterization of the solid phenytoin nano-extrudate material. (A) topographical (height) image of a cross section of the phenytoin/Soluplus® nano-extrudate. (B) AFM phase image of the block face of the same samples. Interaction of the AFM tip with harder materials led to a larger positive frequency and phase shift (white regions) than with a soft material (dark region). White arrows indicate the phenytoin nano-crystals incorporated into the Soluplus® matrix.*

Next, the aqueous solubility (24–96 h) and in-vitro dissolution studies (considering sink conditions: C_s in 0.05 M Tris buffer = 100.6 ± 0.9 µg/ml) of the pure substances/mixtures and the extrudates were performed, to carefully investigate which parameters impact the release behavior. A significant increase in the solubility (Table 2; $p < 0.05$) of phenytoin formulated as a nano-suspension and later as a nano-extrudate was observed. Compared with the bulk-phenytoin powder, phenytoin nano-crystals showed a significant increase in solubility by a factor of 2.1. Specifically, untreated phenytoin had a solubility of 11.5 ± 0.8 µg/ml (after 24 h). Over the same period of time, a concentration of 23.6 ± 0.6 µg/ml was achieved for the nano-crystals. To assess whether the increase of the solubility is only a function of the stabilizer, we performed in-vitro dissolution studies of the bulk phenytoin and the nano-suspension in 0.05 M Tris buffer comprising 1% (w/v) stabilizer. The results showed that regarding bulk phenytoin 45.6% ± 4.3 of the drug dissolved after 10 min and the concentration did not significantly increase with increasing time (Fig. 8). In contrast, the drug release of the nano-suspension was markedly enhanced – after 5 min the entire drug was dissolved. This implies that although the stabi-

lizer impacts the solubility of the drug due to increased wetting of the material and solubilization (Kawakami et al., 2006), the reduced particle size increases the “kinetic” solubility. This is also in accordance with Müller et al., 1999b (Müller and Akkar, 2004) and Keck et al. (Keck and Müller, 2006), who reported that the higher solubility of nano-suspensions is actually a “kinetic” solubility (which is higher than the “thermodynamic equilibrium solubility” of particles <2 µm).

Table 2. *Aqueous solubility of untreated phenytoin, phenytoin nano-suspension, phenytoin bulk extrudates and phenytoin nano-extrudates (24–96 h).*

	Aqueous solubility ± SD [µg/ml]		Increase in aqueous solubility (24 h)
	24 h	96 h	
Bulk-phenytoin	11.5 ± 0.8	10.8 ± 0.1	
Phenytoin nano-suspension	23.6 ± 0.6	20.5 ± 0.6	2.1-fold higher compared to bulk material
Phenytoin bulk-extrudate	1737.5 ± 116.7	2352.9 ± 174.4	150-fold higher compared to bulk material
Phenytoin nano-extrudate	2112.8 ± 181.2	2709.2 ± 66.2	184-fold higher compared to bulk material

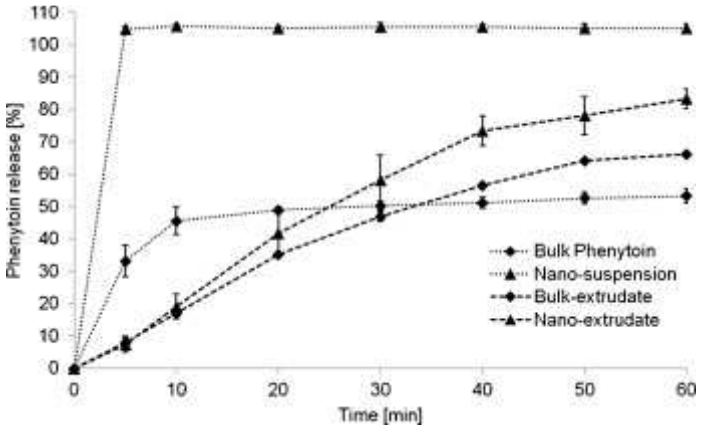

Fig. 8. *In vitro drug release profiles from bulk phenytoin, phenytoin nano-suspension, phenytoin bulk-extrudate and phenytoin nano-extrudate in 0.05 M Tris buffer (pH 7.5) over 1 h. Mean values ± SD (*n = *3).*

Apart from the stabilizer the matrix polymer is likely to impact the solubility of the drug. Soluplus® is a graft co-polymer well known for enhancing the solubility of poorly-soluble BCS Class II and IV APIs (Kolter et al., 2012). The results of the solubility experiments (see Table 2) showed that nano-sized phenytoin embedded in Soluplus® had a 184-fold

higher solubility than bulk-phenytoin. The concentration of dissolved phenytoin after 24 h in water was 2112.8 ± 181.2 µg/ml (nano-extrudates). Additionally, extrudates containing untreated phenytoin crystals were prepared and tested for solubility. The results indicated that the aqueous solubility of phenytoin from bulk-extrudates was 1737.5 ± 116.7 µg/ml which was 1.2-fold lower compared to the nano-extrudates and did not significantly change over a period of 96 h (see Table 2). Comparing the in-vitro release profiles of the extrudates (see Fig. 8), it was demonstrated that Soluplus® formed a gelous layer at pH 7.5, resulting in a decreased release of the bulk, as well as the nano-sized phenytoin due to encapsulation of the drug (Terife et al., 2012). However, extrudates comprising nano-crystals showed a markedly higher and faster release profile compared to bulk-extrudates (83.4 ± 3.0% and 66.3 ± 0.8%, respectively; see Fig. 8). The release rate was 1.3-fold increased, which is in accordance with the results of the solubility studies.

In summary, the results clearly show that the increase in the solubility is a function of the stabilizer and the matrix material. However, particle size strongly determines the kinetic solubility and thus, causes a faster and higher dissolution rate. These data agree with the Ostwald–Freundlich equation and the Kelvin equation (Beckman and Ames, 1998,Nyström and Bisrat, 1988 and Torrado et al., 1998).

4. Conclusions

To handle poorly soluble and/or degradation-prone molecules and to replace cost-and time intensive conventional multi-step processes, the pharmaceutical industry requires new, safe and efficient strategies that combine existing conventional know how with innovative drug delivery knowledge and novel processing methods. In this context, manufacturing techniques, where a complex product is produced continuously are of significant interest. In this study, a continuous hot melt extrusion process was tailored and its capability was demonstrated to produce a product encompassing dispersion of nano-particles in a polymer matrix in a single processing unit.

Stabilized nano-suspensions were prepared via MM and directly embedded via liquid side feeding in a molten polymer in a single process step. Devolatilization of the residual water was performed and the nano-crystals were de-aggregated distributed in the Soluplus® matrix. No changes in the crystalline structure were detected. As expected, upon contact with water, an enhanced aqueous solubility was observed. Apart from solubilizing effects of the stabilizer and the used matrix polymer, particle size impacted the kinetic solubility of the drug.

Thus, NANEX proves to be a promising platform technology for making solid nano-formulations in a single step, thereby improving solubility and bioavailability of the drug and enhancing patient compliance.

Acknowledgments

This work was funded through the Austrian COMET Program by the Austrian Federal Ministry of Transport, Innovation and Technology (BMVIT), the Austrian Federal Ministry of Economy, Family and Youth (BMWFJ) and by the State of Styria (Styrian Funding Agency SFG).

The authors thank Leistritz Extrusionstechnik GmbH (Nürnberg, Germany) for providing the equipment and the extrusion team of the RCPE GmbH, Graz, Austria, for their assistance with the hot melt extrusion process. We furthermore acknowledge Bruker (Bruker AXS, Karlsruhe, Germany) for support with the SWAXS measurement system.

References

Beckman, K.B., Ames, B.N., 1998. The free radical theory of aging matures. Physiol. Rev. 78, 547–581. http://www.ncbi.nlm.nih.gov/pubmed/9562038.

Chingunpituk, J., 2011. Nanosuspension technology for drug delivery. Walailak J. Sci. Technol. 4, 139–153.

Crowley, M.M., et al., 2007. Pharmaceutical applications of hot-melt extrusion: part I. Drug Dev. Ind. Pharm. 33, 909–926. http://www.ncbi.nlm.nih.gov/pubmed/ 17891577.

Fasano, A., 1998. Innovative strategies for the oral delivery of drugs and peptides. Trends Biotechnol. 16, 152–157.

Kawakami, K., et al., 2006. Solubilization behavior of a poorly soluble drug under combined use of surfactants and cosolvents. Eur. J. Pharm. Sci. 28, 7–14. doi: http://dx.doi.org/10.1016/j.ejps.2005.11.012.

Kayaert, P., Van den Mooter, G., 2012. Is the amorphous fraction of a dried nanosuspension caused by milling or by drying? A case study with Naproxen and Cinnarizine. Eur. J. Pharm. Sci. 81, 650–656. doi:http://dx.doi.org/10.1016/j. ejpb.2012.04.020.

Keck, C.M., Müller, R.H., 2006. Drug nanocrystals of poorly soluble drugs produced by high pressure homogenisation. Eur. J. Pharm. Biopharm. 62, 3–16. doi:http:// dx.doi.org/10.1016/j.ejpb.2005.05.009.

Kesisoglou, F., et al., 2007. Nanosizing-oral formulation development and biopharmaceutical evaluation. Adv. Drug Deliv. Rev. 59, 631–644. doi:http:// dx.doi.org/10.1016/j.addr.2007.05.003.

Khinast, J., et al., 2013. Nano-extrusion: a one-step process for manufacturing of solid nanoparticle formulations directly from the liquid phase. AAPS PharmSciTech doi:http://dx.doi.org/10.1208/s12249-013-9946-0.

Kohlgrüber, K., Wiedmann, W., 2008. Co-Rotating Twin-Screw Extruders - Fundamentals, Technology, and Applications. Carl Hanser Verlag GmbH & CO., KG.

Kolter, K., et al., 2012. Hot-Melt Extrusion with BASF Pharma Polymers. BASF SE, Pharma Ingredients & Services, 67056 Ludwigshafen, Germany.

Leuner, C., Dressman, J., 2000. Improving drug solubility for oral delivery using solid dispersions. Eur. J. Pharm. Biopharm. 50, 47–60 Retrieved from http://www. ncbi.nlm.nih.gov/pubmed/10840192.

Liversidge, G., & Cundy, K. (1992). Surface modified drug nanoparticles. US Patent 5,145,684.

Merisko-Liversidge, E., et al., 2003. Nanosizing: a formulation approach for poorly- water-soluble compounds. Eur. J. Pharm. Sci. 18, 113–120.

Möschwitzer, J., et al., 2004. Development of an intravenously injectable chemically stable aqueous omeprazole formulation using nanosuspension technology. Eur. J. Pharm. Biopharm. 58, 615–619. doi:http://dx.doi.org/10.1016/j.ejpb.2004.03.022.

Müller, R.H., et al., 1999. Nanosuspensions: formulations for poorly soluble drugs with poor bioavailability. Pharm. Ind. 61, 175–178.

Müller, R.H. et al. (1999). Pharmaceutical nanosuspensions for medicament administration as systems with increased saturation solubility and rate of solution. US Patent 5858,410.

Müller, R.H., et al., 2001. Nanosuspensions as particulate drug formulations in therapy. Rationale for development and what we can expect for the future. Adv. Drug Deliv. Rev. 47, 3–19.

Müller, R.H., 1996. Zetapotential und Partikelladung in der Laborpraxis. Wissenschaftliche Verlagsgesellschaft mbH, Stuttgart.

Müller, R.H., Akkar, A., 2004. Drug nanocrystals of poorly solible drugs. Encycl. Nanosci. Nanotechnol. 2, 627–638.

Müller, R.H., Jacobs, C., 2002. Buparvaquone mucoadhesive nanosuspension: preparation, optimisation and long-term stability. Int. J. Pharm. 237, 151–161 Retrieved from http://www.ncbi.nlm.nih.gov/pubmed/11955813.

Müller, R.H., Peters, K., 1998. Nanosuspensions for the formulation of poorly soluble drugs: I: preparation by a size-reduction technique. Int. J. Pharm. 160, 229–237.

Müller, R.H., Schuhmann, R., 1996. Teilchengrößenbestimmung in der Laborpraxis. Wissenschaftliche Verlagsgesellschaft mbH, Stuttgart.

Munson, E.J., 2009. Analytical techniques in solid-state characterization, In Developing Solid Oral Dosage Forms: Pharmaceutical Theory And Practice. 1st ed. Oxford: Elsevier, pp. 61–74.

Nokhodchi, A., et al., 2003. Crystal modification of phenytoin using different solvents and crystallization conditions. Int. J. of Pharm. 250, 85–97 Retrieved from http://www.ncbi.nlm.nih.gov/pubmed/12480275.

Nyström, C., Bisrat, M., 1988. Physicochemical aspects of drug release: VIII. The relation between particle size and surface specific dissolution rate in agitated suspensions. Int. J. Pharm. 47, 223–231.

Pardeike, J., et al., 2011. Nanosuspensions as advanced printing ink for accurate dosing of poorly soluble drugs in personalized medicines. Int. J. Pharm. 420, 93– 100. doi:http://dx.doi.org/10.1016/j.ijpharm.2011.08.033

Patil, S., Wagh, K., 2011. Strategies for solubility enhancement of poorly soluble drugs. Int. J. Pharm. Sci. Rev. Res. 8, 74–80 Retrieved from http://www.globalresearchonline.net/journalcontents/volume8issue2/Article-013 pdf.

Patravale, V., et al., 2004. Nanosuspensions: a promising drug delivery strategy. J. Pharm. Pharmacol. 56, 827–840. doi:http://dx.doi.org/10.1211/0022357023691.

Paudel, A., et al., 2013. Manufacturing of solid dispersions of poorly water soluble drugs by spray drying: formulation and process considerations. Int. J. Pharm. 453, 253–284. doi:http://dx.doi.org/10.1016/j.ijpharm.2012.07.015.

Peltonen, L., Hirvonen, J., 2010. Pharmaceutical nanocrystals by nanomilling: critical process parameters, particle fracturing and stabilization methods. J. Pharm. Pharmacol. 62, 1569–1579. doi:http://dx.doi.org/10.1111/j. 2042– 7158.2010.01022. x.

Rabinow, B.E., 2004. Nanosuspensions in drug delivery. Nat. Rev. Drug. Disc. 3, 785–796. doi:http://dx.doi.org/10.1038/nrd1494.

Radl, S., et al., 2010. A novel design for hot-melt extrusion pelletizers. Chem. Ing. Sci. 65, 1976–1988. doi:http://dx.doi.org/10.1016/j.ces.2009.11.034.

Roblegg, E., et al., 2011. Development of sustained-release lipophilic calcium stearate pellets via hot melt extrusion. Eur. J. Pharm. Biopharm. 79, 635–645. doi:http://dx.doi.org/10.1016/j.ejpb.2011.07.004.

Shah, S., et al., 2012. Melt extrusion with poorly soluble drugs. Int. J. Pharm. 001, 1– 20. doi:http://dx.doi.org/10.1016/j.ijpharm.2012.11.001.

Terife, G., et al., 2012. Hot melt mixing and foaming of Soluplus1and indomethacin. Polym. Eng. Sci. 52, 1629–1639. doi:http://dx.doi.org/10.1002/pen.23106.

Thakur, R., Gupta, R.B., 2006. Formation of phenytoin nanoparticles using rapid expansion of supercritical solution with solid cosolvent (RESS-SC) process. Int. J. Pharm. 308, 190–199. doi:http://dx.doi.org/10.1016/j.ijpharm.2005.11.005.

Torrado, G., et al., 1998. Process-induced crystallite size and dissolution changes elucidated by a variety of analytical methods. Int. J. Pharm. 166, 65–73.

Treffer, D., et al., 2013. Hot melt extrusion as a continuous pharmaceutical manufacturing process. In: Repka, M.A., Langley, N., Dinunzio, J.C. (Eds.), Melt Extrusion: Materials, Technoloy and Drug Product Design, , pp. 363–396 Retrieved from http://scholar.google.com/scholar?hl=en&btnG&9552;Search&-q=intitle:AAPS+Advances+in+Pharmaceutical+Sciences+Series#6.

Treffer, D., et al., 2014. In-line implementation of an image-based particle size measurement tool to monitor hot-melt extruded pellets. Int. J. Pharm. 466, 181– 189. doi:http://dx.doi.org/10.1016/j.ijpharm.2014.03.022.

Van Eerdenbrugh, B., et al., 2008. Top-down production of drug nanocrystals: nanosuspension stabilization, miniaturization and transformation into solid products. Int. J. Pharm. 364, 64–75. doi:http://dx.doi.org/10.1016/j. ijpharm.2008.07.023.

Van Eerdenbrugh, B., et al., 2009. A screening study of surface stabilization during the production of drug nanocrystals. J. Pharm. Sci. 98, 2091–2103. doi:http://dx.doi.org/10.1002/jps.

Verma, R., Garg, S., 2001. Current status of drug delivery technologies and future directions. Pharm. Tech. 25, 1–14 Retrieved from http://www.pharmanet.com.br/pdf/drugdelivery.pdf.

4. NANEX: process design and optimization

Ramona Baumgartner [a], Josip Matić [a,b], Simone Schrank [c], Stephan Laske [a], Johannes Khinast [a,b], Eva Roblegg [a,c*]

[a] *Research Center Pharmaceutical Engineering GmbH, Inffeldgasse 13, 8010 Graz, Austria*

[b] *Institute for Process and Particle Engineering, Graz University of Technology, Inffeldgasse 13, 8010 Graz, Austria*

[c] *Institute of Pharmaceutical Sciences, Department of Pharmaceutical Technology, University of Graz, Universitätsplatz 1, 8010 Graz, Austria*

* Corresponding author at: Institute of Pharmaceutical Sciences, Department of Pharmaceutical Technology, University of Graz, Universitätsplatz 1, 8010 Graz, Austria. Tel.: +43 316 380 8888.

Published in: International Journal of Pharmaceutics 506 (2016) 35-45.
DOI: 10.1016/j.ijpharm.2016.04.029

Abstract

Previously, we introduced a one-step nano-extrusion (NANEX) process for transferring aqueous nano-suspensions into solid formulations directly in the liquid phase. Nano-suspensions were fed into molten polymers via a side-feeding device and excess water was eliminated via devolatilization. However, the drug content in nano-suspensions is restricted to 30 % (w/w), and obtaining sufficiently high drug loadings in the final formulation requires the processing of high water amounts and thus a fundamental process understanding. To this end, we investigated four polymers with different physicochemical characteristics (Kollidon® VA64, Eudragit® E PO, HPMCAS and PEG 20000) in terms of their maximum water uptake/removal capacity. Process parameters as throughput and screw speed were adapted and their effect on the mean residence time and filling degree was studied. Additionally, one-dimensional discretization modeling was performed to examine the complex interactions between the screw geometry and the process parameters during water addition/removal. It was established that polymers with a certain water miscibility/solubility can be manufactured via NANEX. Long residence times of the molten polymer in the extruder and low filling degrees in the degassing zone favored the addition/removal of significant amounts of water. The residual moisture content in the final extrudates was comparable to that of extrudates manufactured without water.

Graphical abstract

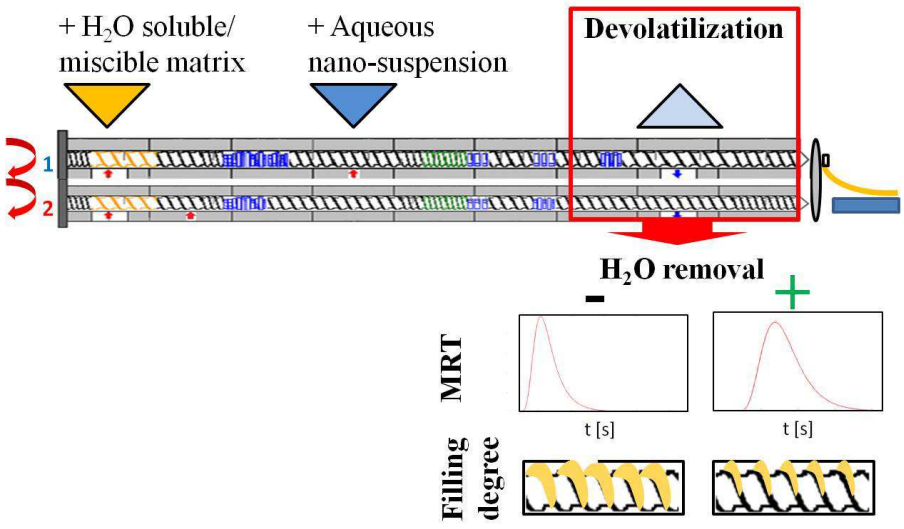

Keywords

One-step nano-extrusion process; NANEX design and optimization; Screw configuration; Water integration capacity; Mean residence time; Devolatilization

1. Introduction

Among the various routes for drug administration, oral administration with intestinal absorption is by far the most common one [1]. However, oral drug delivery is often associated with numerous obstacles, such as pH-variations, enzymatic conditions and selective barrier properties, which may either lead to degradation and inactivation of active pharmaceutical ingredients (APIs) or prevent their absorption [2]–[5]. Apart from the physiological conditions, the physicochemical properties of the administered drug may dictate whether it reaches systemic circulation [4]. Only dissolved molecules can diffuse across membranes. Thus, poorly soluble/permeable drugs are expected to have a low drug efficacy [6], [7]. Notably, nearly a third of APIs listed in the United States Pharmacopeia and about 70% of potentially effective molecules in the pipeline of pharmaceutical companies have physicochemical characteristics that are unfavorable for passing the gastrointestinal barriers [8]. In order to solve this problem, scientists have increasingly developed strategies for improving drug solubility/permeability [4], [11].

In the past decade, nano-technology has generated much research interest [57]. Nano-sizing of a material results in a larger specific surface area and a decreased hydrodynamic boundary layer thickness (comparable with the particle`s diameter), promoting higher dissolution rates [58], [59], [149]. Moreover, the apparent solubility of nano-sized materials is increased due to the increased energy level of surface molecules. Particle size reduction can be achieved via top-down (i.e., breakage of large particles into nano-crystals, such as NanoCrystal® [69], [70] and DissoCubes™ [65], [75], [79] technologies) or bottom-up (i.e., nano-particles are formed from molecules via, e.g., precipitation) methods [65], [69], [86], [150]–[153]. Generally, these preparation techniques are applied in the liquid phase, resulting in so-called nano-suspensions. To prevent nano-particles from agglomeration, stabilizing agents (i.e., polymers and/or surfactants) are added [57], [64], [71], [82]–[86]. However, since sedimentation and/or crystal growth over time limits the long-term stability of nano-suspensions [93], [94], they are often transferred into more stable solid oral dosage forms [57], [82]. For this purpose, freeze- and spray-drying with a subsequent compression of the dry intermediate into tablets is commonly used [82], [93], [95]–[100]. Alternatively, nano-suspensions can be layered onto an appropriate core material via fluidized bed granulation or spray-layering prior to compression into tablets or filling into capsules. Moreover, nano-suspensions may be directly layered onto the tablets (Rapamune®) [57], [101]–[103]. Nevertheless, due to the multiple processes involved, these approaches are time-consuming and cost-intensive [111]. In addition, a continuous implementation is hard to achieve. Recently, inkjet and flexographic printing technologies created new opportunities for a flexible and continuous production of solid nano-formulations, with nano-suspensions printed on substrates for (intra-)oral administration

[104]–[112]. Yet the process is often restricted to low-viscosity fluids, and the drug dose that can be deposited on such substrates is limited, which makes this technology only attractive for low-dose drugs.

To overcome such dosing problems, we developed a nano-extrusion (NANEX) process, which converts stabilized aqueous nano-suspensions directly into solid formulations in a continuous way [147], [154]. This is achieved via feeding of a nano-suspension directly into a hot melt extruder and removing the water (of the suspension) from the molten polymer via devolatilization. This one-step process allows not only the handling of poorly soluble drugs but also provides precise control of product quality and increased manufacturing capacity. However, the API content in an aqueous nano-suspension is restricted to about 30 % (w/w) [153]. Thus, to reach sufficiently high API loadings, addition (integration) and removal of significant water amounts (stemming from the nano-suspension) must be possible.

In previous studies we used the NANEX process for the preparation of nano-extrudates based on the co-polymer Soluplus® [147], [154]. In an attempt to extend the NANEX process to a number of different matrix materials we evaluated several polymers with regard to their maximum water integration and removal capacity, considering such process parameters as throughput and screw speed. To this end, four matrix materials i.e., Kollidon® VA64, Eudragit® E PO, AQOAT® (hypromellose acetate succinate, HPMCAS) and poly(ethylene glycol) 20000 (PEG 20000), which are commonly used as excipients in hot melt extrusion [5], [12], [155]–[164], were selected. In addition to the experimental studies, one-dimensional (1D) modeling was performed based on our novel simulation approach [165]–[168] to achieve a sound understanding of the complex interactions between the screw geometry, the material properties and the operating conditions during the NANEX process.

2. Materials and Methods

Kollidon® VA64, Eudragit® EPO, AQOAT® (hypromellose acetate succinate, HPMCAS) and poly(ethylene glycol) 20000 (PEG 20000) were used as potential matrix materials for the NANEX experiments. To achieve extrudability of HPMCAS, Kolliphor® P188 was added as a plasticizing agent. Ultrapurified water (i.e.; Milli-Q®-water, Millipore S.A.S., Molsheim, France) was used in all experiments.

2.1. NANEX process: experimental set-up

All extrusion experiments were carried out using a MICRO 27 GL co-rotating twin-screw extruder (Leistritz Extrusionstechnik GmbH, Nürnberg, Germany). The barrel had nine

sections (barrel zones), eight of which were temperature controlled and individually heated with electric heaters. Initially, the temperatures of the barrel zones were adapted to the requirements of each matrix material to allow for melting, mixing and extrusion of the pure polymers (see Table 1). Two different screw configurations (SC 1 and SC 2; Table 1 and Fig. 1) were used based on the physicochemical properties of the polymers. Since the integration and removal of water is crucial during the NANEX process, the same experimental conditions were used as previously described [154]. For this, the matrix materials were starve-fed gravimetrically into barrel 1 of the extruder with a K-tron twin-screw feeder (K-tron LLC, Switzerland). Water was added via a side-feeding device (zone 4 or zone 2) with a flow–controlled micro angular gear pump (mzr7205 G, HNP Microsystems GmbH, Germany). The water and volatile components were removed (devolatilization) by applying a vacuum of 200 mbar (i.e., absolute pressure of 800 mbar) in a degassing unit in barrel 8.

Table 1. *Process temperatures of the investigated matrix materials.*

Matrix material	**Barrel temperatures [°C]**								**Die plate temperatures [°C]**		**SC**
	2	**3**	**4**	**5**	**6**	**7**	**8**	**9**	**1**	**2**	
Eudragit® EPO	50	100	100	100	100	100	100	100	105	105	1
HPMCAS/plasticizer	100	150	140	140	140	140	145	145	155	175	1
Kollidon® VA64	100	150	140	140	140	140	145	145	150	155	1
PEG 20000	55	60	65	70	70	65	60	50	58	58	2

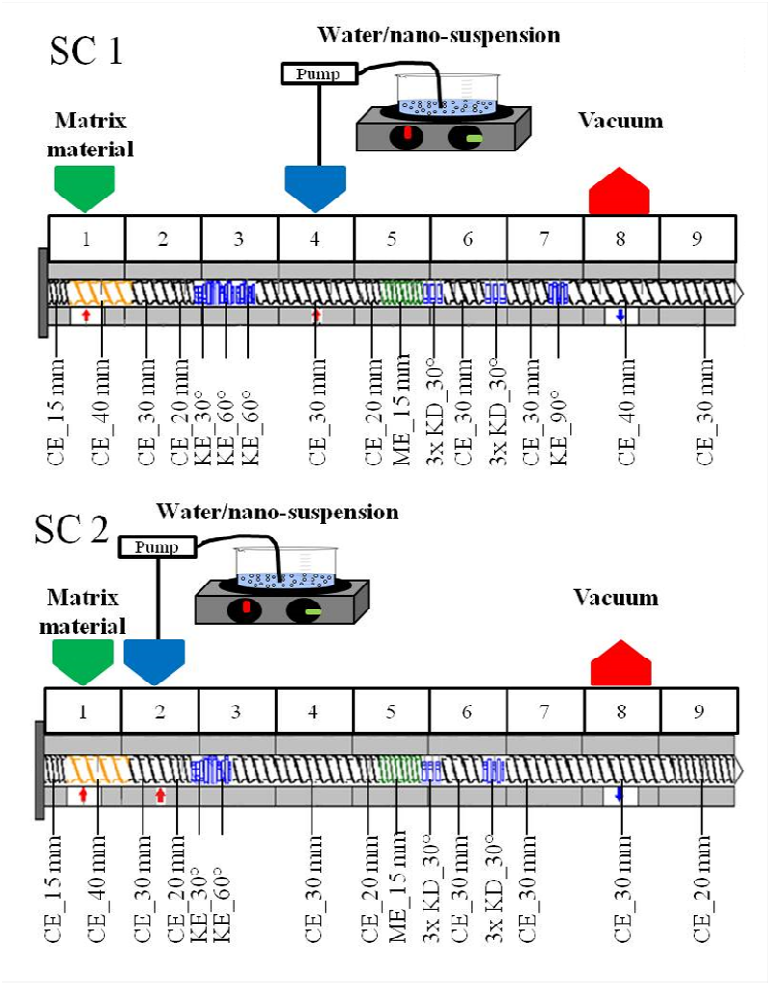

Fig. 2. *Schematic of the experimental set-up for screw configurations (SC) 1 and 2. CE= conveying element; KE= kneading element; ME= mixing element; 40, 30, 20 mm = pitch of conveying and mixing elements; and 30, 60, 90°= offset angles of kneading elements.*

Each matrix material was processed using six sets of process conditions, i.e., various screw speeds and throughputs (see Table 2), which theoretically result in different mean residence times (MRTs) and filling degrees. For a better overview, the predefined sets of process parameters were assigned to two groups: group one for high throughputs and high screw speeds (i.e., 2 kg/h at 400 rpm, 4 kg/h at 300 rpm, 4 kg/h at 200 rpm) and group two for low throughputs and slow screw speeds (i.e., 1 kg/h, 1.5 kg/h and 2 kg/h at 60 rpm).

To estimate the filling degrees as a function of the set process parameters in a first attempt, the dimensionless throughput characteristics were calculated via $\dot{V}/nD^3$, with $\dot{V}$ being the throughput (m^3/s), n the screw speed (1/s), D the barrel diameter of the extruder (m) as shown in Table 2. Lower dimensionless throughput characteristics indicate lower filling degrees. The exact filling degrees, as well as the mean residence times, were determined based on simulations as discussed below in section 2.3.

Table 2. *Process parameters for all matrix materials, which were selected to result in different filling degrees f(x) [-] and mean residence times [MRT, s] with the corresponding dimensionless throughput characteristics (V̇/nD³, [-]). The presented values for MRT and filling degree f (f=0: unfilled; f=1: completely filled) were simulated via 1 D simulation.*

	Throughput **[kg/h]**	**Screw speed** **[rpm]**	**Dimensionless throughput characteristics V̇/nD³*** **[-]**	**MRT** **[s]**	**Filling degree *f(x)*** **[-]**
Group one	2	400	0.004	82	0.016
	4	300	0.011	55	0.031
	4	200	0.017	66	0.039
Group two	1	60	0.014	237	0.034
	1.5	60	0.021	191	0.055
	2	60	0.028	170	0.070

**The density of the material is taken as constant with 1000 kg/m³*

All polymers were tested in terms of processability, specifically focusing on the integration and removal of water, which are two distinct phenomena. For this, the water feeding rate was increased stepwise from 0.11 kg/h to 1.23 kg/h (corresponding to pump settings of 25 – 250 ml/min). Clogging of the degassing unit (i.e., unintended material discharge into the degassing unit) and/or inclusions of water within the strands were visually evaluated and were taken as indicators for a too high water supply rate. To better illustrate the water integration and removal capacity of each polymer, the maximum water amount is given as maximum added water concentration (w/w %) relative to the throughput of the polymer (i.e., via feeder 1).

Moreover, process conditions (i.e., melt temperature and pressure, torque) were monitored in-line without and with the addition of water. The specific mechanical energy consumption (SMEC), which is a scale-independent measure of the mechanical energy input into the extrudates, was determined to assess the effect of the water addition on the mechanical energy input. SMEC was calculated according to Equation 1,

Equation 1 $$SMEC = \frac{\tau * \omega}{\dot{m}} \left[\frac{kWh}{kg}\right]$$

where $\tau\,[Nm]$ represents the screw torque, $\omega\,[rad/s]$ the angular screw velocity and $\dot{m}\,[kg/h]$ the material (i.e., polymer and liquid) throughput. The angular screw velocity and the throughput are the set process parameters. In contrast, the screw torque is a consequence of the set process parameters and the material properties and was measured during the extrusion process (Table 3).

2.2. Determination of the moisture content

To verify the elimination of water during the NANEX process, the extrudates' residual moisture content was measured directly after extrusion via Karl Fisher titration (Titroline 7500 KF, SI Analytics, Mainz, Germany). Typically, the moisture content of stable solid dosage forms is below 2% [169] and was our target value. The mean residual moisture content of strands prepared without the addition of water and with the highest possible amount of added water was determined for comparative purposes. Karl Fisher titration was performed by dissolving 2.5 g of crushed strands in anhydrous methanol and analyzing the obtained solution.

2.3. 1D simulation

In addition to the experiments, semi-mechanistic 1D simulations were carried out for the chosen process parameters (i.e., screw speed and throughput) in order to evaluate the filling degree of the screw in axial direction and the residence time distribution (RTD; and mean residence time, MRT). The underlying mathematical model was proposed by Eitzlmayr et al. [167], [168], adapting the approach described by Choulak et al. [170], who modeled the extruder as a cascade of continuously-stirred tank reactors. Screw-specific model parameters were computed using the 3D particle-based simulation method Smoothed Particle Hydrodynamics (SPH) [165], [171]. The twin-screw extruder was discretized in the axial direction, obtaining N numerical elements connected with three mass flow rates accounting for the mass transfer along the screws. Two of the contributions account for the conveying screw effects: $\dot{m}_{f,i}$ for the forward conveying elements and $\dot{m}_{b,i}$ for the backward conveying elements. Depending on the screw's conveying direction, either one (or for non-conveying screw elements both) of the terms are zero. The third mass flow contribution accounts for pressure-driven flow $\dot{m}_{p,i}$ resulting from a pressure gradient in the axial direction. Its sign depends on the actual pressure difference between the two adjacent screw elements and the filling degree of the screw ($\dot{m}_{p,i}$ = 0 for partially filled).

The inherent conveying capacity (A_1), i.e., the dimensionless volume conveyed without a pressure gradient, and the pressure build-up capacity at zero throughput (A_2) are characteristic for a specific screw element and form the basis for modeling the overall extruder performance [172]. These parameters can be established via experiments or, as in our case, via 3D SPH simulations of individual screw elements [165], [171]. Our model also accounts for the highly-variable material properties of the melt: we use the Menges [173] model for density approximation based on pressure and temperature and the Carreau [174] viscosity model based on the shear rate and temperature. Moreover, we account for the thermal conductivity and heat capacity of the melt, screws and barrel. Heat generated

due to viscous dissipation was also considered, since it is the main source of heat input during the extrusion process.

The material data were chosen based on Eitzlmayr et al. [167] since RTD (and the corresponding MRT) and filling degree are rather independent of the matrix material properties [175]. The barrel temperature profile was taken from HPMCAS/plasticizer and Kollidon® VA64 (table 1), thus SC 1 was considered. This allowed evaluating the filling degree profiles and RTDs (and the corresponding MRTs). Due to the fact that there are no models available, which describe the solid conveying zone and the melting process appropriately, it is assumed, that the processed material was molten from start. Furthermore, these calculations do not account for liquid side feeding and resemble only the polymer melt transport. Although this may seem like a coarse simplification, it does not have a pronounced influence on the filling degree and RTD/MRT calculated. Hence, this model allows qualitative assessment of the effect of process parameters to select optimal processing conditions.

3. Results

3.1. NANEX process

3.1.1. Screw configuration and experimental set-up

To achieve a stable HME-process, the screw configurations (SCs) were adapted to the respective polymers. SC 1 (Fig. 1) was used for the matrix materials Eudragit® EPO, Kollidon® VA64 and HPMCAS/plasticizer. For a detailed screw description the reader is referred to the supporting information. The liquid (i.e., water) was fed into barrel 4 of the hot melt extruder via a micro-angular gear pump and the matrix material was added into barrel 1. Degassing of the added water was conducted in barrel 8 (vacuum of 800 mbar).

PEG 20000 was processed using SC 2 (Fig. 1, supporting information), because less energy input is required for processing PEG 20000 due to its comparatively low melting point (i.e., 63-66 °C). Moreover, the liquid side feeding was changed to barrel 2 to achieve a stable process.

3.1.2. Process stability and water integration and removal capacity

All polymers were tested in terms of processability and their maximum water integration and removal capability. For these purposes, various process parameters, i.e., screw speeds, throughputs and combinations thereof, were investigated. Process conditions without and with the addition of water (i.e., melt temperature and pressure, torque) resulting from the applied process parameters were monitored in-line. Finally, the measured

values for the generated torque were used to calculate the corresponding SMEC values for each matrix material and set of process conditions (Fig. 2 a-f).

First, the matrix materials were manufactured via conventional HME (without the addition of water). The results showed that the torque and the melt pressure were slightly decreased for group one compared to group two parameters (Fig. 2 a-f), whereas the melt temperatures were slightly increased. However, for PEG 20000 (Fig. 2 e-f) no melt pressure could be recorded and the melt temperature was not affected markedly by the set process conditions. Calculated values for SMEC clearly demonstrated that the introduced energy is strongly dependent on the amount of processed polymer: the higher the $\dot{V}/nD^3$ (i.e., a function of the throughput and the screw speed) the less energy is exerted on the material (Fig. 2 e-f). As expected, with a decrease in the screw speed, the mechanical energy input decreased.

Second, water was added via side feeding and the results are displayed in Table 3. Eudragit® EPO was not suitable for the NANEX process. Although it was possible to process Eudragit® EPO at the applied screw speeds and throughputs, the water integration and removal properties of the polymer were not suitable, thus leading to direct clogging of the degassing unit.

Similar to Eudragit® EPO, processing of plasticized HPMCAS at throughputs of 2 - 4 kg/h and screw speeds of 200, 300 and 400 rpm led to clogging of the degassing unit and air pockets in the final extrudates. By decreasing the screw speed to 60 rpm and the feeding rate to 1, 1.5 and 2 kg/h, water integration (1.1 kg/h) and removal in the degassing zone were achieved. Based on the throughput of the matrix material (feeder 1), the calculated added water concentration ranged from 55 to 110 % (w/w). The amount of water that could be integrated and subsequently, removed decreased with increasing throughputs (for the same screw speed and the same water feeding rate) and was highest compared to the other polymers processed at the same conditions (Fig. 3). The addition of water yielded lower torque values, which in turn reduced the SMEC; the melt temperature and the melt pressure did not change significantly (Fig. 2 a-b).

Kollidon® VA64 could be processed at all applied process parameters with a range of water feeding rates (0.55 - 1.1 kg/h). For the low screw speed of 60 rpm, the added water concentration decreased with increasing throughput (for the same water feeding rate; Fig. 3). The combination of a low screw speed and a throughput of 1 kg/h resulted in the highest added water concentration of 88% (w/w). Increasing the screw speed and the throughput (group one) lowered the water integration and removal capacity. The combination of a high screw speed of 300 rpm, a high throughput of 4 kg/h and a low water feeding rate of 0.55 kg/h yielded the lowest amount of integrated/removed water (i.e., 14% (w/w)) (Fig. 3). Similar to HPMCAS, water integration slightly decreased the resulting

torque and thus SMEC, whereas the melt temperature and the melt pressure were not affected noticeably (Fig. 2 c-d).

PEG 20000 could also be processed at all applied conditions (Table 3). The water feeding rates ranged from 0.66 to 0.88 kg/h (i.e., 17 - 88 % (w/w)). Again, a low screw speed (60 rpm) and a low throughput (1 kg/h; group two) resulted in a maximum added water concentration of 88% (Fig. 3). The addition of water lowered the resulting torque and the SMEC, while not affecting the melt temperature markedly. As already mentioned, for PEG 20000, no melt pressure could be recorded – independent upon the water concentration (Fig. 2 e-f).

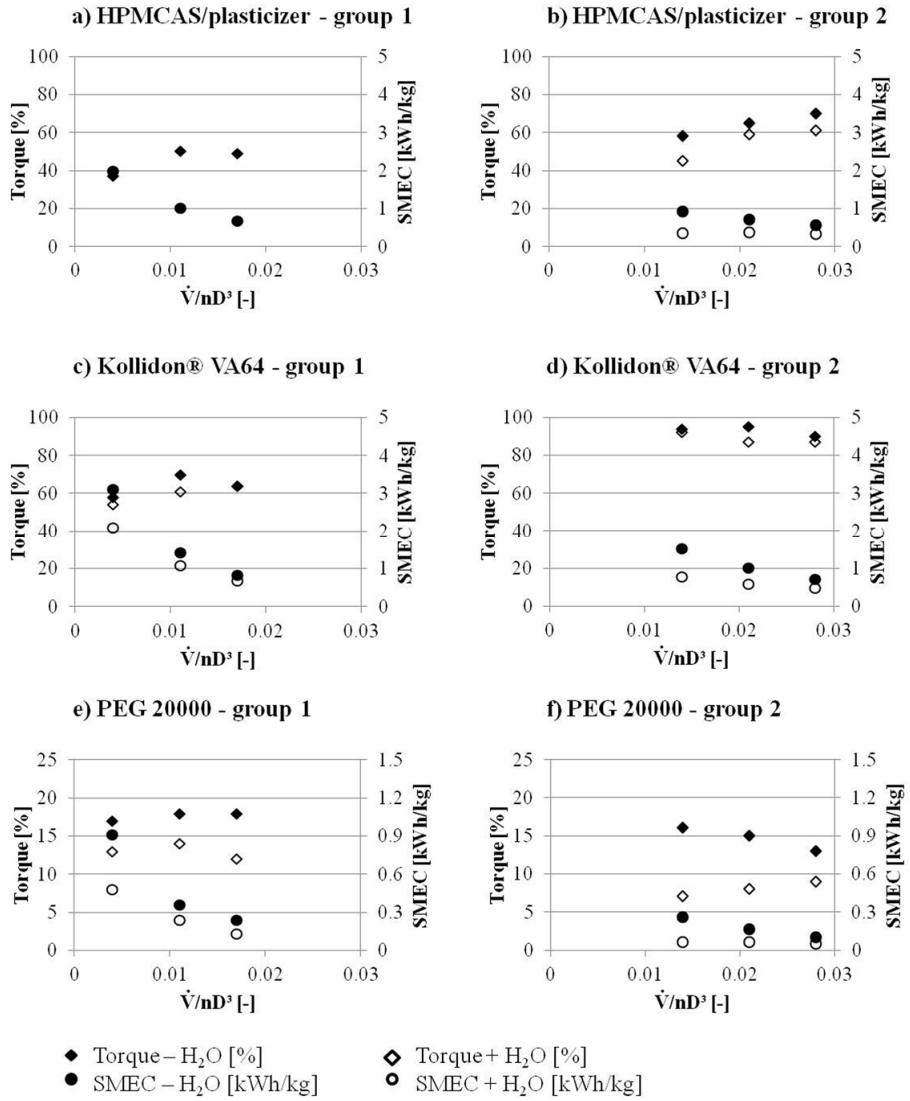

Fig. 2. *In-line monitored process conditions and calculated SMEC values (without and with the addition of water): a) b) HPMCAS/plasticizer, c) d) Kollidon® VA64 and e) f) PEG 20000 at the different sets of process parameters (expressed as V̇/nD³ [-], which is a function of the throughput and the screw speed).*

Table 3. *Maximum added water concentration [%, w/w] at the various set of process parameters.*

Matrix material	Throughput feeder 1 [kg/h]	Screw speed [rpm]	Throughput feeder 2 [kg/h]	Max. added water conc. [%, w/w]
HPMCAS/ Plasticizer	2	400	N.A.	N.A.
	4	300	N.A.	N.A.
	4	200	N.A.	N.A.
	1	60	1.10	110
	1.5	60	1.10	73
	2	60	1.10	55
Kollidon® VA64	2	400	0.77	39
	4	300	0.55	14
	4	200	1.10	28
	1	60	0.88	88
	1.5	60	0.88	59
	2	60	0.88	44
PEG 20000	2	400	0.88	44
	4	300	0.66	17
	4	200	0.77	19
	1	60	0.88	88
	1.5	60	0.71	47
	2	60	0.66	33
N.A.: not applicable				

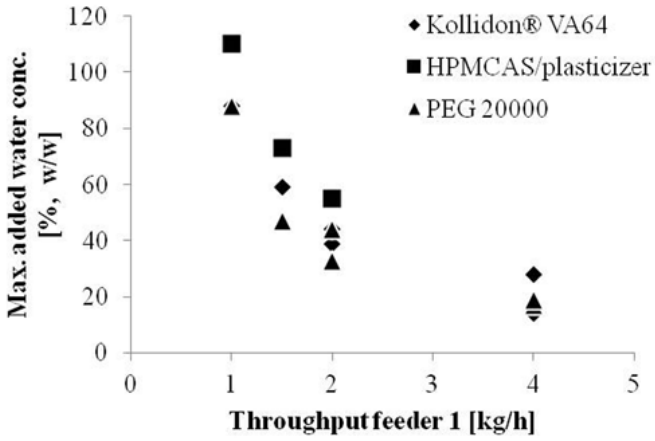

Fig. 3. *Maximum added water concentration [%, w/w; relative to the throughput of feeder 1] at the distinct sets of process parameters dependent on the throughput of feeder 1 [kg/h] for all tested matrix materials.*

3.1.3. Mean residual moisture content

To verify the removal of water during the NANEX process, the mean residual moisture content of the extrudates prepared with the highest possible amount of added water was determined and compared to those obtained from extrudates without adding liquid (Table 4). The water was nearly entirely removed from extrudates based on Kollidon® VA64 and HPMCAS/plasticizer – independent of the addition of water during processing. Thereby, the residual moisture content was below 2% (Table 4). The residual moisture content was decreased for low throughputs and screw speeds. In contrast, extrudates based on PEG 20000 that were prepared with the addition of water had higher mean residual moisture contents, ranging from 3.4 to 4.1%, implying that the water removal was not sufficient.

Table 4. *Mean residual moisture content [%] of extrudates without and with the addition of water at high throughputs and high screw speeds (group one) and at low throughputs and low screw speeds (group two).*

	Mean residual moisture content [%]			
	Without water addition		**With water addition**	
	High throughputs/ high screw speeds	*Low throughputs/ low screw speeds*	*High throughputs/ high screw speeds*	*Low throughputs/ low screw speeds*
HPMCAS/plasticizer	1.0 ± 0.1	0.7 ± 0.2	N.A.	0.7 ± 0.3
Kollidon® VA64	1.9 ± 0.0	0.6 ± 0.1	1.9 ± 0.2	0.6 ± 0.1
PEG 20000	1.6 ± 0.1	1.0 ± 0.0	4.1 ± 0.1	3.4 ± 0.0
N.A.: not applicable				

3.1.4. 1D simulations

A 1D model according to Eitzlmayr et al. [167], [168] was used, first, to model the RTDs – and the corresponding MRTs - at various throughputs and screw speeds and, second, to evaluate the filling degree profile of the screw in axial direction, especially in the degassing zone (twin-screw extruder screws are only partially filled in many sections).

MRTs increased with decreasing throughputs and screw speeds (Table 2, Fig. 4). Hence, MRTs generated with group one settings were markedly shorter, with the shortest MRT of 55 s at a throughput of 4 kg/h and a screw speed of 300 rpm. When the screw speed was reduced to 200 rpm, the MRT increased to 66 s. The longest MRT (i.e., 82 s) was calculated for a throughput of 2 kg/h and a screw speed of 400 rpm. In contrast, for group two the molten materials had a MRT of 170 s at a throughput of 2 kg/h and a screw speed of 60 rpm. With decreasing throughputs (i.e., 1 and 1.5 kg/h), the MRTs significantly increased to 191 s and 237 s for the identical screw speed.

The filling degree *f(x)* is defined as the actual filled volume divided by the total fillable volume at a certain axial position x. The filling degree in the degassing zone increased with

increasing throughput and decreasing screw speed (Table 2, Fig. 4). Consequently, group one setups yielded lower filling degrees with the lowest obtained at a screw speed of 400 rpm and a feeding rate of 2 kg/h (i.e., 0.016). For group two, the filling degrees were increased with the highest obtained for a throughput of 2 kg/h and a screw speed of 60 rpm (i.e., 0.070).

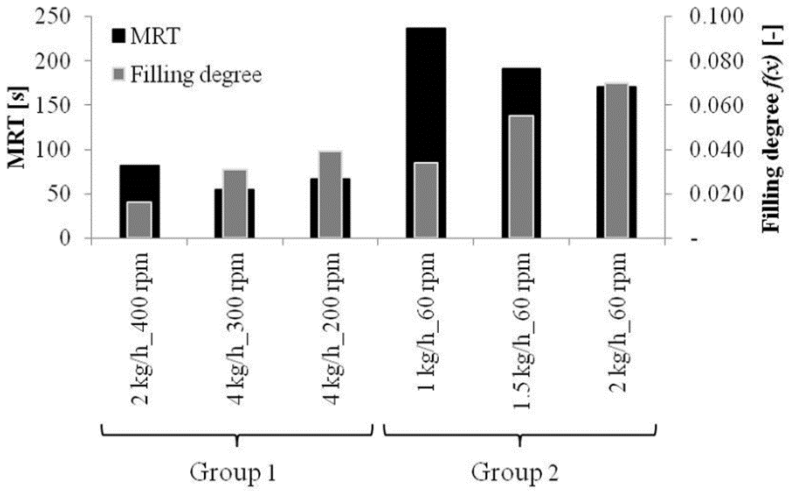

Fig. 4. *Calculated MRTs [s] and filling degrees f(x) [-] of the screw for various sets of process parameters.*

4. Discussion

The API content in an aqueous nano-suspension is restricted to about 30 % (w/w) [153]. Thus, the ability to add a significant amount of suspension/water to the molten polymeric mass during the NANEX process is important, in order to obtain sufficiently high drug loadings in the final nano-extrudates. To ensure stability of the final extrudates, the excess water needs to be removed in a subsequent step.

In this study, various matrix materials were investigated with respect to their suitability for the NANEX process. The matrices were chosen based on the following requirements: i) the matrix material should be processed via HME and ii) the material should be miscible with or soluble in water to allow for water integration. In a subsequent step, however, the added water needs to be removed to result in a stable final product [147], [154]. For water integration, the added water molecules, which are present as liquid water and/or water vapor (i.e., dependent on the process temperatures), have to interact with the polymer resulting in either emulsions (i.e., [water-in-polymer melt]-emulsions or [polymer melt-in-water]-emulsions) or solutions (i.e., water dissolved in the polymer melt or polymer melt dissolved in water). It can be assumed that the strength of the water/polymer interactions

varies for the different types of emulsions and solutions and determines the water removal capacity.

Since water integration requires a stable process, we carefully investigated the effect of process parameters, including screw configuration, throughput and screw speed on the processability. Most importantly, we evaluated the maximum amount of water that can be added to each polymer at the defined sets of process parameters under stable process conditions. Moreover, degassing of the integrated water amount was studied and verified by evaluating the mean residual water content of the final extrudates.

In a first step, we designed two SCs based on the physicochemical properties of the matrix materials. The first design (SC1) was used for Eudragit® EPO, HPMCAS/plasticizer and Kollidon® VA64 (Figure 1). In the feeding zone (barrel 1), the major task of the screw is to convey and compress the matrix materials. For this purpose, screw elements with enough free volume (i.e., high pitch, sufficient channel depth and number of threads) were installed in SC 1 [19]. Towards the plastification zone (the transition zone, barrel 2), the pitch was reduced to compress the material and to accomplish a higher filling degree to improve plastification. The main task of the screw in the plastification zone is melting of the matrix material. Generally, this process depends on the applied screw speed and throughput associated with the filling degree and MRT. Fully-filled screws and (thus) long MRTs favor melting. In fact, the influence of the barrel heating is less pronounced [176]. In our set-up, kneading elements were installed around section 3 to induce the fill-up of preceding screw elements. Larger staggering angles enhance the mixing process and increase the MRTs. Moreover, adding narrow kneading disks reduces shear forces in the kneading gaps and improves the mixing process by increasing the leakage stream, which in turn facilitates the melting process [19].

Since the NANEX process includes addition of an aqueous nano-suspension, water was added to the polymers in barrel 4. Here it is critical to provide enough free screw volume to facilitate the addition of liquid. For that purpose, we installed conveying elements with higher pitches. In the subsequent mixing zone (barrel 5-7), the fed liquid/nano-suspension should be homogenously distributed in the melt [19]. Use of toothed mixing elements and kneading elements with narrow off-set angles improves the mixing process due to shear deformation [19].

Finally, the water has to be removed in the devolatilization/degassing zone (barrel 8). Degassing is strongly affected by the screw speed, the filling degree in this section, the available free screw volume and the applied vacuum. High melt temperatures, low filling degrees and low throughputs/screw speed ratios with frequent surface renewal and a high vacuum yield the best efficiency [19]. Thus, we used conveying elements with a large pitch. These elements provide the largest possible surface area for degassing. To avoid

the formation of high gas velocities, which may drag out material into the degassing zone, we applied a vacuum of only 800 mbar and used conveying elements with a large pitch. In the end section of the extruder, conveying elements with a smaller pitch were used to create the necessary pressure build-up to force the molten mass through the die holes.

For PEG 20000, the SC had to be adapted (SC 2, Fig. 1), since the low melting temperature (69.6 ± 0.6 °C) required less energy input. This was especially necessary in the plastification/melting zone (barrel 3), in the mixing zone (barrel 7) and in the devolatilization/degassing zone (barrel 8). During plastification, the last kneading element was replaced by a conveying element and one set of the three kneading disks was eliminated in the mixing zone. Moreover, conveying elements with smaller pitches were used in the degassing zone, to allow sufficient degassing. Since preliminary investigations showed that water should be added earlier in the process to ensure a proper mixing process with PEG, side feeding was performed in barrel 2 with the SC's conveying elements having a sufficiently high pitch.

All polymers could be processed via (conventional) HME applying the process parameters, which are listed in Table 2. The addition of water caused a reduction of the generated torque, and as a consequence, the SMEC was markedly reduced. Water acts as plasticizer due to its capability to lubricate surfaces and to weaken hydrogen bonds. Additionally, water forms dipole-dipole interactions with polymers due to its high dielectric constant and the capability of strong interactions with hydrophilic groups. Consequently, the glass transition and the melt temperature of polymers are lowered, which in turn reduces melt viscosity [177]–[179]. This indicates that the material experienced lower thermal and mechanical forces, when water was present. In contrast, the recorded melt temperatures, as well as the melt pressures, were only marginally affected. Regarding PEG 20000, no melt pressure was recorded due to the low viscosity of the plasticized mass.

Independent upon the process set-up, it was possible to feed water to the Eudragit® EPO melt. However, for all experimental conditions the subsequent water removal was challenging as clogging of the degassing unit occurred due to immiscibility of the matrix material with the liquid. Eudragit® EPO is soluble below a pH of 5, whereas it swells in aqueous systems with a pH above 5. As the MilliQ water had a pH ranging between 6 and 7, swelling (which is a comparatively slow process) was unlikely to occur, as typical residence times in a twin screw extruder are less than 2 min [16]. Apparently, the molten Eudragit® EPO matrix did not interact with the water. The large (unbound) water amount led to excessively high gas velocities in the back and forward vents, which dragged the melt into the degassing unit and clogged the device [19].

In contrast, the other polymers interacted with water and formed an emulsion or even a solution during HME. Nevertheless, the applied process conditions affected their processability.

For HPMCAS/plasticizer clogging of the degassing unit was observed only at high throughputs and high screw speeds (i.e., group one) due to the short MRTs. Thereby, the polymer melt and water did not get mixed properly. Additionally, degassing in partially-filled screws occurs via diffusion of volatile components through the surface of the molten polymer, before removal through openings in the degassing zone. Here, devolatilization is impeded by i) a short MRT of the molten polymer in the degassing zone – corresponding to high throughputs and screw speeds -, ii) low gas-melt interfaces, iii) thick melt layers in the screw flights, iv) insufficient renewal of the surfaces, v) low melt temperatures and vi) a low vacuum [19]. When the MRT was significantly increased by decreasing both, the throughput and the screw speed, integration and removal of water was successful. The amount of water fed into the molten mass was directly related to the throughput (for a constant screw speed) and consequently, to the MRT: the longer the MRT, the more water could be fed into/removed from the molten mass, yielding a maximum water fraction of 110% (Fig. 5). However, not only the applied process parameters and the corresponding process conditions (i.e., MRT, melt surface) were responsible for this effect, but also the presence of Kolliphor® P188. It seems that Kolliphor® P188 did not only act as a plasticizer but also as emulsifier and stabilizer. Thereby, the o/w surfactant in combination with the high water supply and the mixing properties of the used SC favored the formation of an [polymer melt-in-water]-emulsion [180]. Most importantly, this kind of an emulsion, where water is the continuous phase, allows for effective degassing of high amounts of water, which was reflected by a residual moisture content of 0.7% . It can be assumed that water removal is facilitated for o/w emulsion compared to w/o emulsions. For the latter one, water needs to diffuse through the continuous polymer melt phase first to reach the system´s surface, from which it can be removed via devolatilization. In contrast, for an o/w emulsion, the water is readily available on the system´s surface.

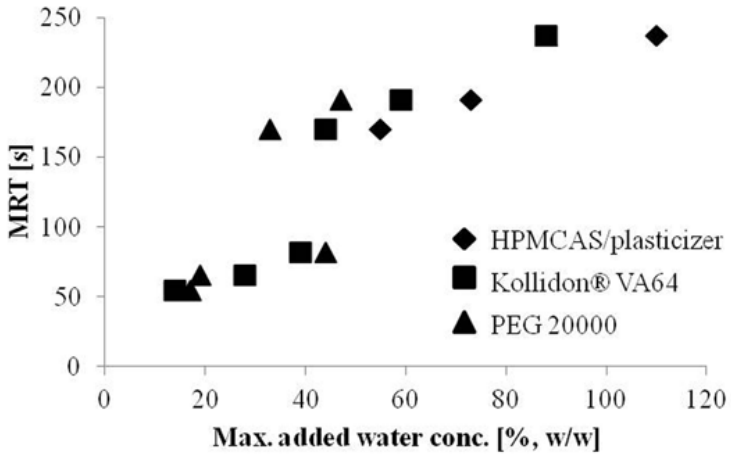

Fig. 5. *Maximum added water concentration [%, w/w; relative to the throughput of feeder 1] at the distinct sets of process parameters dependent on the MRTs [s] for all tested matrix materials. (R^2 for HPMCAS/plasticizer = 0.9998; R^2 for Kollidon® VA 64 = 0.9695 (at process parameters of group one) and 0.9991 (at process parameters of group two); R^2 for PEG 20000 = 0.8821 (at process parameters of group one) and 0.9959 (at process parameters of group two).*

For Kollidon® VA64 water integration and removal was possible for all conditions. Due to the high water solubility of Kollidon VA64 (> 10%) the molten polymer and the liquid were likely to be mixed rather fast yielding a single phase system. It can be assumed that mixing was complete even for the low MRTs. Again, the added water concentration increased with decreasing throughput and screw speed and consequently, with increasing MRT. The residual moisture content of Kollidon® VA64-based extrudates was below 2% and decreased with increasing MRTs (corresponding to low throughputs and screw speeds). However, water incorporation was limited by the subsequent water removal. Hence, less water could be added and removed from Kollidon® VA64 compared to HPMCAS/plasticizer. Kollidon® VA64 and water formed a single phase system, in which the water molecules were incorporated via comparatively strong intermolecular interactions. During water removal, the majority of the water molecules had to diffuse towards the system´s surface to be removed. This process may be time consuming and may not have been completed within the applied MRTs. Hence, water removal was impeded compared to the o/w HPMCAS system, where water was freely accessible on the system´s surface.

In the case of PEG 20000, stable processes were obtained for all tested process set ups and different rates of water addition (i.e., ranging from 0.66 to 0.88 kg/h). Considering the throughput of the matrix material, the highest water integration was again reached at low screw speeds and low throughputs, corresponding to long MRTs. It can be reasonably assumed that water interacted with PEG 20000 (i.e., hydrogen bondings) in a similar manner as with Kollidon® VA 64 due to its high water solubility. Thus, a single phase system was likely to be formed. However, extrudates prepared with the addition of water had

slightly increased mean residual moisture contents. This can be attributed, firstly, to the comparatively strong intermolecular interactions of the water molecules with the polymer, hence, diffusion of entrapped water molecules from the matrix system was partly inhibited [181]. Secondly, process temperatures of 70 °C and a vacuum of 800 mbar were not sufficient. Theoretically, the pressure should be decreased to at least 300 mbar to ensure complete devolatilization.

Our data also demonstrate that the filling degree strongly affects the water uptake/release capacity of all polymers (Fig. 6). However, a direct correlation between the filling degree and water integration and removal capacity was only found at low screw speeds and low throughputs (group two). Here, lower filling degrees yielded increased water integration and removal capacity. Lower filling degrees decrease the material´s volume-to-surface ratio, which facilitates mixing of the polymer melt and water. Moreover, it improves water removal via devolatilization.

Although high throughputs and high screw speeds resulted in lower filling degrees, the time for conveying the polymer through the degassing zone was apparently insufficient for devolatilization.

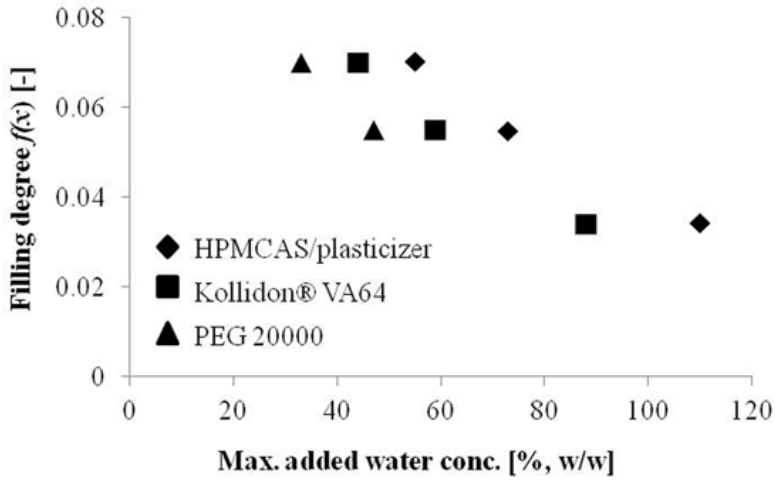

Fig. 6. *Maximum added water concentration [%, w/w; relative to the throughput of feeder 1] dependent on the prevailing filling degree f(x) [-] in the degassing zone for all tested matrix materials applying the process parameters of group two. (R^2 for HPMCAS/plasticizer = 0.9853; for Kollidon® VA 64 = 0.9927 and for PEG 20000 = 0.9679).*

Summarizing, our data showed that the NANEX process requires the application of water soluble/miscible polymers or polymer/emulsifier mixtures to allow for integration of an aqueous nano-suspension. We anticipate that the physicochemical properties of the polymer determine the type of system formed (i.e., emulsion, solution) and consequently, the water removal capability. For o/w emulsions, the water removal via devolatilization was

facilitated, as water formed the continuous phase and was thus, readily available at the systems surface.

Apart from the physicochemical properties of the system, water removal is a strong function of the process conditions and especially, of the resulting MRT of the material in the degassing zone. The residual moisture contents decreased with increasing MRTs (Table 4) as the time during which degassing can occur was increased. The effect of the process parameters on the residual moisture content implies that even the initial moisture is removed during the degassing and this process can be used even for very low moisture levels. Additionally, the filling degree affects the water removal capacity. Low filling degrees result in large gas-melt interfaces, which favor water removal.

5. Conclusions

NANEX is a promising platform technology for making solid nano-formulations in a continuous process. Such formulations do not only improve the solubility and bioavailability of drugs but also enhance patient compliance, since oral uptake is still the most accepted route of drug administration. However, the processing of nano-suspensions via HME requires the addition and removal of an extensive amount of water in order to yield i) high drug doses and ii) sufficient product stability. To that end, a fundamental process understanding concerning distinct matrix materials with respect to their processability is necessary. Four matrix systems were processed with various sets of screw geometries, speeds and throughputs and their effect on the water uptake/release capacity and residual moisture content was determined. It was established that a long MRT of the molten polymer in the extruder and low filling degrees in the degassing zone increase the amount of water that can be added to and removed from the molten material. The amount of water that can be added is proportional to the MRT of the melt and low filling degrees lead to large gas-melt interfaces, allowing effective devolatilization. The final products had a mean residual water content that was similar to that of extrudates processed without the addition of water.

In summary, our data suggest that API loadings of 25 % (w/w) can be achieved once appropriate polymers and nano-suspensions associated with the right process conditions are defined. Future work will address the integration of nano-suspensions that provide high API loadings and homogeneous nano-particle distribution in the final dosage form.

Acknowledgements

This work was funded through the Austrian COMET Program by the Austrian Federal Ministry of Transport, Innovation and Technology (BMVIT), the Austrian Federal Ministry of

Economy, Family and Youth (BMWFJ) and by the State of Styria (Styrian Funding Agency SFG). The authors further acknowledge Andreas Eitzlmayr for fruitful discussions and his valuable support with the 1D simulations, Lisa Mannsberger and the extrusion team of the RCPE GmbH, Graz, Austria, for their assistance with the hot melt extrusion process and Leistritz Extrusionstechnik GmbH (Nuremberg, Germany) for providing the equipment.

Appendix A. Supplementary data

Supplementary data associated with this article can be found, in the online version, at http://dx.doi.org/10.1016/j. ijpharm.2016.04.029.

References

Akay, G., Tong, L., 2001. Preparation of Colloidal Low-Density Polyethylene Latexes by Flow-Induced Phase Inversion Emulsification of Polymer Melt in Water. J. Colloid Interface Sci. 239, 342–357. doi:10.1006/jcis.2001.7615

Amidon, G.L., Lennernas, H., Shah, V.P., Crison, J.R., 1995. A theoretical basis for a biopharmaceutic drug classification: the correlation of in vitro drug product dissolution and in vivo bioavailability. Pharm. Res. doi:10.1023/a:1016212804288

Bastian, M., Gabor, T., 2002. Plastifizierung von Polymeren in Gleichdrall-Doppelschneckenextrudern, in: VDI-Tagung Polymeraufbereitung 2002. Baden-Baden.

Baumgartner, R., Eitzlmayr, A., Matsko, N., Tetyczka, C., Khinast, J., Roblegg, E., 2014. Nano-extrusion: A promising tool for continuous manufacturing of solid nano-formulations. Int. J. Pharm. 477, 1–11.

Baumgartner, R., Teubl, B., Tetyczka, C., Roblegg, E., 2016. Rational design and characterization of a nano-suspension for intraoral administration. J. Pharm. Sci. 105, 257–267.

Bierdel, M., 2008. Computational Fluid Dynamics, in: Co-Rotating Twin-Screw Extruders, K.Kohlgrüber. Carl Hanser Verlag GmbH & CO. KG, Ed. Munich.

Borm, P., Klaessig, F.C., Landry, T.D., Moudgil, B., Pauluhn, J., Thomas, K., Trottier, R., Wood, S., 2006. Research strategies for safety evaluation of nanomaterials, Part V: Role of dissolution in biological fate and effects of nanoscale particles. Toxicol. Sci. 90, 23–32. doi:10.1093/toxsci/kfj084

Breitenbach, J., 2002. Melt extrusion: from process to drug delivery technology. Eur. J. Pharm. Biopharm. Off. J. Arbeitsgemeinschaft fur Pharm. Verfahrenstechnik eV 54, 107–117.

Campbell, K., Craig, D.Q.M., McNally, T., 2008. Poly(ethylene glycol) layered silicate nanocomposites for retarded drug release prepared by hot-melt extrusion. Int. J. Pharm. 363, 126–131.

Chaubal, M. V., Popescu, C., 2008. Conversion of nanosuspensions into dry powders by spray drying: A case study. Pharm. Res. 25, 2302–2308.

Chen, X., Young, T.J., Sarkari, M., Williams, R.O., Johnston, K.P., 2002. Preparation of cyclosporine A nanoparticles by evaporative precipitation into aqueous solution. Internaitonal J. Pharm. 242, 3–14.

Chokshi, R.J., Sandhu, H.K., Iyer, R.M., Shah, N.H., Malick, A.W., Zia, H., 2005. Characterization of physico-mechanical properties of indomethacin and polymers to assess their suitability for hot-melt extrusion processs as a means to manufacture solid dispersion/solution. J. Pharm. Sci. 94, 2463–2474.

Choulak, S., Couenne, F., Le Gorrec, Y., Jallut, C., Cassagnau, P., Michel, A., 2004. Generic Dynamic Model for Simulation and Control of Reactive Extrusion. Ind. Eng. Chem. Res. 43, 7373–7382. doi:10.1021/ie0342964

Chung, N.O., Lee, M.K., Lee, J., 2012. Mechanism of freeze-drying drug nanosuspensions. Int. J. Pharm. 437, 42–50. doi:10.1016/j.ijpharm.2012.07.068

Claeys, B., Coen, R. De, De Geest, B.G., de la Rosa, V.R., Hoogenboom, R., Carleer, R., Adriaensens, P., Remon, J.P., Vervaet, C., 2013. Structural modifications of polymethacrylates: Impact on thermal behavior and release characteristics of glassy solid solutions. Eur. J. Pharm. Biopharm. 1–9. doi:10.1016/j.ejpb.2013.01.027

Eitzlmayr, A., Khinast, J., 2015a. Co-Rotating Twin-Screw Extruders: Detailed Analysis of Conveying Elements based on Smoothed Particle Hydrodynamics. Part 1: Hydrodynamics. Chem. Eng. Sci. 134, 861–879.

Eitzlmayr, A., Khinast, J., 2015b. Co-rotating twin-screw extruders: Detailed analysis of conveying elements based on smoothed particle hydrodynamics. Part 2: Mixing. Chem. Eng. Sci. 134, 880–886. doi:10.1016/j.ces.2015.05.035

Eitzlmayr, A., Khinast, J., 2013. Experimental Characterization and Modeling of Twin-Screw Extruder Elements for Pharmaceutical Hot Melt Extrusion. AIChE J. 59, 4440–4450. doi:10.1002/aic

Eitzlmayr, A., Koscher, G., Khinast, J., 2014a. A novel method for modeling of complex wall geometries in smoothed particle hydrodynamics. Comput. Phys. Commun. 185, 2436–2448. doi:10.1016/j.cpc.2014.05.014

Eitzlmayr, A., Koscher, G., Reynolds, G., Huang, Z., Booth, J., Shering, P., Khinast, J., 2014b. Mechanistic Modeling of Modular Co-Rotating Twin-Screw Extruders. Int. J. Pharm. 474, 157–176. doi:10.1016/j.ijpharm.2014.08.005

Gabor, F., Fillafer, C., Neutsch, L., Ratzinger, G., Wirth, M., 2010. Improving Oral Delivery, Phospholipase A2. doi:10.1007/978-3-642-00477-3

Galli, C., 2006. Experimental determination of the diffusion boundary layer width of micron and submicron particles. Int. J. Pharm. 313, 114–122. doi:10.1016/j.ijpharm.2006.01.030

Gao, J., Walsh, G.C., Bigio, D., Briber, R.M., Wetzel, M.D., 1999. Residence-Time Distribution Model for Twin-Screw Extruders. AIChE J. 45, 2541–2549.

Gao, L., Zhang, D., Chen, M., 2008. Drug nanocrystals for the formulation of poorly soluble drugs and its application as a potential drug delivery system. J. Nanoparticle Res. 10, 845–862.

Gao, Y., Qian, S., Zhang, J., 2011. Physicochemical and pharmacokinetic characterization of a spray-dried cefpoxodine proxetil nanosuspension. Chem. Pharm. Bull. 414, 186–192. doi:10.1016/j.ijpharm.2011.05.032

Genina, N., Fors, D., Palo, M., Peltonen, J., Sandler, N., 2013a. Behavior of printable formulations of loperamide and caffeine on different substrates - Effect of print density in inkjet printing. Int. J. Pharm. 453, 488–497. doi:10.1016/j.ijpharm.2013.06.003

Genina, N., Fors, D., Vakili, H., Ihalainen, P., Pohjala, L., Ehlers, H., Kassamakov, I., Haeggström, E., Vuorela, P., Peltonen, J., Sandler, N., 2012. Tailoring controlled-

release oral dosage forms by combining inkjet and flexographic printing techniques. Eur. J. Pharm. Sci. 47, 615–623. doi:10.1016/j.ejps.2012.07.020

Genina, N., Janßen, E.M., Breitenbach, A., Breitkreutz, J., Sandler, N., 2013b. Evaluation of different substrates for inkjet printing of rasagiline mesylate. Eur. J. Pharm. Biopharm. 85, 1075–1083. doi:10.1016/j.ejpb.2013.03.017

Huilier, D.G.F., 1990. Modeling of injection mold post-filling: a review and some critical problems to solve. J. Polym. Eng. 9, 237–302.

Jinno, J.I., Kamada, N., Miyake, M., Yamada, K., Mukai, T., Odomi, M., Toguchi, H., Liversidge, G.G., Higaki, K., Kimura, T., 2008. In vitro-in vivo correlation for wet-milled tablet of poorly water-soluble cilostazol. J. Control. Release 130, 29–37. doi:10.1016/j.jconrel.2008.05.013

Kalivoda, A., Fischbach, M., Kleinebudde, P., 2012. Application of mixtures of polymeric carriers for dissolution enhancement of fenofibrate using hot-melt extrusion. Int. J. Pharm. 429, 58–68. doi:10.1016/j.ijpharm.2012.03.009

Kayaert, P., Anné, M., Van Den Mooter, G., 2011. Bead layering as a process to stabilize nanosuspensions: Influence of drug hydrophobicity on nanocrystal reagglomeration following in-vitro release from sugar beads. J. Pharm. Pharmacol. 63, 1446–1453. doi:10.1111/j.2042-7158.2011.01351.x

Keck, C.M., Müller, R.H., 2006. Drug nanocrystals of poorly soluble drugs produced by high pressure homogenisation. Eur. J. Pharm. Biopharm. 62, 3–16.

Keen, J.M., Martin, C., Machado, A., Sandhu, H., McGinity, J.W., Dinunzio, J.C., 2014. Investigation of process temperature and screw speed on properties of a pharmaceutical solid dispersion using corotating and counter-rotating twin-screw extruders. J. Pharm. Pharmacol. 66, 204–17. doi:10.1111/jphp.12106

Khinast, J.G., Baumgartner, R., Roblegg, E., 2013. Nano-extrusion: a one-step process for manufacturing of solid nanoparticle formulations directly from the liquid phase. AAPS Pharm. Sci. Technol. 14, 601–4.

Kipp, J.E., 2004. The role of solid nanoparticle technology in the parenteral delivery of poorly water-soluble drugs. Int J Pharm 284, 109–22. doi:10.1016/j.ijpharm.2004.07.019

Kohlgrüber, K., Wiedmann, W., 2008. Co-Rotating Twin-Screw Extruders - Fundamentals, Technology, and Applications. Carl Hanser Verlag GmbH & CO. KG.

Krause, K.P., Müller, R.H., 2001. Production and characterisation of highly concentrated nanosuspensions by high pressure homogenisation. Int. J. Pharm. 214, 21–4.

Langguth, P., Fricker, G., Wunderli-Allenspach, H., 2004. Biopharmazie. Wiley, Weinheim.

Lee, J., 2003. Drug nano- and microparticles processed into solid dosage forms: Physical properties. J. Pharm. Sci. 92, 2057–2068. doi:10.1002/jps.10471

Lennernäs, H., Abrahamsson, B., 2005. The use of biopharmaceutic classification of drugs in drug discovery and development: current status and future extension. J. Pharm. Pharmacol. 57, 273–285. doi:10.1211/0022357055263

Liu, H., Wang, P., Zhang, X., Shen, F., Gogos, C.G., 2010. Effects of extrusion process parameters on the dissolution behavior of indomethacin in Eudragit?? E PO solid dispersions. Int. J. Pharm. 383, 161–169. doi:10.1016/j.ijpharm.2009.09.003

Liversidge, G., Cundy, K., 1992. Surface modified drug nanoparticles. US Pat. 5145684.

Liversidge, G.G., Conzentino, P., 1995. Drug particle size reduction for decreasing gastric irritancy and enhancing absorption of naproxen in rats. Int. J. Pharm. 125, 309–313.

Liversidge, G.G., Cundy, K.C., 1995. Particle size reduction for improvement of oral bioavailability of hydrophobic drugs: I. Absolute oral bioavailability of nanocrystalline danazol in beagle dogs. Int. J. Pharm. 125, 91–97.

Marieb, E.N., Hoehn, K., 2007. Human Anatomy & Physiology, 7th Editio. ed. Pearson Benjamin Cummings.

Matveev, Y.I., Grinberg, V.Y., Tolstoguzov, V.B., 2000. The plasticizing effect of water on proteins, polysaccharides and their mixtures. Glassy state of biopolymers, food and seeds. Food Hydrocoll. 14, 425–437. doi:10.1016/S0268-005X(00)00020-5

Merisko-Liversidge, E., Liversidge, G.G., Cooper, E.R., 2003. Nanosizing: a formulation approach for poorly-water-soluble compounds. Eur. J. Pharm. Sci. 18, 113–20.

Möschwitzer, J., Müller, R.H., 2006. Spray coated pellets as carrier system for mucoadhesive drug nanocrystals. Eur. J. Pharm. Biopharm. 62, 282–7. doi:10.1016/j.ejpb.2005.09.005

Möschwitzer, J.P., 2013. Drug nanocrystals in the commercial pharmaceutical development process. Int. J. Pharm. 453, 142–156. doi:10.1016/j.ijpharm.2012.09.034

Mrsny, R.J., 2012. Oral drug delivery research in Europe. J. Control. Release 161, 247–253. doi:10.1016/j.jconrel.2012.01.017

Müller, R. et al, n.d. Nanosuspensions: formulations for poorly soluble drugs with poor bioavailability. Pharm Ind 61, 175–178.

Müller, R.H., Akkar, A., 2004. Drug nanocrystals of poorly soluble drugs. Encycl. Nanosci Nanotechnol. 2, 627–638.

Müller, R.H., Jacobs, C., Kayser, O., 2001. Nanosuspensions as particulate drug formulations in therapy. Rationale for development and what we can expect for the future. Adv. Drug Deliv. Rev. 47, 3–19.

Müller, R.H., Peters, K., 1998. Nanosuspensions for the formulation of poorly soluble drugs. Int. J. Pharm. 160, 229–237. doi:10.1016/S0378-5173(97)00311-6

Nakarani, M., Misra, A.K., Patel, J.K., Vaghani, S.S., 2010. Itraconazole Nanosuspension for Oral delivery: formulation, characterization and in vitro comparison with marketed formulation 2, 162–171.

Newsletter, 2002. Oral drug delivery. drugDel.com.

Palo, M., Kolakovic, R., Laaksonen, T., Määttänen, A., Genina, N., Salonen, J., Peltonen, J., Sandler, N., 2015. Fabrication of drug-loaded edible carrier substrates from nanosuspensions by flexographic printing. Int. J. Pharm. 1–8. doi:10.1016/j.ijpharm.2015.01.027

Pardeike, J., Strohmeier, D.M., Schrödl, N., Voura, C., Gruber, M., Khinast, J.G., Zimmer, A., 2011. Nanosuspensions as advanced printing ink for accurate dosing of poorly soluble drugs in personalized medicines. Int. J. Pharm. 420, 93–100.

Peltonen, L., Hirvonen, J., 2010. Pharmaceutical nanocrystals by nanomilling: critical process parameters, particle fracturing and stabilization methods. J. Pharm. Pharmacol. 62, 1569–79.

Petereit, H.U., Weisbrod, W., 1999. Formulation and process considerations affecting the stability of solid dosage forms formulated with methacrylate copolymers. Eur. J. Pharm. Biopharm. 47, 15–25. doi:10.1016/S0939-6411(98)00083-6

Pissis, P., Apekis, L., Christodoulides, C., Niaounakis, M., Kyritsis, A., Nedbal, J., 1996. Water effects in polyurethane block copolymers. J. Polym. Sci. Part B-Polymer Phys. 34, 1529–1539.

Planchette, C., Pichler, H., Wimmer-teubenbacher, M., Gruber, M., Khinast, J., 2015. Printing medicines as orodispersible dosage forms : Effect of substrate on the printed micro-structure. Int. J. Pharm. in press. doi:10.1016/j.ijpharm.2015.10.054

Preis, M., Breitkreutz, J., Sandler, N., 2015. Perspective: Concepts of printing technologies for oral film formulations. Int. J. Pharm. 494, 578–584.

Rabinow, B.E., 2004. Nanosuspensions in drug delivery. Nat. Rev. Drug Discov. 3, 785–96.

Raijada, D., Genina, N., Fors, D., Wisaeus, E., Peltonen, J., Rantanen, J., Sandler, N., 2013. A Step Toward Development of Printable Dosage Forms for Poorly Soluble Drugs. J. Pharm. Sci. 102, 3694–3704. doi:10.1002/jps.23678

Rauwendaal, C., 2001. Polymer extrusion. Hanser Publishers, Munich, Germany.

Rowe, R.C., Sheskey, P.J., Quinn, M.E., 2009. Handbook of Pharmaceutical Excipients, Sixth Edition, Journal of Controlled Release. Pharmaceutical Press, American Pharmacists Association.

Sandler, N., Määttänen, A., Ihalainen, P., Kronberg, L., Meierjohann, A., Viitala, T., Peltonen, J., 2011. Inkjet Printing of Drug Substances and Use of Porous Substrates-Towards Individualized Dosing. J. Pharm. Sci. 100, 3386–3395. doi:10.1002/jps

Sarkari, M., Brown, J., Chen, X., Swinnea, S., Williams, R.O., Johnston, K.P., 2002. Enhanced drug dissolution using evaporative precipitation into aqueous solution. Int. J. Pharm. 243, 17–31.

Sarode, A.L., Obara, S., Tanno, F.K., Sandhu, H., Iyer, R., Shah, N., 2014. Stability assessment of hypromellose acetate succinate (HPMCAS) NF for application in hot melt extrusion (HME). Carbohydr. Polym. 101, 146–53. doi:10.1016/j.carbpol.2013.09.017

Sarode, A.L., Sandhu, H., Shah, N., Malick, W., Zia, H., 2013. Hot melt extrusion (HME) for amorphous solid dispersions: Predictive tools for processing and impact of drug-polymer interactions on supersaturation. Eur. J. Pharm. Sci. 48, 371–384. doi:10.1016/j.ejps.2012.12.012

Shah, S., Maddineni, S., Lu, J., Repka, M.A., 2012. Melt extrusion with poorly soluble drugs. Int J Pharm 001, 1–20. doi:10.1016/j.ijpharm.2012.11.001

Surikutchi, B., Patil, S., Shete, G., 2013. Drug-excipient behavior in polymeric amorphous solid dispersions. J. Excipients Food Chem. 4, 70–94.

Tho, I., Liepold, B., Rosenberg, J., Maegerlein, M., Brandl, M., Fricker, G., 2010. Formation of nano/micro-dispersions with improved dissolution properties upon dispersion of ritonavir melt extrudate in aqueous media. Eur. J. Pharm. Sci. Off. J. Eur. Fed. Pharm. Sci. 40, 25–32.

Van Eerdenbrugh, B., Froyen, L., Van Humbeeck, J., Martens, J. a, Augustijns, P., Van den Mooter, G., 2008. Drying of crystalline drug nanosuspensions-the importance of surface hydrophobicity on dissolution behavior upon redispersion. Eur. J. Pharm. Sci. 35, 127–35.

Van Eerdenbrugh, B., Van den Mooter, G., Augustijns, P., 2008. Top-down production of drug nanocrystals: nanosuspension stabilization, miniaturization and transformation into solid products. Int. J. Pharm. 364, 64–75.

Wang, P., Luo, Q., Miao, Y., Ying, L., He, H., Cai, C., Tang, X., 2012. Improved dissolution rate and bioavailability of fenofibrate pellets prepared by wet-milled-drug layering. Drug Dev. Ind. Pharm. 38, 1344–1353. doi:10.3109/03639045.2011.650647

Wang, R., Wang, Q., Li, L., 2003. Evaporation behaviour of water and its plasticizing effect in modified poly(vinyl alcohol) systems. Polym. Int. 52, 1820–1826. doi:10.1002/pi.1385

Wu, L., Zhang, J., Watanabe, W., 2011. Physical and chemical stability of drug nanoparticles. Adv. Drug Deliv. Rev. 63, 456–469.

Zhang, G.G.Z., Zhou, D., 2009. Developing Solid Oral Dosage Forms: Pharmaceutical Theory And Practice, Developing Solid Oral Dosage Forms: Pharmaceutical Theory And Practice. doi:10.1016/B978-0-444-53242-8.00002-3

5. Summary of major findings

In this thesis, it was aimed to develop solid nano-formulations of the poorly soluble model API phenytoin in a single step, using the NANEX process. The obtained nano-extrudates were supposed to comprise de-agglomerated embedded phenytoin nano-crystals showing an improved drug release. To carefully justify this assumption, a stable aqueous nano-suspension of the poorly soluble API (phenytoin) was prepared and carefully characterized. Before nano-sizing the bulk material via wet media milling, relevant aqueous non-ionic stabilizer solutions were investigated regarding their wetting properties, surface tension and viscosity and the most stable formulation was identified. Dissolution experiments were conducted and in-vitro and ex-vivo permeability studies across a buccal cell culture model (TR 146 cultured on transwells) and freshly excised porcine buccal mucosa were performed. Moreover, CLSM investigations and cytotoxicity studies were carried out to assess the uptake route of the nano-crystals and exclude possible adverse effects. Finally, the results of nano-phenytoin were compared to those achieved with bulk (untreated) phenytoin. The major findings of this study include:

- Among all tested stabilizers, the addition of Tween® 80 resulted in the most stable system corresponding with a particle size of 335 ± 6 nm and a zeta potential value of -18.3 ± 0.4 mV.
- Nano-sizing did not affect the crystalline structure of the API, since bragg peaks in the WAXS region (SWAXS studies) were identical to those of the bulk material. Only a marginal shift of the melting endotherm (DSC measurements) was observed for nano-crystalline phenytoin.
- Evaluation of the saturation solubility of nano-phenytoin in a Tween® 80 solution yielded a 1.4-fold higher solubility compared to the bulk material. Moreover, the time-dependent dissolution displayed higher and faster drug dissolution of nano-phenytoin, due to the increased specific surface area of the nano-sized material.
- Stability tests of nano-suspensions in physiological media revealed that nano-particles tended to agglomerate during dispersion due to the presence of mono- and divalent cations. Nevertheless, nano-crystals showed markedly higher saturation solubility in all tested media.
- Nano-phenytoin permeated across the buccal membrane (in-vitro as well as ex-vivo) to a higher extent compared to the bulk material. Since it was shown that the nano-material was not internalized by the cells, it can be anticipated that the improved permeability behavior is related to the enhanced solubility characteristics of nano-phenytoin.
- Due to size reduction no impact on the cell viability was observed.

In chapter 3, the Tween® 80 stabilized phenytoin nano-suspension was transferred into a solid nano-formulation via the NANEX process. Since an industrial more relevant extruder was employed for this study, a scale-up was necessary and a rational screw design was conducted. Moreover, the process set-up was adapted compared to the initial proof-of-concept study. The obtained nano-extrudates were carefully investigated regarding their crystalline structure, morphology and particle distribution in the matrix. Most importantly, solubility characteristics and dissolution profiles were recorded and the results were compared to those obtained for the pure API and the bulk-extrudates (i.e., extrudates prepared by extruding a blend of Soluplus® and bulk API). The major findings of this study are listed below:

- Analytical TEM as well as AFM investigations evidently confirmed that nano-crystals were successfully embedded in a de-agglomerated manner into Soluplus®.
- The nano-crystals remained in their crystalline state during and after the NANEX process, which was established by DSC measurements.
- The incorporation of nano-sized phenytoin into Soluplus® yielded a 184-fold higher solubility compared to bulk-phenytoin. To investigate whether the increased solubility is due to the nano-sizing and/or the solubilizing effects of the matrix material, bulk-extrudates were prepared. A 1.2-fold higher solubility of nano-particles embedded in the matrix was achieved, which highlights the beneficial effect of size-reduction on the solubility characteristics.
- Finally, extrudates comprising nano-crystals showed a markedly (i.e., 1.3-fold) higher and faster release profile compared to bulk-extrudates. Thus, particle size of embedded nano-particles strongly determined the kinetic solubility resulting in a faster and higher dissolution rate.

To reach sufficiently high drug loadings in the final product, we investigated distinct matrix materials with regard to their “NANEX processability” and optimized the process parameters (chapter 4). To this end, four carrier systems, i.e., Eudragit® EPO, AQOAT® (HPMCAS), Kollidon® VA 64 and PEG 20000, were used and tested for their applicability. To meet the requirements of each polymer, different sets of screw geometries were employed and the position of liquid side feeding was adapted. By varying process parameters such as throughput and screw speed, the maximum nano-suspension integration as well as water removal capacity of each polymer was determined. In addition to the experimental studies, one-dimensional discretization modeling was performed and the influence of the mean residence time and the filling degree was carefully evaluated. The findings of this study are summarized below:

- The data of this study showed that the physicochemical nature of the applied matrix material strongly determines its applicability for the NANEX process: only water soluble/miscible polymers or polymer/emulsifier mixtures, which interact with the added water molecules and form emulsions or solutions were identified as appropriate candidates.
- It was possible to add and remove water to HPMCAS/plasticizer, Kollidon® VA 64 and PEG 20000.
- In contrast, it was not possible to remove the added liquid from Eudragit® EPO because of too weak interactions between water and the molten polymer: Eudragit® EPO was neither soluble in water nor swelled upon water addition due to short process times. As a consequence, a large (unbound) water amount led to excessively high gas velocities dragging out melt into the degassing unit resulting in an unstable process and a final product of inferior quality.
- It was found that the strength of the water-polymer interactions determined the water removal capacity: emulsions, where water is the continuous phase and readily available on the system´s surface for degassing, showed the highest water removal capacity (e.g., HPMCAS/plasticizer mixture). Solutions, showing a stronger interaction of polymer and water (i.e., water molecules are entrapped in the matrix), exhibited a reduced water removal capacity (i.e., Kollidon® VA64 and PEG 20000)
- Simulation studies revealed that the water removal capacity is a strong function of the applied process conditions and especially, of the resulting MRT and the filling degree of the material in the degassing zone. The amount of water that can be added is proportional to the MRT: the longer the MRT the more water can be added and removed from the system. Additionally, low filling degrees lead to large gas-melt interfaces, allowing for effective devolatilization.
- In summary, it was shown that it is theoretically possible to reach an API loading of 25 % (w/w) in the final nano-extrudates when a nano-suspension with 30 % (w/w) API content is processed. Adapting the process parameters allows fast and continuous control over the final API loading in the extrudates, once more highlighting the benefits of the NANEX process.

6. Outlook

The NANEX process is a continuous in-line controlled hot melt extrusion process that converts a stabilized aqueous nano-suspension into a solid oral formulation in a single step. Due to particle size reduction, solubility, dissolution velocity and consequently, the permeability of poorly soluble substances can be significantly improved. Moreover, this technology circumvents time-consuming and cost-intensive multi-batch processes and allows to precisely control the product quality. Hence, this innovative platform technology will open new pathways for the pharmaceutical industry.

Films or patches intended for intraoral application can be designed continuously with the respective processing units and downstream equipment. Incorporated nano-crystals will enhance transmucosal permeation for local and systemic therapy. Moreover, degradation prone drug candidates such as proteins and peptides can be encapsulated in (biodegradable) nano-carriers that can be further processed via NANEX. This solid oral dosage forms would enable to improve the drug´s (enzymatic) stability and thus, its performance along the GI route. For this, the NANEX process needs to be adapted with regard to the prevailing process temperatures and shear forces. Additionally, nano-crystallization processes can be directly integrated.

The NANEX approach can not only be applied for the preparation of tablets, multiparticulate dosage forms or films but also for the development of controlled-release drug delivery systems such as implants (e.g., intravaginal applications). The rational selection and design of an appropriate matrix/reservoir system and the incorporation of nano-crystals with uniform shape, size and crystalline structure would help to control API release over a long period and eliminate stability problems associated with the amorphous state of an incorporated API.

Apart from technological advantages, also high potent active substances, which have to be manufactured at the highest technical level, can be handled via NANEX. On that account, high potent compound materials can be fed as solutions, suspensions or emulsions to an appropriate matrix material. Thus, dust formation as well as the contact time between the manufacturer and the material will be reduced during the production process, which will further minimize the risk of hazardous materials to human health

The concept of the NANEX process can also be used to manufacture solids with very low doses. The main problems associated with low-dosable drugs are insufficient content uniformities due to segregation problems during blending and mixing. The installation of highly precise pumping devices would enable to achieve accurate dosing of sensitive APIs in

their dissolved, suspended, emulsified or nano-sized form. Moreover, adaption of mixing, kneading and conveying elements of the screw will support a homogenous distribution of the API in the final dosage form.

Finally, the NANEX set-up can be used to enable HME processability of matrix systems that require the supply of water during the manufacturing process for plastification. This includes natural products like starch, xanthan, and gummi arabicum. Hence, a prior granulation step will be omitted and the matrix carriers can be directly manufactured via feeding the required amount of water (integrating the drug) during the NANEX process.

Summarizing, NANEX is an enabling platform technology that can revolutionize the development of complex drug systems, by reducing risks and costs of development, significantly accelerating market launch in the future.

7. List of publications

Articles in peer-reviewed journals

R. Baumgartner, A. Eitzlmayr, N. Matsko, C. Tetyczka, J. Khinast, E. Roblegg, *Nano-extrusion: A promising tool for continuous manufacturing of solid nano-formulations*, Int. J. Pharm. 477 (2014) 1-11

R. Baumgartner, B.J. Teubl, C. Tetyczka, E. Roblegg, *Rational Design and Characterization of a Nanosuspension for Intraoral Administration Considering Physiological Conditions,* J. Pharm. Sci. 105 (2016) 257-267

R. Baumgartner, J. Matić, S. Schrank, S. Laske, J. Khinast, E. Roblegg, *NANEX: Process Design and Optimization*, Int. J. Pharm. 506 (2016) 35-45

Co-authored articles in peer-reviewed journals

J. Khinast, R. Baumgartner, E. Roblegg, *Nano-extrusion: a One-Step Process for Manufacturing of Solid Nanoparticle Formulations Directly from the Liquid Phase*. AAPS PharmSciTech, 14 (2013) 601-604

H.M.A. Ehmann, R. Baumgartner, B. Kunert, A. Zimmer, E. Roblegg, O. Werzer, *Morphologies of Phenytoin Crystals at Silica Model Surfaces: Vapor Annealing versus Drop Casting*, J. Phys. Chem. C. 118 (2014) 12855-12861

O. Werzer, R. Baumgartner, M. Zawodzki, E. Roblegg, *Particular Film Formation of Phenytoin at Silica Surfaces*, Mol. Pharm. 11 (2014) 610-616

H.M.A. Ehmann, R. Baumgartner, D. Reischl, E. Roblegg, A. Zimmer, R. Resel, O. Werzer, *One Polymorph and Various Morphologies of Phenytoin at a Silica Surface Due to Preparation Kinetics*, Cryst. Growth Des. 15 (2015) 326-332

M. Llusa, S. Mohr, R. Baumgartner, A. Paudel, G. Koscher, J. Khinast, *Continuous Low-dose Feeding of Highly Active Pharmaceutical Ingredients in Hot-Melt Extrusion.* Drug Dev Ind Pharm. (2016)

C. Röthel, H.M.A. Ehmann, R. Baumgartner, D. Reischl, O. Werzer, *Alteration of texture and polymorph of phenytoin within thin films and its impact on dissolution.* Cryst Eng Comm. (2016)

Patent

R. Baumgartner, G. Koscher, T. Klein, E. Roblegg, J. Khinast, *System for producing a solid preparation from a suspension*, UK Patent Application, GB 2503710 A

Presentations

R. Baumgartner, J. Khinast, E. Roblegg, *Nano-Extrusion: Herstellung einer festen nano-partikulären Formulierung durch das Verarbeiten von Nano-suspensionen mittels Schmelzextrusion*, 17.-18.04.2013, Leoben, Austria; 9. Minisymposium der Verfahrenstechnik

E. Roblegg, R. Baumgartner, J. Khinast, *Nano-Extrusion: A Novel One-step Process for the Manufacturing of Solid Drug Nanoparticle-Formulations*, 03.-08.11.2013, San Francisco, California, United States of America, 2013 AIChE Annual Meeting

R. Baumgartner, J. Khinast, E. Roblegg, *Nano-extrusion (NANEX): A promising tool for the Oral Drug Delivery Market*, 1.-12.06.2014, Nuernberg, Germany; Pharmaworkshop Leistritz

R. Baumgartner, J. Khinast, E. Roblegg, *NANEX: A Rational Design of the Manufacturing of a Solid Oral Nanoparticle Formulation,* 16.-17.06.2014, Graz, Austria; 6th International Congress on Pharmaceutical Engineering (ICPE)

R. Baumgartner, J. Khinast, E. Roblegg, NANEX: Process design with potential matrix materials, 05.02.2015, Graz, Austria; 5th Pharma DocDay 2015

R. Baumgartner, J. Khinast, E. Roblegg, *Evaluation of potential matrix materials for the nano-extrusion (NANEX) process*, 18.-19.05.2015, Graz, Austria; Seventh pan European QbD & PAT Science Conference

R. Baumgartner, B. Teubl, C. Tetyczka, E. Roblegg, *Nano-Drug Delivery across the Buccal Mucosa*, 04.-06.06.2015, Graz, Austria; International Student Congress 2015

Posters used within an academic meeting

R. Baumgartner, J. Khinast, E. Roblegg, Nano-Extrusion (NANEX): Manufacturing of Solid-Nanoparticle Formulations Directly from the Liquid Phase via Hot-Melt Extrusion, 17.-18.04.2013, Leoben, Austria; 9. Minisymposium der Verfahrenstechnik

R. Baumgartner, J. Khinast, E. Roblegg, *Nano-Extrusion (NANEX): A One-step Process for Manufacturing Solid API Nanoparticle-Formulations Directly from the Liquid Phase,* 10.-14.11.2013, San Antonio, Texas, United States of America, AAPS Annual Meeting and Exposition 2013

R. Baumgartner, J. Khinast, E. Roblegg, *Überführung einer Phenytoin-Nanosuspension in eine feste orale Darreichungsform mittels Nano-Extrusion (NANEX),* 23.-28.02.2014, Schladming, Österreich, 47. Wissenschaftliche Fortbildung der Österreichischen Apothekerkammer

R. Baumgartner, J. Khinast, E. Roblegg, *Manufacturing of a Solid Phenytoin Nanoparticle Formulation via Nanoextrusion,* 31.03.-03.04.2014, Lisbon, Portugal, 9th World Meeting on Pharmaceutics, Biopharmaceutics and Pharmaceutical Technology

R. Baumgartner, A. Eitzlmayr, N. Matsko, J. Khinast, E. Roblegg, *Nanoextrusion: A Promising Strategy for the Oral Drug Delivery Market*, 23.-25.04.2014, Graz, Austria, 23.Wissenschaftliche Tagung der Österreichischen Pharmazeutischen Gesellschaft (ÖPHG); awarded

R. Baumgartner, J. Khinast, E. Roblegg, *NANEX: Process design with potential matrix materials*, 13.-14.04.2015, Reims, France, 1st European Conference on Pharmaceutics – Drug Delivery

R. Baumgartner, G. Koscher, J. Khinast, (S. Laske), E. Roblegg*, NANEX: A Continuous Hot-Melt Extrusion (HME) Process for Nano-Based Formulations*, 8.-13.11.2015, Salt Lake City, United States of America, AIChe Annual Meeting

R. Baumgartner, J. Matić, J. Khinast, E. Roblegg, *Nano-extrusion: A continuous hot melt extrusion process for nano-based formulations,* 19.-21.04.2016, Nuremberg, Germany, PARTEC 2016, International Congress on Particle Technology